Structural and functional analysis

of human sweat glands

(ヒト汗腺の構造機能解析)

A Doctoral Dissertation

Presented to Osaka University

2015

Ryuichiro Kurata

Contents

Chapter II

Identification of human sweat gland stem cells

Abbreviations

Ab: antibody

αSMA: alpha-smooth muscle actin

BABB: benzyl alcohol/benzyl benzoate

BSA: bovine serum albumin

AQP5: aquaporin 5

CD29: integrin β1

CD31: platelet endothelial cell adhesion molecule

CD49f: integrin α6

HE: hematoxylin and eosin

HRP: horseradish peroxidase

K18: keratin 18

K8: keratin 8

PBS: phosphate-buffered saline

PBTT: PBS, 0.1% Tween-20 and 0.1% Triton-X 100

PFA: paraformaldehyde

PGP9.5: protein gene product 9.5

S100A2: S100 calcium binding protein A2

S100P: S100 calcium binding protein P

Summary

Human eccrine sweat glands are complex coiled tubular organs that maintain body temperature by secreting sweat. Understanding the cellular mechanisms that govern the structures and functions of eccrine sweat glands may lead to clinical benefits for burn victims and patients with hyperhidrosis. Although the structures and functions of these glands have been assessed histologically, the cellular mechanisms underlying sweat activity of eccrine sweat glands have not been determined. I therefore utilized three-dimensional imaging to clarify the detailed coiled structures of eccrine sweat glands. Whole-organ analysis showed that the elongated myoepithelial cells are three-dimensionally arranged parallel to the entangled secretory portions of coiled structures, suggesting that sweat secretion is due to the mechanical stress of myoepithelial cells on the entangled tubules. I also found that these myoepithelial cells contain large numbers of sweat gland stem cells with self-renewal ability and multipotency. Myoepithelial cells generated sweat gland-like spheres, with their apical and basal cell layers expressing markers for luminal and myoepithelial cells, respectively, suggesting that myoepithelial cells possess the ability to regenerate eccrine sweat glands. These findings enabled the visualization of the three-dimensional coiled structures of eccrine sweat glands, as well as identifying the sweat gland stem cells able to regenerate sweat gland-like organs. These results provide insights into the cellular mechanisms that govern the structures and functions of eccrine sweat glands.

General Introduction

Vital role of the skin in maintaining homeostasis of the body

The skin, which is located at the interface between the body and the environment, is the largest organ of the human body. The vital role of skin is to prevent loss of water and other components of the body to the environment and protect the body from a variety of environmental stimuli. The skin is an intricate structure composed of the epidermis and dermis, including the subcutaneous adipose tissue. The epidermis possesses an effective barrier function that defends the body against dehydration, infection by invading microorganisms, and environmental influences, e.g., physical and chemical stimuli (Fuchs, 2009; Proksch et al., 2008). The epidermal appendages, including the hair follicles, sebaceous glands, and sweat glands, also help maintain and protect the skin. For example, sweat glands act to maintain skin homeostasis, including moisturization, host defenses, and thermoregulation.

The dermis is separated from the epidermis by the basement membrane (Watt and Fujiwara, 2011). Dermal components contribute to epidermal homeostasis through epidermal-dermal interactions via the basement membrane (Alonso and Fuchs, 2006; Blanpain and Fuchs, 2009). For example, dermal papilla cells of hair follicles stimulate epidermal cells to downwardly extend and induce hair follicle morphogenesis (Alonso and Fuchs, 2006; Driskell et al., 2011). Dermal blood vessels provide nourishment to and remove wastes from epidermal cells. Body temperature is maintained near 37°C primarily by action of the blood vessels and sweat glands. Dermal sensory nerve fibers wrap around hair bulbs, allowing the sense of touch to extend beyond the skin surface. Sweat glandular nerve fibers, also called sudomotor fibers (Kennedy et al, 1994; Low et al, 2006),

innervate sweat glands, which initiate sweat secretion. Thus, the epidermis and epidermal appendages, together with the assistance of the dermis, protect the body against environmental stimuli and maintain skin homeostasis.

Epidermal components individually maintain skin homeostasis

As the outermost layer of the organism, the epidermis is constantly exposed to multiple types of injury. Therefore, the structures and functions of the epidermis must persistently protect the organism against harmful environmental stimuli. The epidermal components, hair follicles, sweat glands, and interfollicular epidermis, possess distinct functions that maintain epidermal homeostasis against environmental insults (Figure I-1).

The interfollicular epidermis is a stratified squamous epithelium, maintenance of which relies on the proliferation and differentiation of the basal layer of the epidermis (Figure I-2). As basal epidermal cells differentiate and move toward the surface, they eventually terminally differentiate into the stratum corneum (Leblond, 1964). The stratum corneum is the barrier to the passive diffusion of water out of the skin, allowing individuals to live in air without becoming dehydrated, as well as being is the barrier to the entrance of other molecules, including irritants, into the skin.

The hair follicles develop from epidermal downgrowths induced by specialized mesenchymal cell condensations. Each hair follicle forms a cylinder-like structure that generates a hair shaft through hair cycles. The hair on the scalp serves as an insulator against heat and cooling, as well as protecting against ultraviolet radiation. Hair follicles are associated with sebaceous glands and arrector pili muscles. The sebaceous gland releases sebum to the skin surface, which helps keep the skin surface flexible and moist. The arrector pili muscle is innervated by sympathetic nerve fibers

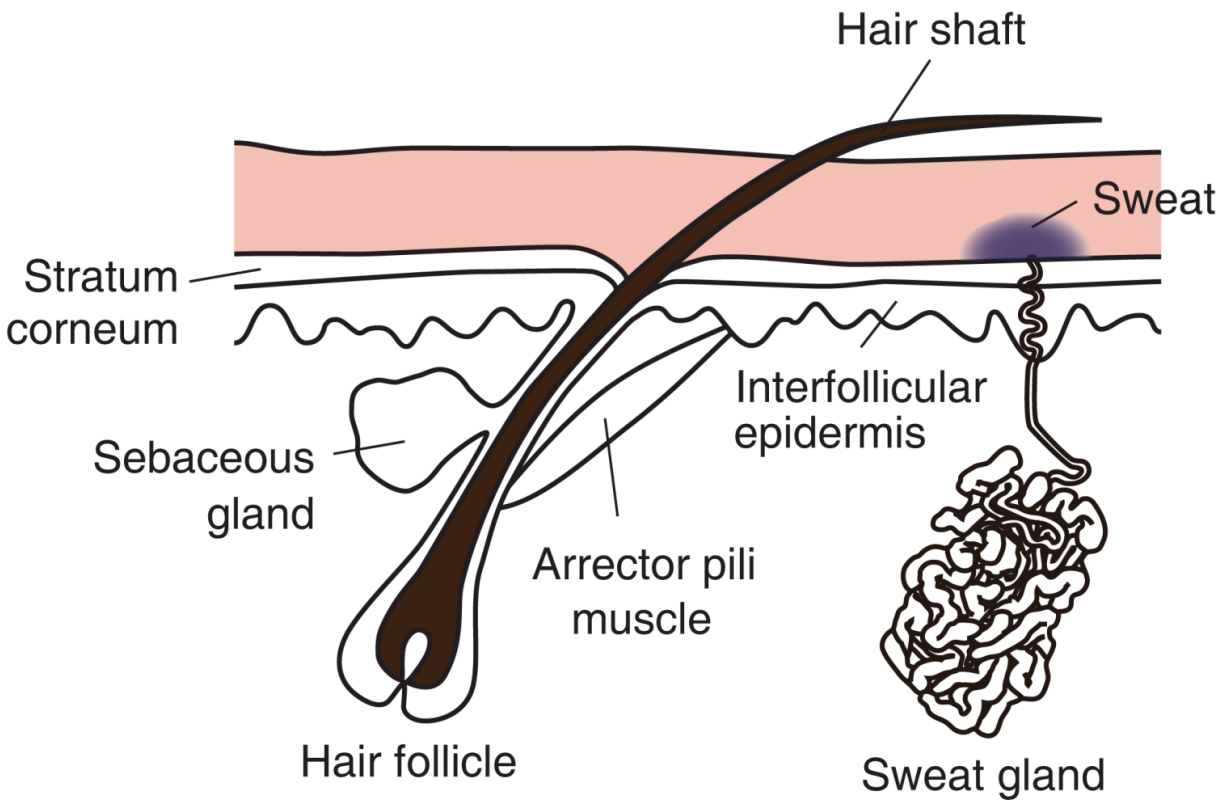

Figure I-1. Histological analysis of the epidermis and epidermal appendages in human skin.
The skin consists of three primary layers, the epidermis, dermis, and hypodermis. The epidermis mainly consists of the interfollicular epidermis, hair follicles, and sweat glands. Each hair follicle is associated with a sebaceous gland and arrector pili muscle.

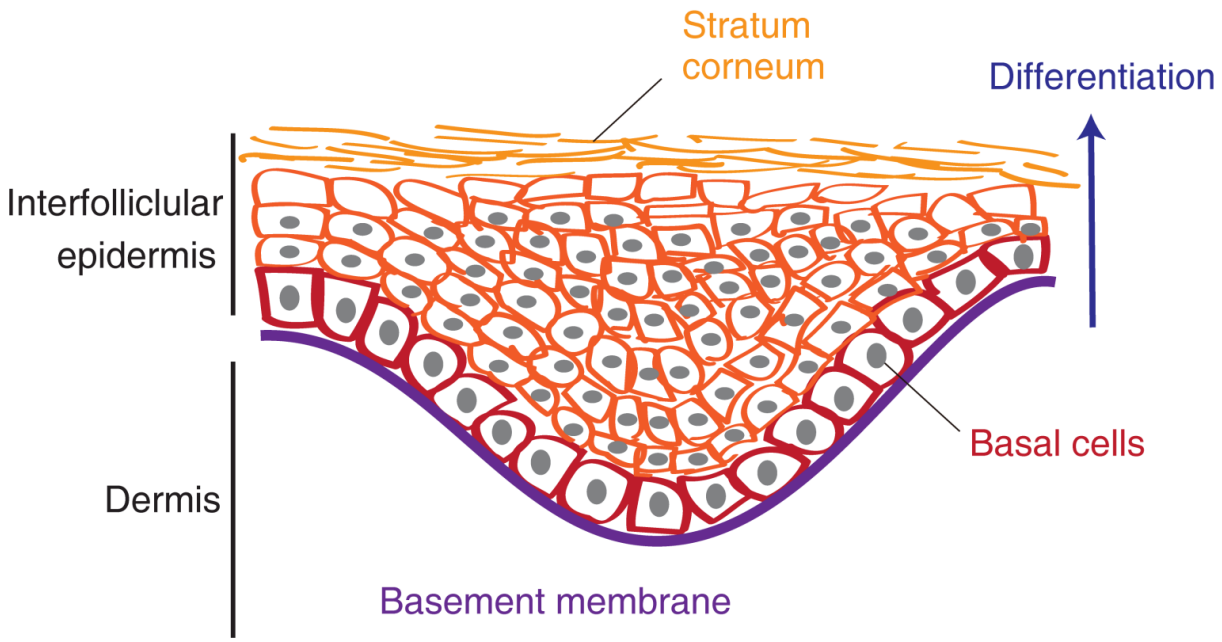

Figure I-2. Architecture of the interfollicular epidermis.
The epidermis is a type of stratified epithelium, consisting of several layers of keratinocytes. Keratinocytes start as basal keratinocytes, differentiating as they move through the cell layers.

and induces piloerection by contraction and suppression of heat loss (Fujiwara et al., 2011).

The sweat glands are epidermal appendages that regulate body temperature by secreting sweat. These glands not only participate in thermoregulation but protect the organism from dryness by preventing the evaporation of moisture from the body (Luebberding et al., 2013). Sweat, together with sebum, creates a hydrolipidic film that covers skin surface and functions as the skin's front-line barrier (Shelmire, 1959). Furthermore, sweat contains antimicrobial peptides and secretory IgA, both of which act to defend against infection (Murakami et al., 2002; Schittek et al., 2001; Shiohara et al., 2011). Thus, human sweat glands are indispensable in maintaining skin homeostasis. Understanding the cellular and molecular mechanisms that govern sweat gland activity may lead to clinical benefits for patients with symptoms associated with abnormalities in perspiration.

Human eccrine sweat glands are the only apparatus regulating body temperature by sweating

Sweat glands are divided into two major types, eccrine and apocrine sweat glands (Figure I-3). Eccrine sweat glands secrete sweat, which contains water, sodium chloride, urea, lactic acid, and potassium ions, by merocrine secretion from sweat duct orifices at the skin surface. Apocrine sweat glands secrete an oil-based fluid containing proteins, lipids, and steroids by apocrine secretion through the follicle orifices (Sato et al., 1989a; Wilke et al., 2007).

Eccrine sweat glands are derived from the epidermis, and their morphogenesis is completed during pregnancy. Apocrine sweat glands are also completely generated during the embryonic stage, but the origin of these glands remains unknown. Eccrine sweat glands are distributed throughout the human body, including in the palms and soles, whereas most animals do not possess eccrine sweat glands. In mice, eccrine sweat glands are confined to the pads of the paws, with few present in the

	Eccrine	Apocrine
		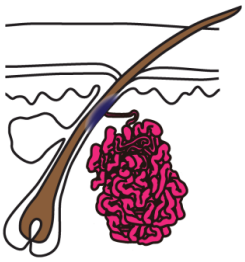
Secreted substances	Water, sodium chloride, etc.	Lipids, steroids, etc.
Opening	Skin surface	Hair follicle
Exocrine secretion	Merocrine secretion	Apocrine secretion
Origin	Epidermis	Unknown
Morphogenesis	During embryonic stage	During embryonic stage
Distribution in skin	Most regions	Axillae, grion, etc.

Figure I-3. Features of human eccrine and apocrine sweat glands

trunk. Although horses and camels control body temperature using sweat glands distributed throughout the body, their sweat glands are apocrine glands (Jenkinson et al., 2007; Schmidt-Nielsen et al., 1957). In contrast, human apocrine sweat glands are confined to the axillae, groin, and submammary, perianal and perineal regions. Thus, compared with other animals, human eccrine sweat glands are unique, in that they play a major role in regulating body temperature by sweating.

Cellular and structural properties of eccrine sweat glands

Eccrine sweat glands, like salivary and mammary glands, are exocrine glandular organs. Exocrine glands produce substances to be released externally, such as mucus, breast milk, and sweat (Debnath and Brugge, 2005). Eccrine sweat glands and mammary glands are thought to have evolved from apocrine sweat glands. However, eccrine sweat glands comprised of straight single tubules must be distinguished from mammary glands comprised of branched tubules.

The eccrine sweat gland mainly consists of a secretory portion and a duct (Figure I-4). The secretory portion shapes the spatial coiled structure and has a narrow lumen for sweat secretion. The secretory portion comprises luminal cells, which encompass myoepithelial cells. These myoepithelial cells are thought to modulate sweating through contraction of the secretory portion (Sato, 1977; Sato et al., 1989b). Secretory luminal cells are classified as light (serous) and dark (mucous) cells, which can be distinguished by the presence of different types of granules (Montagna et al., 1953; Munger, 1961). The light cells are larger luminal cells, which possess slightly acidophilic cytoplasmic granules positively for mucopolysaccharides, whereas the dark cells are smaller luminal cells that contain basophilic granules.

The sweat gland duct is generally formed by an outer layer of peripheral cells and an inner layer

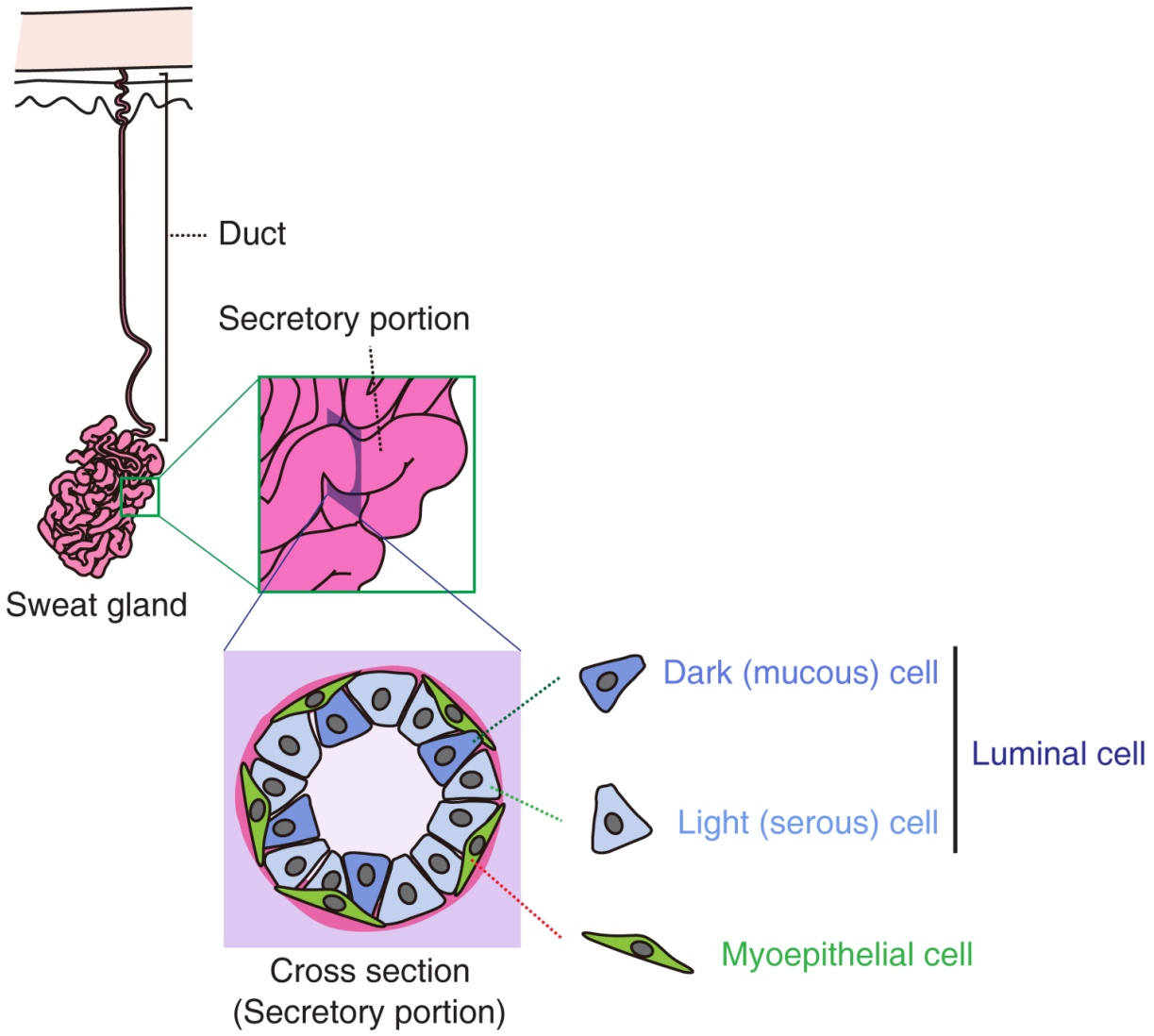

Figure I-4. Cell arrangement in the secretory portion of a human sweat gland.
The sweat gland mainly consists of a duct and a secretory portion, with the latter comprised of luminal and myoepithelial cells. Luminal cells can be subdivided into dark (mucous) and light (serous) cells.

of luminal cells. The duct is subdivided into three segments, i.e., coiled, straight, and intraepidermal ducts (Figure I-5). The coiled duct forms the coiled structure and is connected to the secretory portion. The straight duct, which is connected to the coiled duct, forms a slightly rippled structure. The intraepidermal duct, which is connected to the straight duct, forms a spiral structure and opens onto the epidermal surface. Thus, an eccrine sweat gland is a simple unbranched tubular gland consisting of a duct and a secretory portion but with a characteristic spatial coiled structure.

Morphogenesis of eccrine sweat glands

The development of eccrine sweat glands has been assessed by ultrastructural examination in mice. Mouse eccrine sweat glands are confined to palmoplantar skin. The first sign of sweat gland germ formation in mice is observed at embryonic day 17.5 in the pad epidermis (Kunisada et al., 2009). After birth, the sweat gland germs grow toward the mesenchyme and start to form a coiled secretory segment. As morphogenesis proceeds, inner cells of the sweat glands differentiate into secretory luminal cells, whereas outer basal cells of the glands differentiate into myoepithelial cells. At the completion of sweat gland morphogenesis, cell proliferation occurs in the ducts and epidermis but hardly in the secretory portions (Lu et al., 2012). Thus, mouse eccrine sweat gland development is completed postnatally.

In humans, eccrine sweat gland morphogenesis is completed during the embryonic stage (Figure I-6). Ultrastructural studies of human eccrine sweat gland morphogenesis were first reported in the 1960s (Hashimoto et al., 1965). These glands originate from the epidermis in human embryos, at 12–13 weeks of gestation. The eccrine sweat gland placode is oblong and palisade in shape. At 14–15 weeks, the tip of the eccrine sweat gland germ penetrates deeper into the dermis and begins to form a

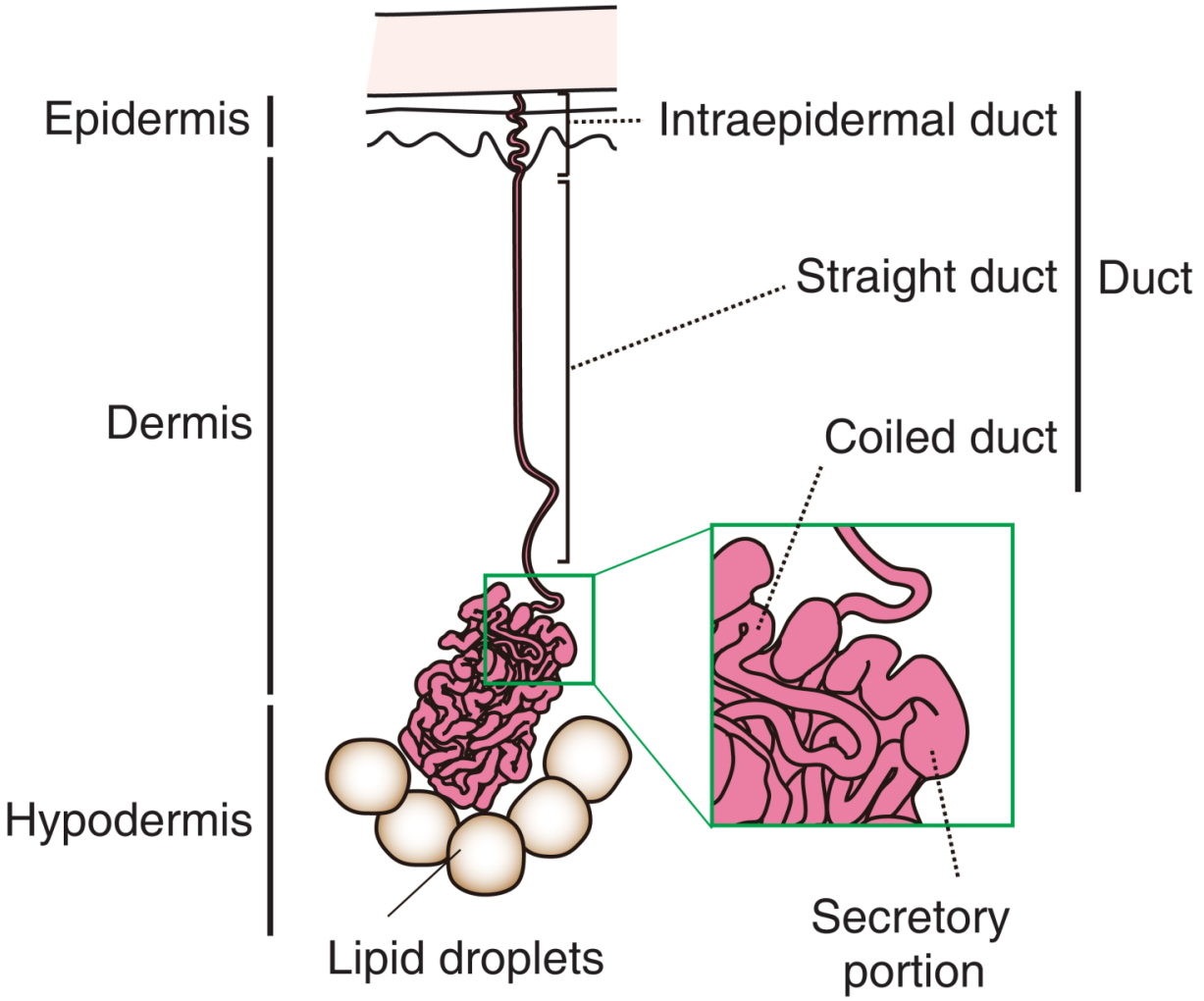

Figure I-5. Schematic illustration of a human sweat gland.
The sweat gland is a simple unbranched tubular structure extending through the epidermis, dermis, and hypodermis and consisting primarily of a duct and a secretory portion. The duct cam be further subdivided into intraepidermal, straight, and coiled ducts.

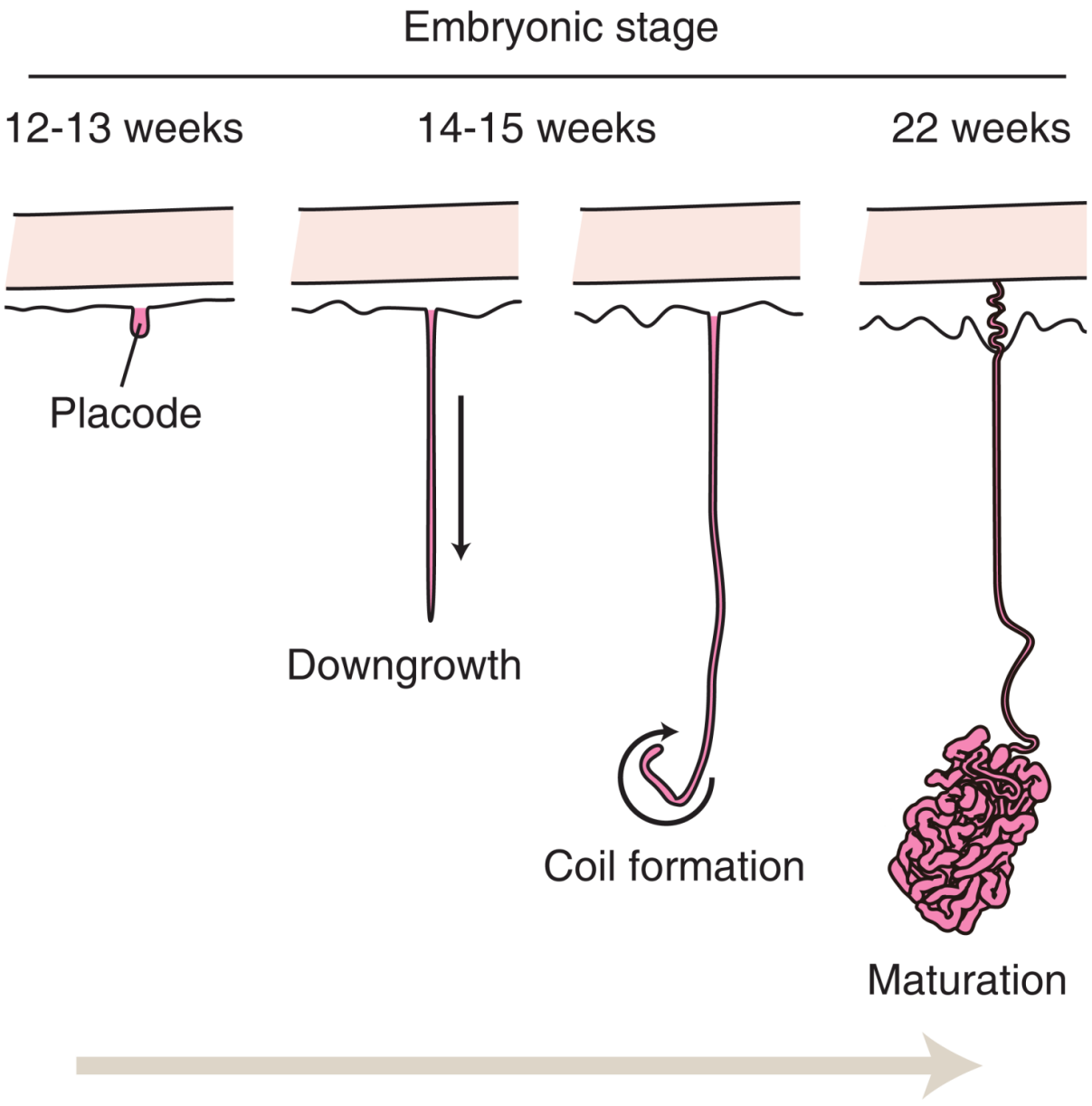

Figure I-6. Schematic illustration of human sweat gland morphogenesis during embryonic stages.

coil. Gland structure matures by 22 weeks and resembles glands in adults (Hashimoto et al., 1965). Myoepithelial and luminal cells in the secretory portion can be detected by 22 weeks (Moll and Moll, 1992; Sun et al., 1979). Thus, the morphogenetic initiation and the maturation of eccrine sweat glands vary according to species, but both human and mouse sweat glands originate from the epidermis.

Stem cells that maintain eccrine sweat gland structure

The homeostasis of eccrine sweat glands following morphogenesis is governed by stem cells. Stem cells are functionally defined as possessing the ability of self-renewal and multipotency. Self-renewal ability is defined as the capacity to sustain a multipotent state during numerous cycles of cell division. Multipotency is defined as the ability to give rise to multiple differentiated cell types. The stem cells are housed in specialized regions and are maintained in unique microenvironments involving humoral factors, extracellular matrix, and cell attachment.

Several types of stem cells that maintain the structure of the epidermis and its appendages have been identified. Keratinocyte stem cells in the interfollicular epidermis progressively provide keratinocytes and maintain interfollicular epidermal structure throughout life. Hair follicle stem cells also provide progenitors and continuously generate hair follicles through hair cycles. Thus, the structures of the interfollicular epidermis and hair follicles are maintained by the persistent provision of progenitors throughout life. However, the mechanism by which eccrine sweat gland structure is maintained during normal homeostasis remains unknown.

The structural maintenance of human eccrine sweat glands has been examined histologically. The existence of stem cells in the ducts has been suggested by the finding that sweat gland residue

following trauma regenerated the duct (Lobitz et al., 1954). Moreover, distinctive stem cell populations have been shown to be present in both the duct and secretory portions of mouse eccrine sweat glands during normal homeostasis (Lu et al., 2012). These results suggest that human eccrine sweat glands harbor glandular stem cells that contribute to the maintenance of sweat gland structure.

Regeneration of eccrine sweat glands

The loss of eccrine sweat glands, such as in burn victims, causes thermoregulatory hypofunction in the human body, making the regeneration of these glands clinically important. Skin grafting using epidermal sheets derived from keratinocyte stem cells has been used to treat patients with extensive burns. Although these keratinocyte stem cells can generate epidermis, they generate few eccrine sweat glands. Since patients with large-scale, deep burns cannot regulate their body temperature, regeneration of eccrine sweat gland organs is important. To date, however, these glands have yet to be regenerated.

Several studies have attempted to regenerate eccrine sweat glands from epithelial cells. For example, rabbit corneal basal cells generate sweat glands when grafted into kidney capsules along with mouse embryonic plantar dermis. However, only embryonic mesenchyme has such inductive capabilities (Ferraris et al., 2000). In mice, the regenerative potential at a single-cell level of various ectodermal appendages, including hair follicles, eccrine sweat glands, mammary glands, and salivary glands, has been evaluated by in vivo engraftment (Blanpain et al., 2004; Lombaert et al., 2008; Lu et al., 2012; Shackleton et al., 2006; Stingl et al., 2006). In eccrine sweat gland regeneration, myoepithelial cells generate glandular structures when grafted into cleared mammary fat pads or shoulder fat pads (Lu et al., 2012). In humans, transplanted epidermal keratinocytes formed eccrine

duct-like structures in the presence of fibroblasts, epidermal growth factors, and serum (Shikiji et al., 2003). Although these observations suggest that eccrine sweat glands can be generated by autologous transplantation, the ability of these regenerated glands to secrete sweat has not been determined.

Function of eccrine sweat glands as a thermoregulatory apparatus

Eccrine sweat glands constitute a functional thermoregulatory apparatus that not only secretes and releases sweat to the skin surface but regulates the body temperature by sweat secretion. Although the anatomical structures of eccrine sweat glands have been assessed histologically, the mechanisms by which these structures undergo contractions mechanically have yet to be identified.

Sweat secretion by eccrine sweat glands is induced by the dermal components of these glands, with their blood vessels and nerve fibers being essential for thermoregulatory sweat secretion. For these glands to effectively secrete sweat, blood vessels are distributed abundantly in proximity to these glands and participate in the reabsorption of HCO_3^- and NaCl from the ducts (Kuno, 1956). Eccrine sweat glands encompassed by nerve fibers receive cholinergic sympathetic innervation (Sato et al., 1989a), with sweat secretion initiated by acetylcholine secreted from the nerve fibers. Neurological disorders that affect the central or peripheral nervous system lead to sweating disorders classified by the amount of sweat secreted, including anhidrosis (absent sweating), hypohidrosis (decreased sweating), and hyperhidrosis (excessive sweating) (Quinton, 1983; Sato et al., 1989a). Thus, the dermal components that encompass eccrine sweat glands are essential for sweat secretion. However, how these glandular dermal components support sweat secretion and sweat gland homeostasis remains unknown.

Aim of the present study

Understanding the mechanisms underlying the structures and functions of human eccrine sweat glands is of clinical importance. Sweating disorders such as eccrine sweat gland depletion and symptoms of excessive perspiration can significantly reduce a patient's quality of life. Although the structures and the functions of eccrine sweat glands have been investigated by conventional histological methods, their glandular natures, including their three-dimensional structures, sweat gland activity, and glandular homeostasis and regeneration, have largely remained unknown. Recent studies of other types of exocrine glands have included analysis of their three-dimensional structures and mechanisms of glandular regeneration. To better understand the structures and functions of eccrine sweat glands, I therefore sought to visualize their three-dimensional structures and to identify sweat gland stem cells.

Chapter I describes the development of a whole-mount immunostaining method with sweat gland cell markers to visualize the three-dimensional structure of human eccrine sweat glands. This method succeeded in visualizing the detailed coiled structures of eccrine sweat glands. Whole-organ analyses at single-cell resolution revealed the three-dimensional arrangements of the sweat gland cell compartments that constitute coiled tubules, suggesting that these arrangements allow effective contraction for sweat secretion. Furthermore, these methods resulted in the visualization of the three-dimensional distributions of blood vessels and nerve fibers, which surround eccrine sweat glands to facilitate effective sweat secretion. These results provide insights into the cellular mechanisms that govern sweat gland activity.

In Chapter II, I histologically examined the localizations of stem cell markers in human eccrine

sweat glands, in order to identify the stem cells that can regenerate eccrine sweat glands. I found that the stem cell markers integrin β1 (CD29) and Notch were highly expressed by myoepithelial cells of these glands. Subsequently, I developed a procedure to isolate each eccrine sweat gland cell population, in order to identify sweat gland stem cells that possess self-renewal ability and multipotency. The myoepithelial cells isolated as a subpopulation of $CD29^{hi}$ integrin α6 $(CD49f)^{hi}$ cells possessed self-renewal ability and multipotency and could be differentiated into luminal cells. These results provide insight into the glandular homeostasis and regeneration of human eccrine sweat glands.

Chapter I

Visualization of the three-dimensional structure of human sweat glands

I-1 Summary

Human eccrine sweat glands maintain body temperature by secreting sweat. Since sweat secretion is facilitated by the mechanical contraction of sweat gland structures, their structural anatomy has been assessed by conventional histological methods. Despite histological evidence that eccrine sweat glands are three-dimensionally coiled tubular structures, consisting of ducts and secretory portions, their detailed structural anatomy has remained unclear. To better understand the details of these three-dimensional coiled structures, the molecular markers that distinguish sweat gland compartments were histologically profiled, by assaying markers of ductal luminal, ductal basal, secretory luminal, and myoepithelial cells. A whole-mount staining method using confirmed sweat gland markers was used to visualize the three-dimensional coiled structures of these glands. Whole-mount staining showed that the ducts and secretory portions of eccrine sweat glands formed three-dimensionally distinct tubular structures. The ductal tubules were occasionally bent, whereas the secretory tubules were not only frequently bent but well entangled. Whole-mount staining also revealed the detailed three-dimensional cellular arrangements of sweat gland compartments constituting complex coiled structures. The ducts were composed of regularly arranged cuboidal shaped cells, whereas the secretory portions were surrounded by myoepithelial cells longitudinally elongated along the entangled secretory tubules. Whole-mount staining was also used to visualize the spatial arrangements of blood vessels and nerve fibers, which facilitate sweat secretion. These blood vessels ran longitudinally parallel to the sweat gland tubules, whereas the nerve fibers wrapped only the secretory, not the ductal, tubules. Together, whole-mount staining of eccrine sweat glands revealed their detailed three-dimensional coiled structures at a single-cell level.

I-2 Introduction

Glands distributed throughout the body develop from epithelial tissue and are categorized as either exocrine or endocrine glands. Exocrine glands secrete their products into ducts, whereas endocrine glands deliver their secretory products directly into the circulatory system. Exocrine glands are classified broadly as unicellular or multicellular. The epithelium of the intestine is unicellular, whereas eccrine sweat glands are multicellular, characterized by a secretory portion, an end portion where epithelial cells secrete a product, and a duct, through which secretions from the secretory portions are delivered to the exterior of the gland. Multicellular exocrine glands can be classified into three major categories, based on the structure of their secretory portions. Tubular glands, e.g., eccrine sweat glands, are straight or coiled; alveolar glands, e.g., mammary glands, have a secretory portion shaped like a flask; and tubuloalveolar glands, e.g., salivary glands, possess combined characteristics of tubular and alveolar secretory portions.

Understanding the mechanisms of secretion by exocrine glands is of clinical importance, because defective secretion by these glands can markedly reduce patient quality of life, resulting, for example, in hyperhidrosis and dry mouth. Since secretions of these glands are facilitated by mechanical stress, i.e., contraction, of myoepithelial cells, which are contractile cells surrounding secretory portions, the structural anatomy of these glands has been assessed by conventional histological methods. The mammary gland is an alveolar gland containing enlarged secretory acini with large lumina that are filled with milk. Contractions of the stellate-shaped myoepithelial cells around the secretory alveoli result in ejection of milk from the mammary glands. Salivary glands are typical tubuloalveolar exocrine glands containing secretory alveolar and tubular elements. The stellate-shaped

myoepithelial cells in salivary glands are present in secretory portions and some parts of ducts, expelling saliva from acini.

Eccrine sweat glands have been also schematically delineated by histological analyses. Eccrine sweat glands are unbranched coiled tubules that mainly consist of secretory portions and ducts, the latter comprising epidermal, straight, and coiled ducts (Figure 1). The secretory portions consist of secretory luminal cells and encompassing myoepithelial cells, whereas the ducts consist of luminal cells and basal cells. The myoepithelial cells are supposed to modulate sweating through contraction of secretory portions (Sato, 1977; Sato et al., 1989b). Although three-dimensional coiled structures of eccrine sweat glands have been assessed histologically, their detailed structural anatomy remains unclear.

Conventional histological methods are limited in determining the three-dimensional complex structures of organs, because some three-dimensional information is lost by sample processing. Whole-mount staining methods have been developed to obtain detailed anatomical information about three-dimensionally complex organs, such as the brain (Dodt et al., 2007; Erturk et al., 2012; Hama et al., 2011; Ke et al., 2013; Tomer et al., 2014). Recently, whole-mount staining of mammary glands resulted in the visualization of the three-dimensional structures of their ducts and secretory portions (Rios et al., 2014), indicating that whole-mount staining is a powerful tool that may determine the detailed structural anatomy of sweat gland coiled regions.

In this study, whole-mount analyses revealed the detailed three-dimensional structures of eccrine sweat glands. Their secretory tubules were found to be intricately entwined and irregularly entangled. Myoepithelial cells of secretory portions were highly elongated and arranged longitudinally in the entangled secretory portion. These results suggest that myoepithelial cells form spatially

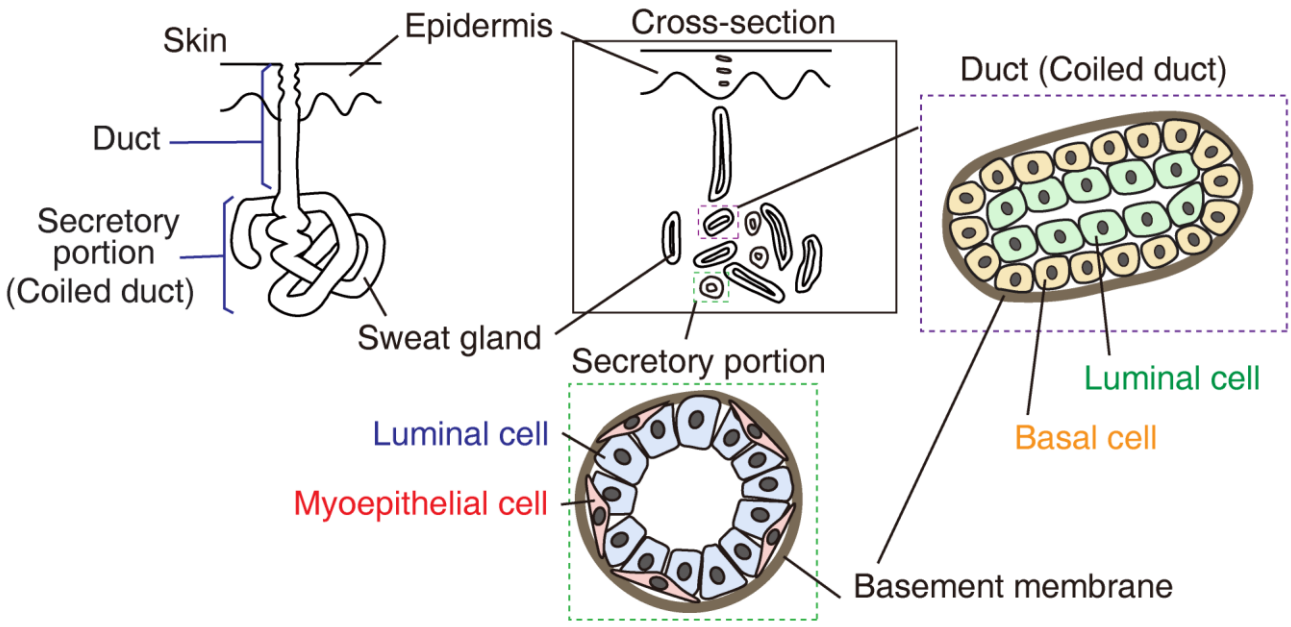

Figure 1. Schematic illustration of a human sweat gland and its main tissue segments. (upper left) Diagram of a sweat gland structure in human skin; (upper center) diagram of a cross section of a sweat gland in human skin; (lower center) diagram of the arrangement of cells in the secretory portion, consisting of luminal and myoepithelial cells surrounded by basement membrane; (upper right) diagram of the arrangement of cells in the duct consisting of luminal and basal cells surrounded by basement membrane.

characteristic arrangements in the secretory portions, in order to effectively expel sweat from tubular structures.

I-3 Materials and Methods

Human skin tissues

Frozen human skin tissues were obtained with informed consent from ILSbio (Chestertown, MD). Fresh human skin tissues were obtained from Osaka University Hospital (Osaka, Japan) and Biopredic International (Rennes, France), with informed consent. Experiments using human skin were approved by the Ethics Committee of Osaka University.

Antibodies

Primary antibodies used for immunohistochemical, immunofluorescence, and whole-mount staining included anti-keratin 8 (K8; Progen, Heidelberg, Germany), anti-α-smooth muscle actin (αSMA; Abcam, Cambridge, MA), anti-S100 calcium binding protein P (S100P; Novus Biologicals, Littleton, CO), anti-S100 calcium binding protein A2 (S100A2; Novus Biologicals), anti-CD29 (Abcam), anti-CD49f (Millipore, Milford, MA), anti-platelet endothelial cell adhesion molecule (CD31; Abcam), and anti-protein gene product 9.5 (PGP9.5; Abcam). Secondary antibodies used in this study included horseradish peroxidase (HRP)-conjugated sheep anti-mouse (Amersham, San Francisco, CA), Envision+System/HRP rabbit (Dako, Glostrup, Denmark), HRP-conjugated goat anti-rat (American Qualex, San Clemente, CA), and species-specific fluorescent secondary antibodies (Invitrogen, Carlsbad, CA). F-actin was stained with Alexa Fluor 488, 633 Phalloidin (Invitrogen).

Immunohistochemical analysis

Human skin tissues were embedded in OCT compound (Sakura Finetechnical Co., Tokyo, Japan)

and frozen in 2-methylbutane chilled in liquid nitrogen. Cryosections were prepared, fixed in 4% formaldehyde in phosphate-buffered saline (PBS), cold methanol, or cold acetone, and blocked with 1% goat serum (Dako, Carpinteria, CA) in PBS, followed by incubation with primary antibodies at 4°C overnight. After three washes with PBS, the sections were treated with HRP-conjugated secondary antibodies, followed by color development using 3,3-diaminobenzidine. After counterstaining with hematoxylin, the sections were examined with an Eclipse E800 microscope (Nikon, Melville, NY). For double immunofluorescence staining, sections were prepared, fixed in 4% formaldehyde in PBS, cold methanol, or cold acetone, and incubated with primary antibodies at 4°C overnight. After washing in PBS, the sections were treated with secondary antibodies for 1 h, washed with PBS, and stained with Hoechst 33342 to visualize the nuclei. All procedures were performed at room temperature. Immunofluorescence images were recorded with an LSM5 confocal microscope (Carl Zeiss, Oberkochen, Germany). Table I shows the sources, clones, and concentrations of primary and secondary antibodies used for immunohistochemical staining.

Whole-mount sweat gland preparation

Connective tissues encasing the secretory regions of sweat glands were surgically separated from the epidermal side of each human skin tissue sample using fine scissors. The resulting dermis was chopped with sharp scissors. The sweat glands in the dermis were visualized using 10 μM neutral red (Sigma, St. Louis, MO) in PBS and picked out with fine forceps (Brayden and Fitzpatrick, 1995). The isolated sweat glands were fixed and incubated overnight at 4°C with 4% formaldehyde in PBS. The sweat glands were washed three times with 2% bovine serum albumin (BSA)/PBTT (PBS, 0.1% Tween-20 and 0.1% Triton-X 100) for 5 min and incubated overnight at 4°C with primary antibodies

Table I. Primary and secondary antibodies used for immunohistochemistry, immunofluorescence and whole-mount staining.

Primary Antibody	Secondary Antibody	Usage
Anti-keratin 8 (K8) (1:100 dilution) Progen, Heidelberg, Germany	HRP-conjugated sheep anti-mouse (1:500) Amersham, San Francisco, CA	Immunohistochemistry
	Alexa Fluor 488 conjugated goat anti-mouse (1:1000 dilution) Alexa Fluor 546 conjugated goat anti-mouse (1:1000 dilution) Invitrogen, Carlsbad, CA	Immunofluorescence and whole-mount staining
Anti-α smooth muscle actin (αSMA) (1:100 dilution) Abcam, Cambridge, MA	Envision system (HRP for rabbit) Dako Cytomation, Glostrup, Denmark	Immunohistochemistry
	Alexa Fluor 488 conjugated goat anti-rabbit (1:1000 dilution) Alexa Fluor 546 conjugated goat anti-rabbit (1:1000 dilution) Invitrogen, Carlsbad, CA	Immunofluorescence and whole-mount staining
Anti-S100 calcium binding protein P (S100P) (1:100 dilution) Novus Biologicals, Littleton, CO	Envision system (HRP for rabbit) Dako Cytomation, Glostrup, Denmark	Immunohistochemistry
	Alexa Fluor 488 conjugated goat anti-rabbit (1:1000 dilution) Alexa Fluor 546 conjugated goat anti-rabbit (1:1000 dilution) Invitrogen, Carlsbad, CA	Immunofluorescence and whole-mount staining
Anti-S100 calcium binding protein A2 (S100A2) (1:100 dilution) Novus Biologicals, Littleton, CO	Envision system (HRP for rabbit) Dako Cytomation, Glostrup, Denmark	Immunohistochemistry
	Alexa Fluor 488 conjugated goat anti-rabbit (1:1000 dilution) Alexa Fluor 546 conjugated goat anti-rabbit (1:1000 dilution) Invitrogen, Carlsbad, CA	Immunofluorescence and whole-mount staining
Anti-integrin β1 (CD29) (1:100 dilution) Abcam, Cambridge, MA	HRP-conjugated sheep anti-mouse (1:500) Amersham, San Francisco, CA	Immunohistochemistry
	Alexa Fluor 488 conjugated goat anti-mouse (1:1000 dilution) Alexa Fluor 546 conjugated goat anti-mouse (1:1000 dilution) Invitrogen, Carlsbad, CA	Immunofluorescence and whole-mount staining
Anti-integrin α6 (CD49f) (1:100 dilution) Millipore, Milford, MA	HRP-conjugated goat anti-rat (1:400) American Qualex, San Clemente, CA	Immunohistochemistry
	Alexa Fluor 488 conjugated goat anti-rat (1:1000 dilution) Alexa Fluor 546 conjugated goat anti-rat (1:1000 dilution) Invitrogen, Carlsbad, CA	Immunofluorescence and whole-mount staining
Anti-platelet endothelial cell adhesion molecule (CD31) (1:100 dilution) Abcam, Cambridge, MA	Alexa Fluor 488 conjugated goat anti-mouse (1:1000 dilution) Invitrogen, Carlsbad, CA	Whole-mount staining
Anti-protein gene product 9.5 (PGP9.5) (1:100 dilution) Abcam, Cambridge, MA	Alexa Fluor 488 conjugated goat anti-mouse (1:1000 dilution) Invitrogen, Carlsbad, CA	Whole-mount staining
Palloidin: Alexa Fluor 488 conjugated (1:100 dilution) Alexa Fluor 546 conjugated (1:100 dilution) Invitrogen, Carlsbad, CA		Immunofluorescence and whole-mount staining

in 2%BSA/PBTT. The sweat glands were subsequently washed and incubated overnight at 4 °C with secondary antibodies plus Hoechst33342 (Molecular Probes, Eugene, OR) and phalloidin (Invitrogen) in 2%BSA/PBTT. The following day, the tissues were washed and incubated in 80% glycerol overnight prior to dissection for three-dimensional imaging. Whole-sweat gland fluorescence images were acquired with a confocal laser-scanning microscope FV1200 (Olympus, Japan), combined with 405 nm, 473 nm, 559 nm, and 635 nm lasers and a FV12-HSD high-sensitivity detector with 10 × (UPlanSApo, NA = 0.40, working distance = 3.1 mm), 20 × (UPlanSApo, NA = 0.75, working distance = 0.6 mm), or 40 × (UPlanSApo, NA = 0.95, working distance = 0.18 mm) objective lenses. Table I details the sources, clones, and concentrations of primary and secondary antibodies used for whole-mount staining.

I-4 Results

Molecular profiling of human sweat gland compartments

Sweat gland coiled structures mainly consist of secretory portions and ducts. To better understand the three-dimensional anatomy of their coiled structures utilizing whole-mount staining, the cross-sectional anatomy of their coiled structures was assessed histologically using sweat gland cell markers. Hematoxylin and eosin staining showed that the coiled structures of eccrine sweat glands were closely clustered rounded tubules (Figure 2). These structures were encased in adipose and collagenous connective tissues and were detected in the deep dermis adjacent to the hypodermis, consistent with previous histological observations (Holyoke and Lobitz, 1952). Sweat gland markers expressed in each eccrine sweat gland compartment were therefore analyzed, by assaying for markers expressed exclusively by secretory luminal, myoepithelial, ductal luminal, and ductal basal cells. K8, a secretory luminal cell marker (Moll and Moll, 1992; Schon et al., 1999), was expressed in the large oblong cells in the luminal layers, but not in the basal layers, of sweat glands (Figure 3). αSMA, a myoepithelial cell marker (Moll and Moll, 1992; Schon et al., 1999), was expressed in the flattened small cells surrounding the eccrine sweat gland basal layers. These results were consistent with previous findings that myoepithelial cells are flattened small cells distinguishable from ductal basal cells (Moll and Moll, 1992). S100 calcium-binding proteins interact with cytoskeletal components and show differential expression and cellular distribution in ducts of eccrine sweat glands. S100P, a ductal luminal cell marker (Zhu et al., 2013), was expressed in the luminal layers of sweat gland ducts (Figure 3). These S100P-positive lumens were narrower than K8-positive lumens, suggesting that S100P and K8 are expressed in the luminal cells of ducts and secretory portions,

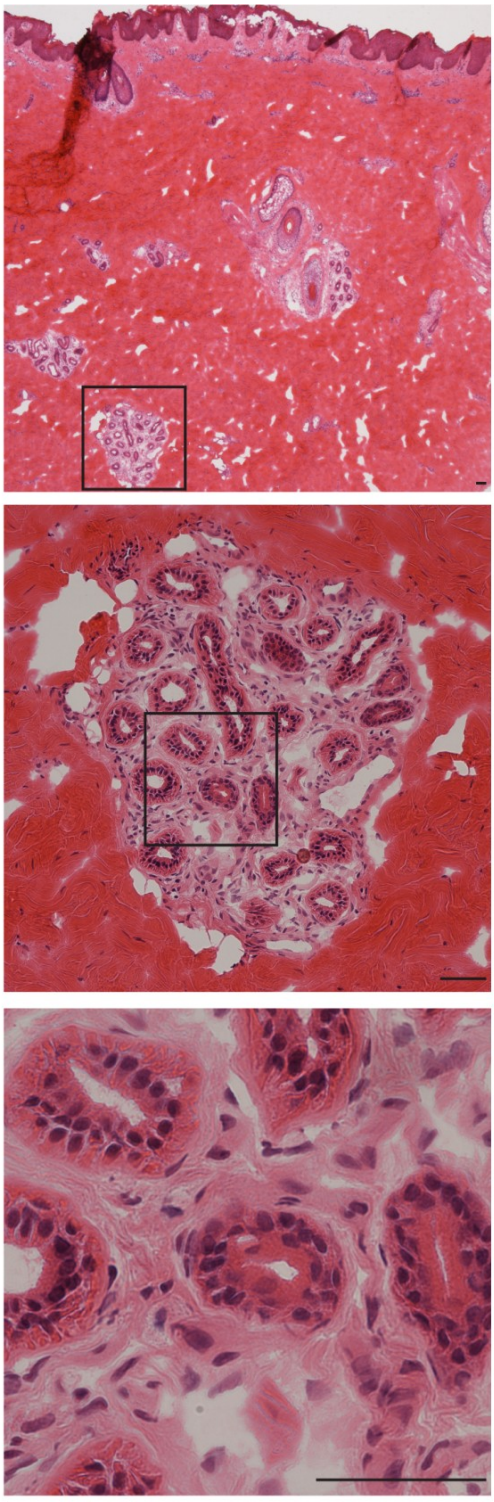

Figure 2. Cross-sectional rounded tubular structures of eccrine sweat gland coiled tubes are present in the deep dermis of human skin.
HE stained skin cross section showing the sweat glands surrounded by adipocytes and connective tissue. The coiled regions of eccrine sweat glands appeared as rounded structures in the hypodermis. Boxed areas in the upper panels are shown at higher magnification in the lower panels. Scale bars: 50 μm.

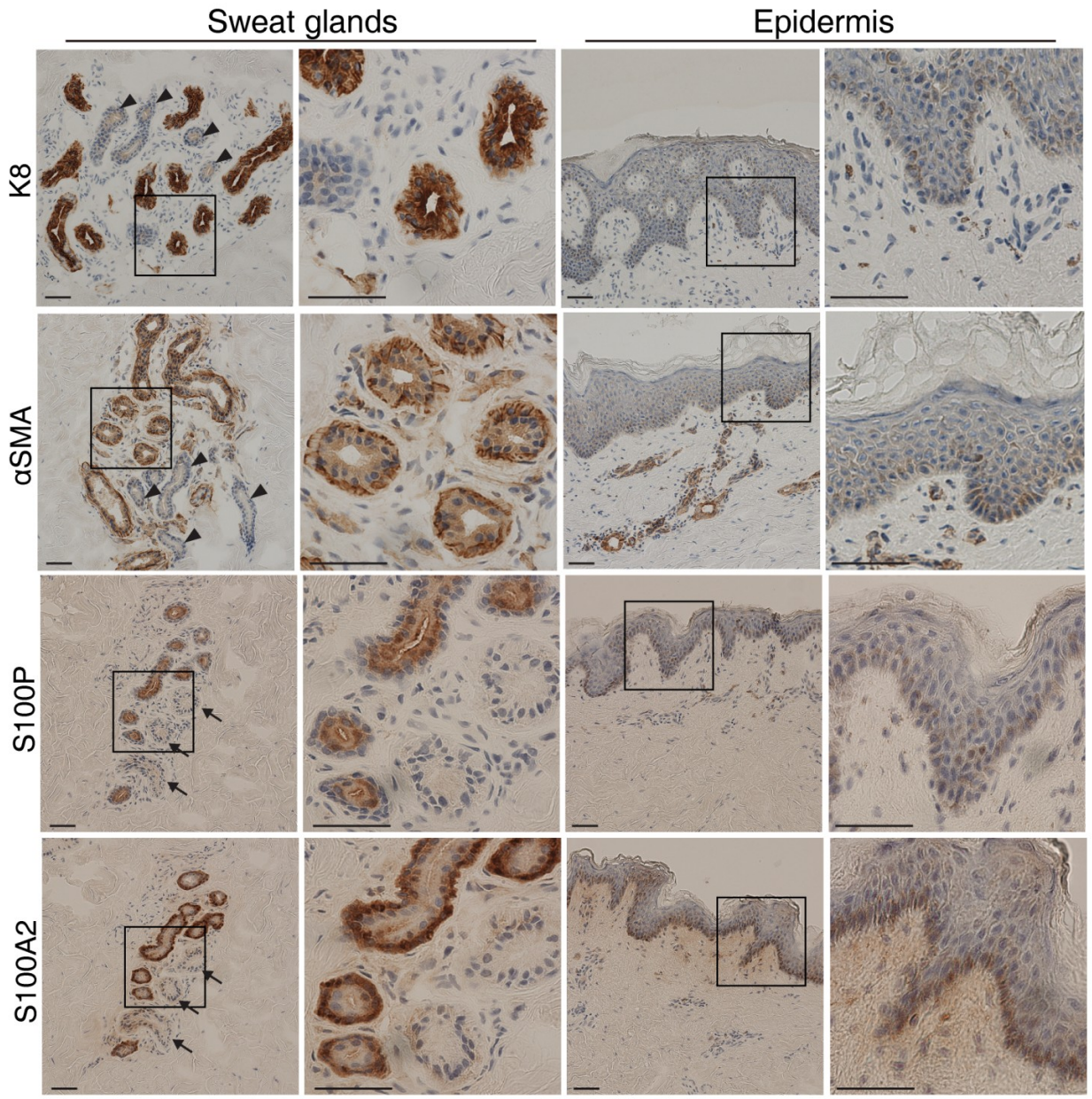

Figure 3. Sweat gland cell marker expression patterns in human eccrine sweat glands. Immunostaining of K8, αSMA, S100P, and S100A2 in human skin. K8 and S100P were expressed in parts of the luminal cell layers, and αSMA and S100A2 in parts of the basal cell layers. Boxed areas in the left panels are shown in the right panels at higher magnification. Arrowheads indicate the portions negative for K8 and αSMA, and arrows indicate the portions negative for S100P and S100A2. Scale bars: 50 μm.

respectively. S100A2, a ductal basal cell marker (Zhu et al., 2013), was expressed in cuboidal basal cells distinguishable from the flattened αSMA-positive basal cells, indicating that S100A2 and αSMA are expressed in basal cell layers in ducts and secretory portions, respectively. Thus, these results demonstrated that the four markers are distinctively expressed in the four sweat gland compartments, i.e., the ductal luminal, ductal basal, secretory luminal, and myoepithelial cell compartments.

Double immunofluorescence staining was utilized to verify whether these markers are exclusively confined to individual sweat gland compartments (Figure 4). K8 and αSMA were exclusively detected in the luminal and basal layers, respectively, of the same tubules. Similarly, S100P and S100A2 were distinctively expressed in luminal and basal cells, respectively. Double immunofluorescence staining also showed that K8 and S100P were expressed in the luminal cell layers, and αSMA and S100A2 in basal cell layers, of different tubules. Since the shapes of K8- and αSMA-positive cells are histologically consistent with those of secretory luminal and myoepithelial cells, respectively (Moll and Moll, 1992), these results indicated that K8/αSMA and S100P/S100A2 are expressed in secretory portions and ducts, respectively, of eccrine sweat glands and are specific markers for the four eccrine sweat gland compartments.

To accurately determine the shapes of sweat gland cells for subsequent three-dimensional analysis, the expression patterns of the basal epithelial cell markers CD29 and CD49f were assayed in the compartments of eccrine sweat gland coiled structures. CD29 was expressed in basal layers of sweat glands (Figure 5). CD49f was also expressed in these basal layers, particularly in myoepithelial-like basal cells, indicating that CD29 and CD49f are co-expressed in myoepithelial cells. Double immunofluorescence staining confirmed that CD29 and CD49f were strongly co-

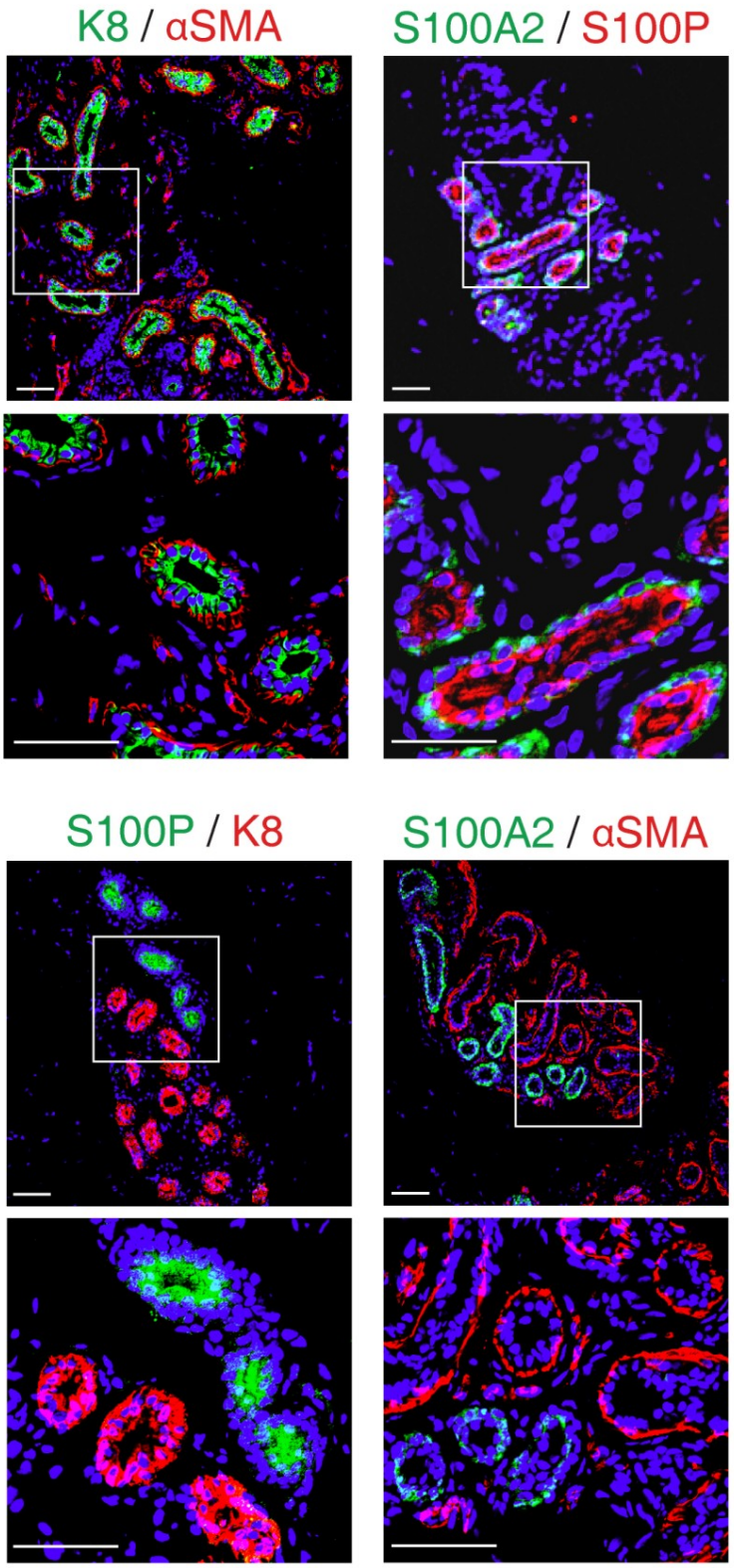

Figure 4. The profiled sweat gland markers are expressed in different human eccrine sweat gland compartments.
Double-immunofluorescence detection of K8, αSMA, S100P, and S100A2 in eccrine sweat glands. Boxed areas in the upper panels are shown in the lower panels at higher magnification. Nuclei (blue) were counterstained with Hoechst 33342. Scale bars: 50 μm.

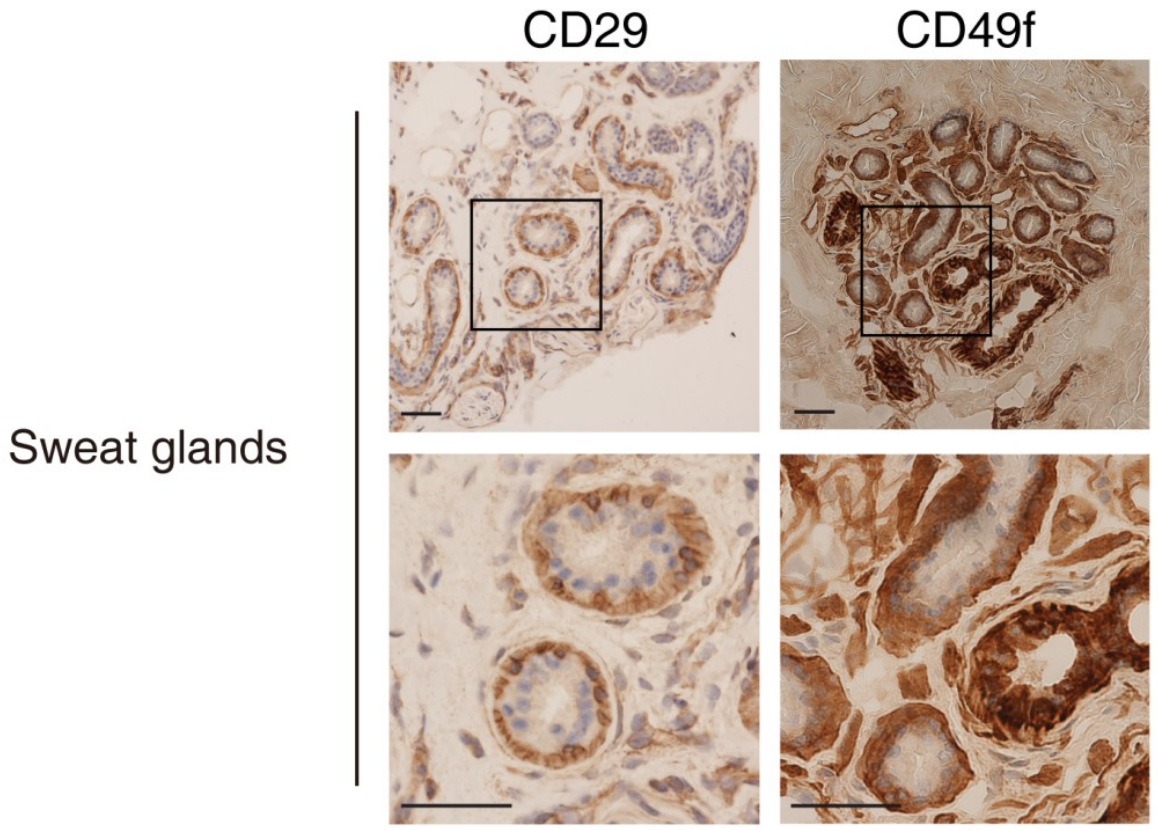

Figure 5. Expression of CD29 and CD49f in the basal layers of eccrine sweat glands. Expression patterns of CD29 and CD49f in human skin. Boxed areas in the upper panels are shown in the lower panels at higher magnification. Scale bars: 50 μm.

expressed in the basal regions of sweat glands (Figure 6). Furthermore, these markers colocalized with αSMA, but not with K8 (Figure 7), indicating that basal cells that strongly express CD29 and CD49f are myoepithelial cells. The expression profiles of these markers used to distinguish among the human sweat gland compartments are summarized in Table II and schematically illustrated in Figure 8.

Imaging of the three-dimensional structure of eccrine sweat glands

Since conventional immunohistochemistry is not sufficient to determine the precise coiled structures of eccrine sweat glands, the detailed three-dimensional anatomy of their coiled structures was determined by whole-mount immunostaining, a method that has been used to visualize the three-dimensional structures of mammary glands (Rios et al., 2014). Eccrine sweat glands are tiny organs scattered throughout the skin; thus, whole-mount staining requires that these glands be distinguished from surrounding dermal connective tissue. Eccrine sweat gland organs were transiently labeled with neutral red, a dye that distinctively stains sweat glands (Quinton, 1981), clearly distinguishing neutral red-stained coiled organs from dermal connective tissue (Figure 9). To histologically determine whether these neutral red-stained organs were eccrine sweat glands, the stained organs were embedded, sectioned, and immunostained with the sweat gland cell markers, αSMA and K8. The luminal and myoepithelial cell layers of neutral red-stained organs were found to express αSMA and K8, respectively (Figure 10), in agreement with histological observations (Figure 4).

Next, the coiled structures of these neutral red-stained eccrine sweat glands were three-dimensionally visualized by whole-mount staining (Figure 11). A skin fragment containing an entire neutral red-stained organ was immunostained for S100A2 and αSMA, markers for ducts and

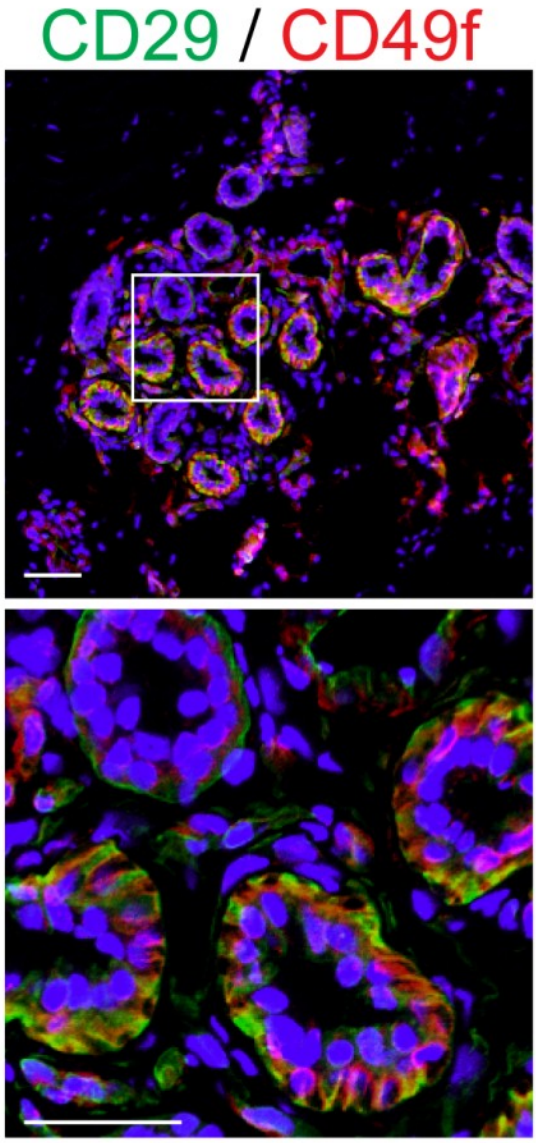

Figure 6. Co-localization of CD29 and CD49f in the basal layers of eccrine sweat glands. Double-immunofluorescence detection of CD29 and CD49f in cross sections of eccrine sweat glands in human skin. Nuclei (blue) were counterstained with Hoechst 33342. Boxed areas in the upper panels are shown in the lower panels at higher magnification. Scale bars: 50 μm.

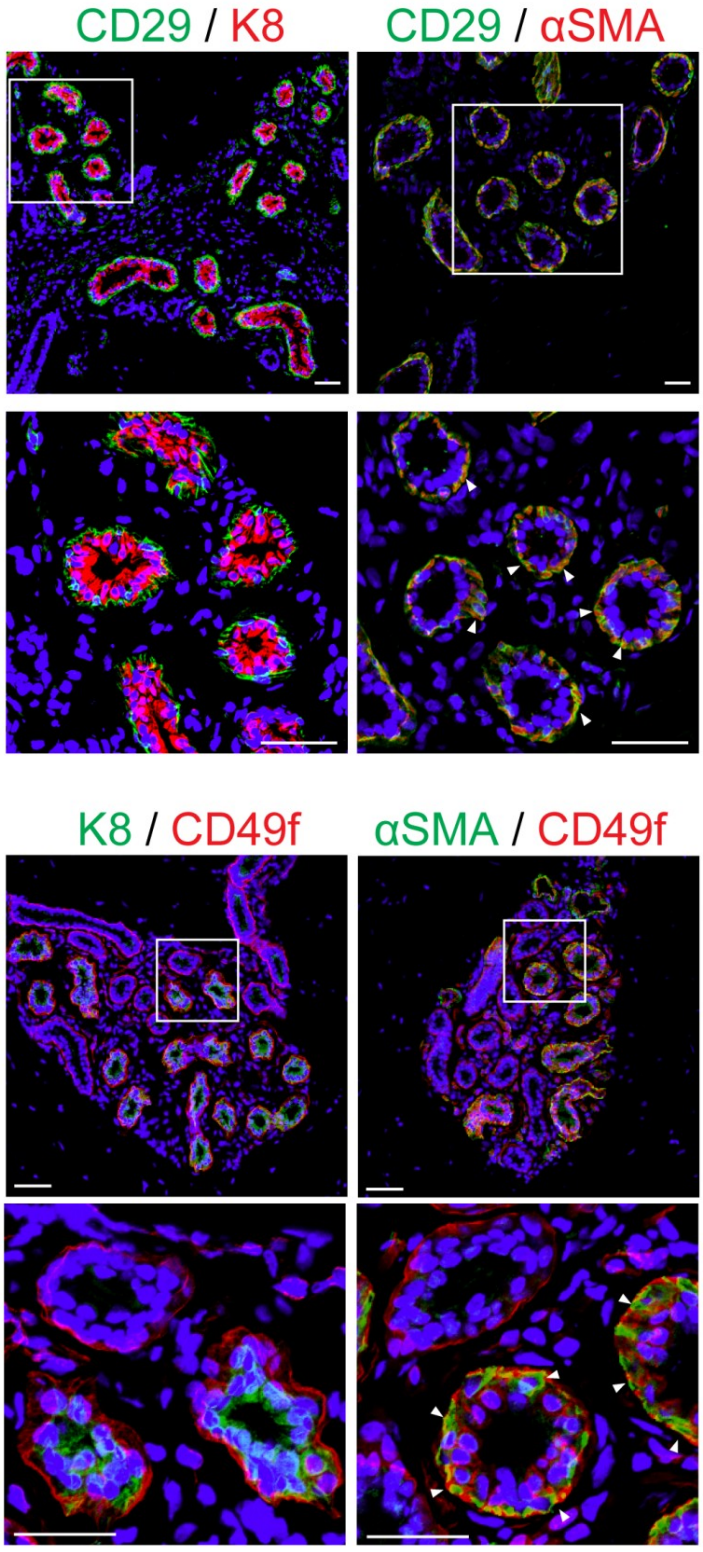

Figure 7. Co-expression of CD29 and CD49f with myoepithelial, but not luminal, cells. Colocalization of epidermal stem cell markers (CD29 and CD49f) and sweat gland cell markers (αSMA and K8) in cross sections of eccrine sweat glands in human skin. Boxed areas in the upper panels are magnified in the lower panels. Arrowheads indicate colocalization of αSMA with CD29 and CD49f. Nuclei (blue) were counterstained with Hoechst 33342. Scale bars: 50 μm.

Table II Expression patterns of cell markers in human eccrine sweat gland compartments.

Minus and plus symbols indicate negative and positive expression, respectively. The number of plus symbols indicates the intensity of expression (++ > +) but is not quantitative.

Marker	Ductal portion		Secretory portion		References
	Luminal cells	Basal cells	Luminal cells	Myoepithelial cells	
S100 calcium binding protein P (S100P)	+	-	-	-	Zhu L et al. (2013)
S100 calcium binding protein A2 (S100A2)	-	+	-	-	
Keratin 8 (K8)	-	-	+	-	Moll I and Moll R (1992) Schon M et al. (1999) Langbein L et al. (2008)
α smooth muscle actin (αSMA)	-	-	-	+	
Integrin β1 (CD29)	-	+	+	++	Lu CP et al. (2012)
Integrin α6 (CD49f)	-	+	+	++	

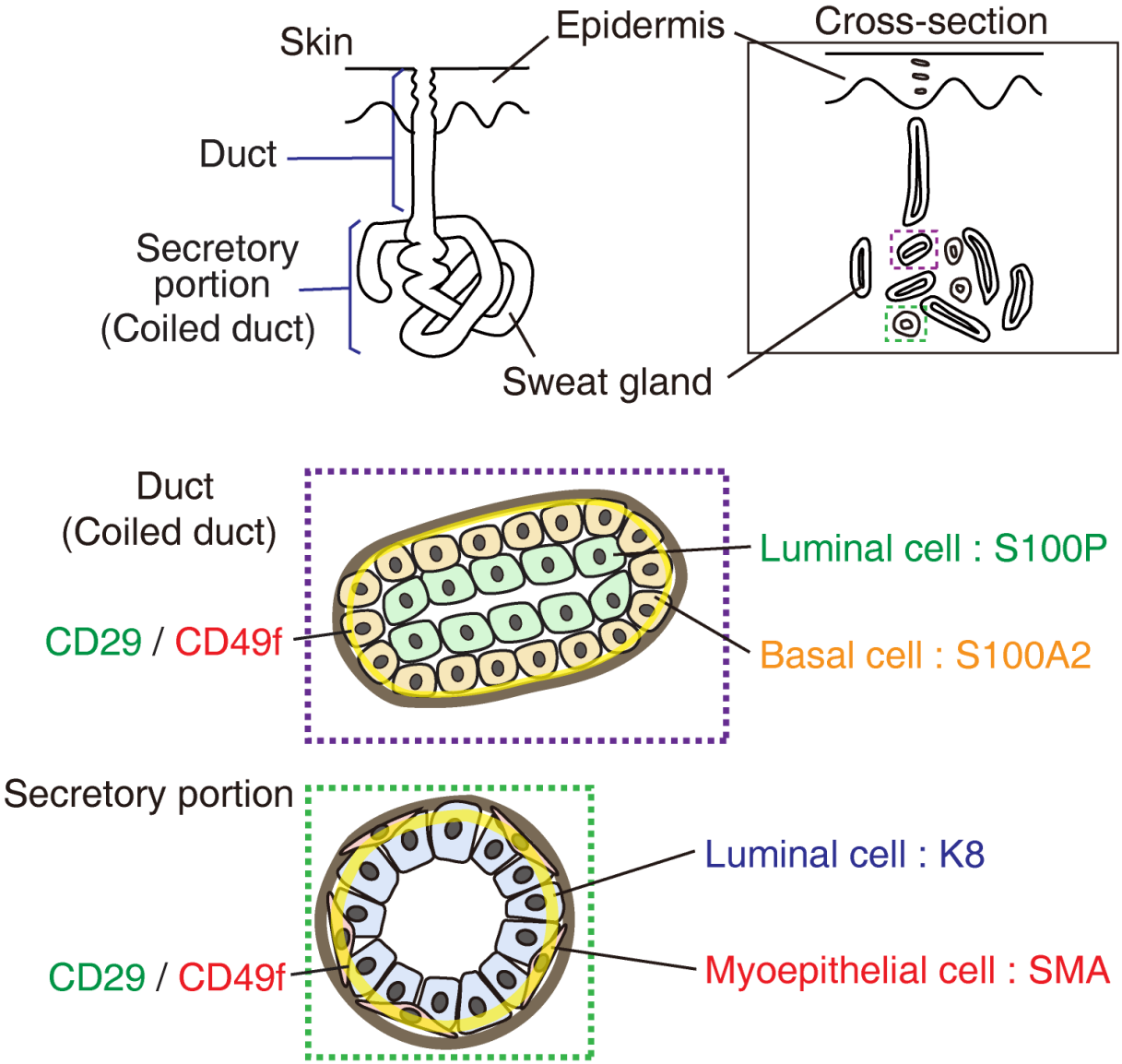

Figure 8. Schematic representation of cell-type specific and cell surface markers in human sweat gland compartments.
(upper) Diagram of a cross section of human skin; (middle) diagram of the arrangement of cells in the duct of a human sweat gland, in which luminal and basal cells express S100P and S100A2, respectively; (lower) diagram of the arrangement of cells in the secretory portion of a human sweat gland, in which luminal and myoepithelial cells express K8 and αSMA, respectively. CD29 and CD49f are expressed in ductal basal, secretory luminal, and myoepithelial cells.

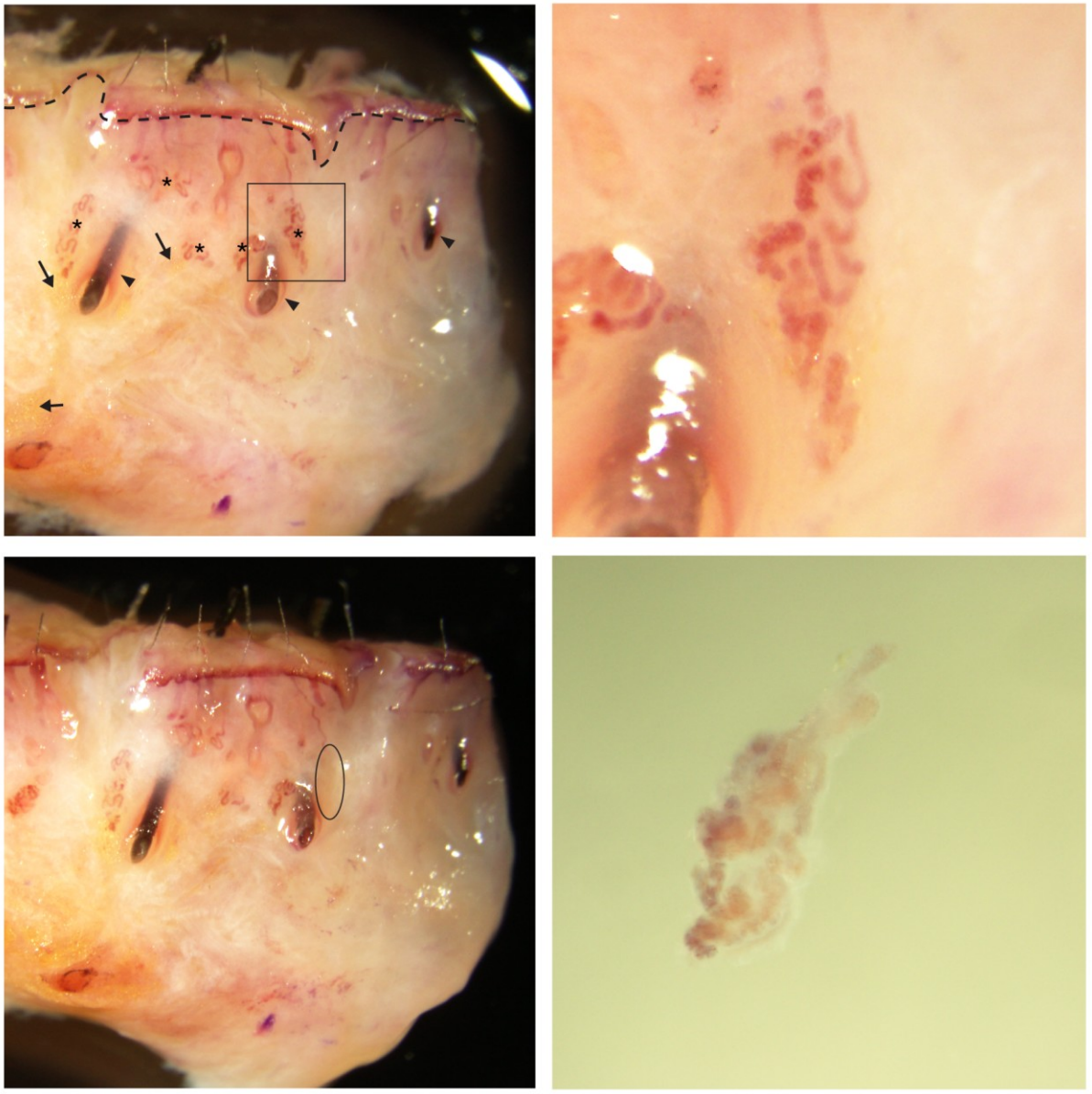

Figure 9. Neutral red positive coiled organs detected in human skin tissue.
The upper left panel shows neutral red-positive coiled structures regarded as eccrine sweat glands in human skin tissue. The boxed area in this panel is shown at higher magnification in the upper right panel. The lower left panel shows the same skin tissue after collection of the neutral red stained organs in the boxed area of the upper left panel. The lower right panel shows the neutral red stained organs in the circled area of the upper left panel. Asterisks, arrowheads, and arrows indicate eccrine sweat glands, hair follicles, and subcutaneous fat, respectively. The dashed line demarcates the border between the epidermis and dermis.

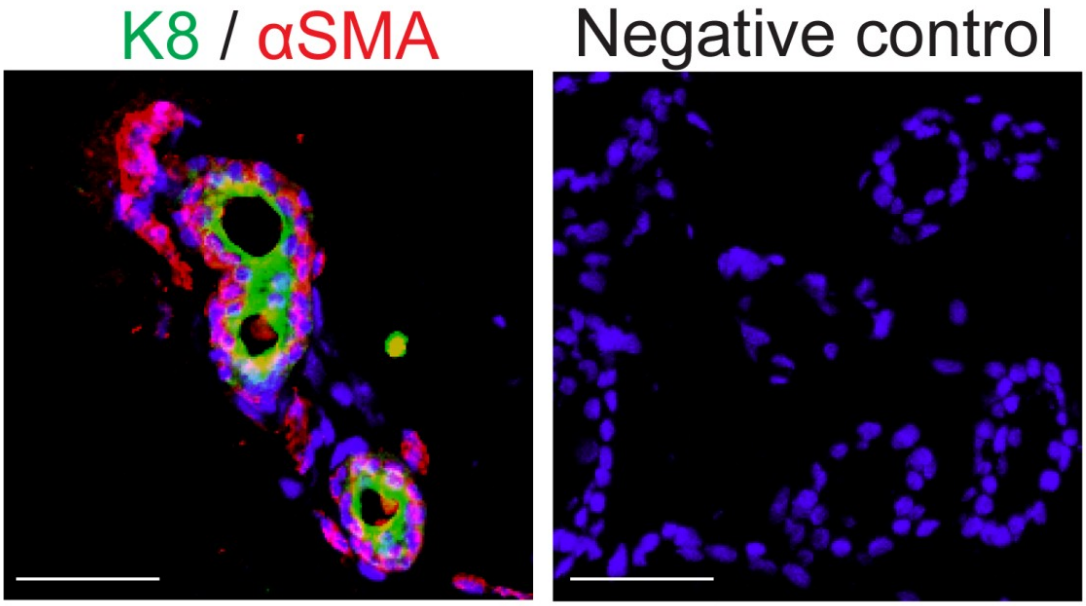

Figure 10. Secretory cell markers detected in cross-sections of coiled eccrine sweat gland fragments.
Double-immunofluorescence detection of K8 and αSMA in cross sections of isolated eccrine sweat glands. The right panel shows a negative control image for dual labeling with Alexa Fluor 488- and 546-conjugated secondary antibodies Nuclei (blue) were counterstained with Hoechst 33342. Scale bars: 50 μm.

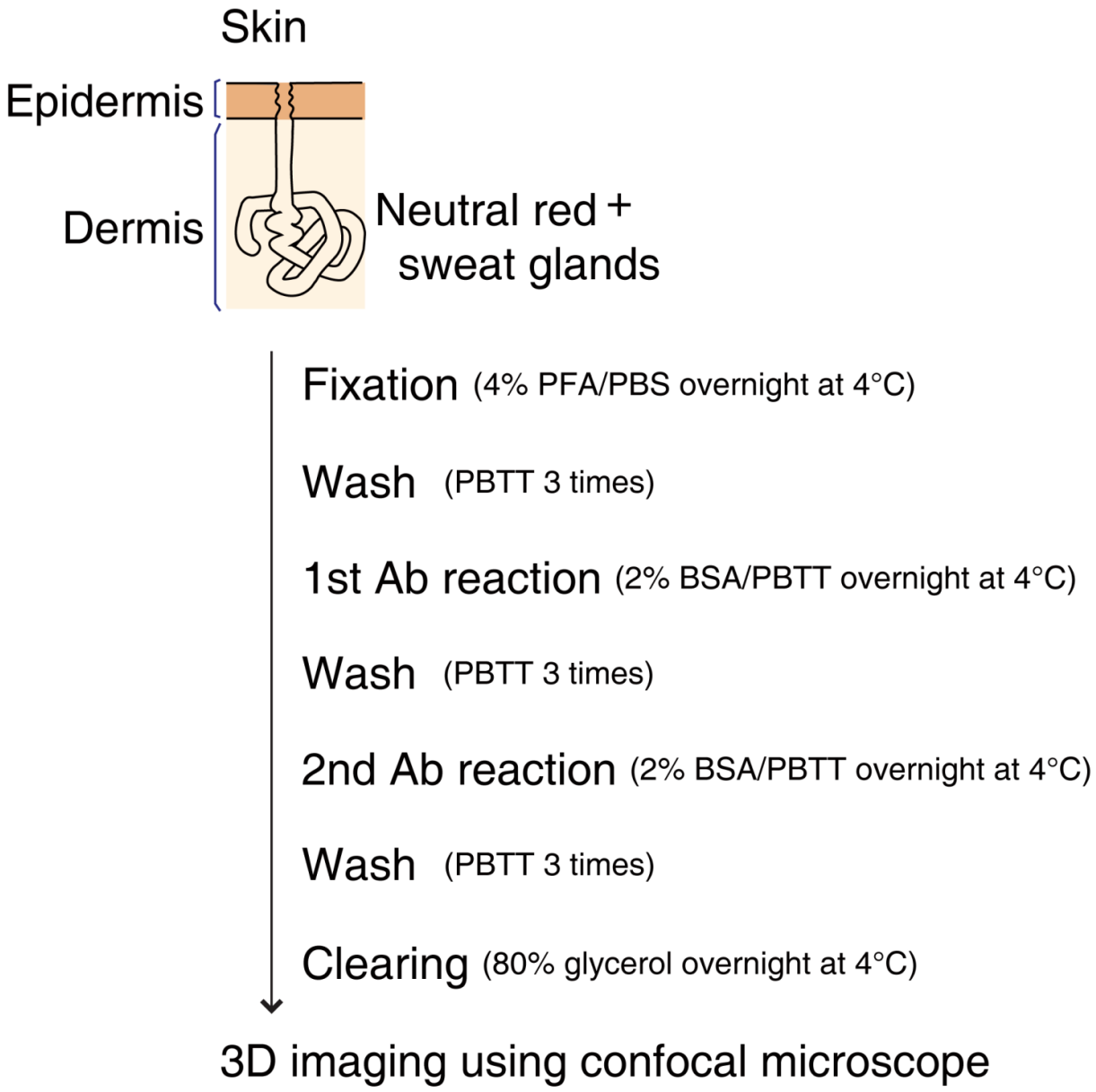

Figure 11. Procedure for whole mount staining of coiled fragments of eccrine sweat glands.

secretory portions, respectively. The spiral, straight, and coiled ducts expressing S100A2 were detected in the epidermis, upper dermis, and deep dermis, respectively (Figure 12). The coiled-like ducts and secretory portions expressing S100A2 and αSMA were partially detected in the deep dermis, respectively, but these coiled structures could be visualized only on surface-exposed regions of skin fragments. Because the coiled regions of eccrine sweat glands are encased in adipose tissue, resulting in a significant loss of fluorescence signals, the coiled fragments of neutral red-stained glands were microsurgically separated using forceps (Figure 9) and the collected coiled fragments assayed for expression of S100A2 and K8, markers for ducts and secretory portions, respectively. Whole-mount analyses of these collected coiled fragments resulted in the successful visualization of the entire coiled structures of eccrine sweat glands, with S100A2- and K8-positive tubules detected in these coiled structures (Figure 13). These findings indicate that the collected organs are coiled regions comprised of ducts and secretory portions, consistent with histological findings.

Whole-mount analyses provided three-dimensional anatomical information about sweat gland coiled structures. The S100A2-positive ductal and K8-positive secretory tubules were distributed throughout the coiled regions and were spatially intertwined. Furthermore, these K8-positive tubules were not only intricately entwined but well entangled. Although histological examination showed that S100A2 and K8 were exclusively detected in sweat glands, whole-mount staining highlighted the regions in which S100A2 co-localized with K8. These S100A2/K8 double positive regions (*asterisks*) may correspond to the junctions between ducts and secretory portions. Thus, whole-mount staining of eccrine sweat glands revealed that their complex coiled structures are three-dimensionally entwined and entangled, a finding not observed by conventional histological analyses.

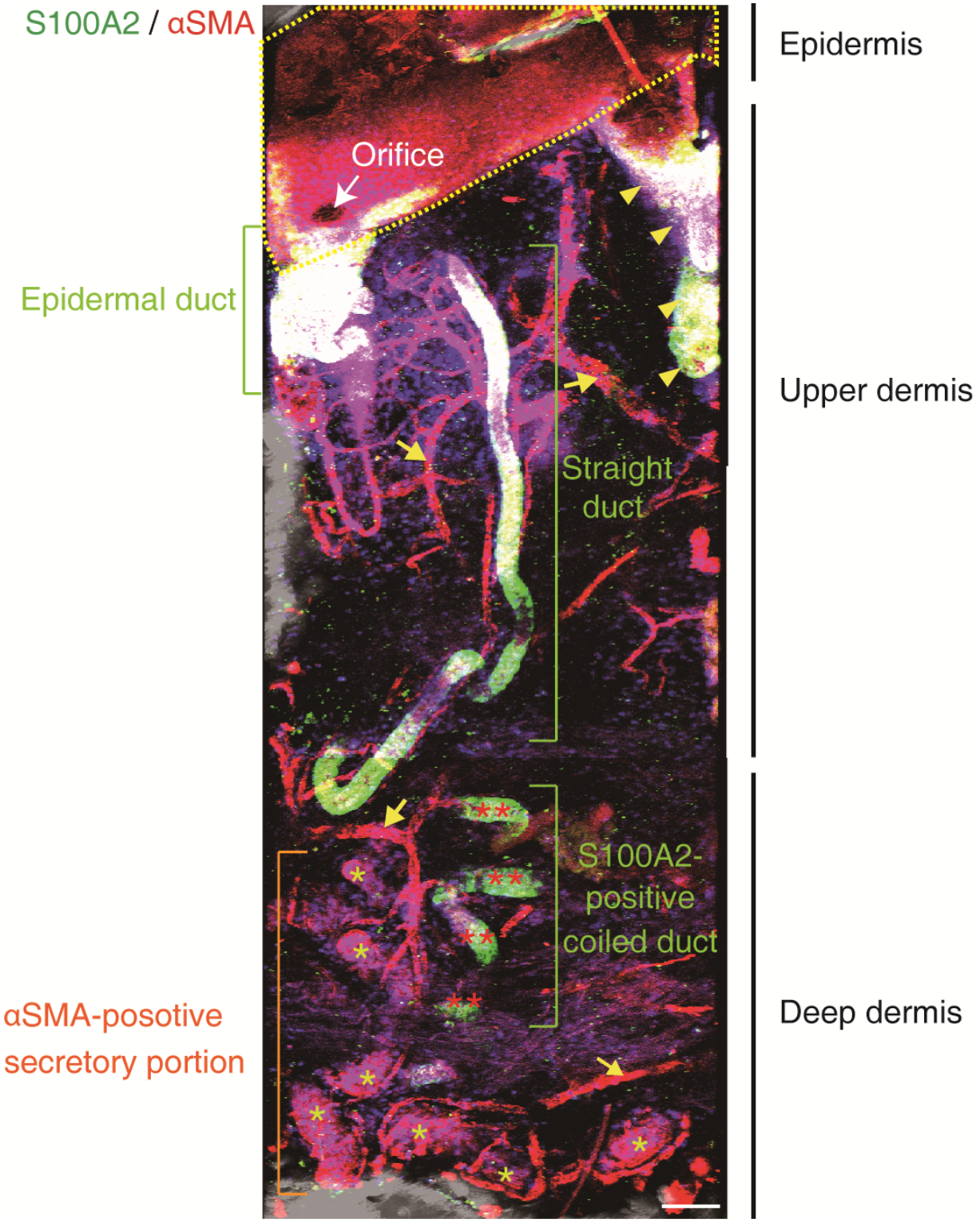

Figure 12. Visualization of an entire eccrine sweat gland embedded in human skin by whole-mount staining.
Double-immunofluorescence detection of αSMA and S100A2 in eccrine sweat glands. Asterisks and double asterisks indicate αSMA-positive secretory portions and S100A2-positive coiled ducts, respectively. Arrowheads and arrows indicate hair follicles and blood vessels, respectively. The dashed line indicates the surface of the skin. Nuclei (blue) were counterstained with Hoechst 33342. Scale bars: 50 μm.

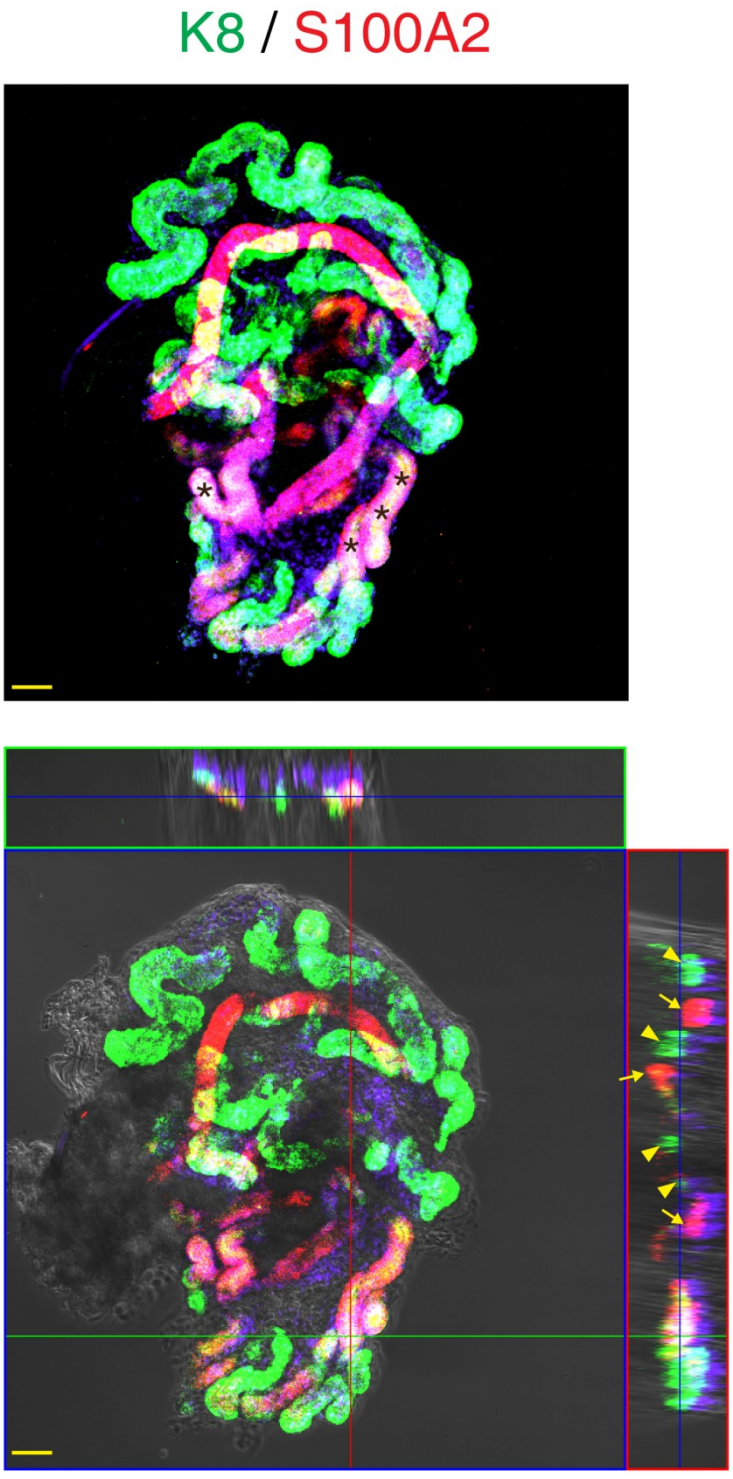

Figure 13. Presence of ductal and secretory portions of coiled fragments dissected from eccrine sweat glands.
Double-immunofluorescence detection of K8 and S100A2 in an isolated eccrine sweat gland. (Upper panel) Projection image of a whole-mount three-dimensional eccrine sweat gland showing K8 and S100A2 expression. Asterisks indicate the areas that form the junctions, in which S100A2 colocalized with K8, between ducts and secretory portions. (Lower panel) Optical section of the whole-mount image. Arrows indicate the S100A2 positive ductal portion, and arrowheads indicate the K8 positive secretory portion. Nuclei (blue) were counterstained with Hoechst 33342. Scale bars: 50 μm.

Three-dimensional imaging of an eccrine sweat gland at single-cell resolution

Whole-mount staining showed that the coiled regions of sweat glands are three-dimensionally complex structures, which are not only folded but well entangled. Since the three-dimensional structures of organs are largely due to cell shapes and arrangements (Eiraku et al., 2011), the shapes and arrangements of sweat gland coiled structures were visualized at single-cell resolution using the cell surface markers CD29 and CD49f. Whole-mount staining showed that CD29 and CD49f co-localized in the basal layers of sweat glands (Figure 14). The expression patterns of these markers distinguished between two types of coiled structures, one composed of cuboidal-shaped cells (*arrowheads*) and the other of elongated-shaped basal cells (*arrows*). To assess the arrangements of cells constituting these structures in greater detail, their F-actin-based cytoskeletal structures were visualized at single-cell resolution by staining with fluorescent phalloidin. These coiled structures were found to be composed of two portions (Figure 15), one consisting of cuboidal shaped cells (*arrowheads*), in which actin filaments accumulated at the apical regions, and the other of highly elongated cells strongly positive for the F-actin-phalloidin complex (*arrows*). Intriguingly, the elongated cells of eccrine sweat glands were found to be longitudinally and uniformly arranged on the secretory portion (Figure 16). Furthermore, anatomical orientation of elongated cells was in agreement with the entangled direction of the secretory portion, suggesting that myoepithelial cells are aligned uniformly along the tubules to induce contractions of the secretory portion, resulting in sweat secretion. In addition, histological analysis showed that these F-actin-phalloidin complexes co-localized with CD49f (Figure 17), suggesting that the elongated cells are myoepithelial cells highly expressing CD29 and CD49f.

Next, this study assessed whether the highly elongated cells are myoepithelial cells and surround

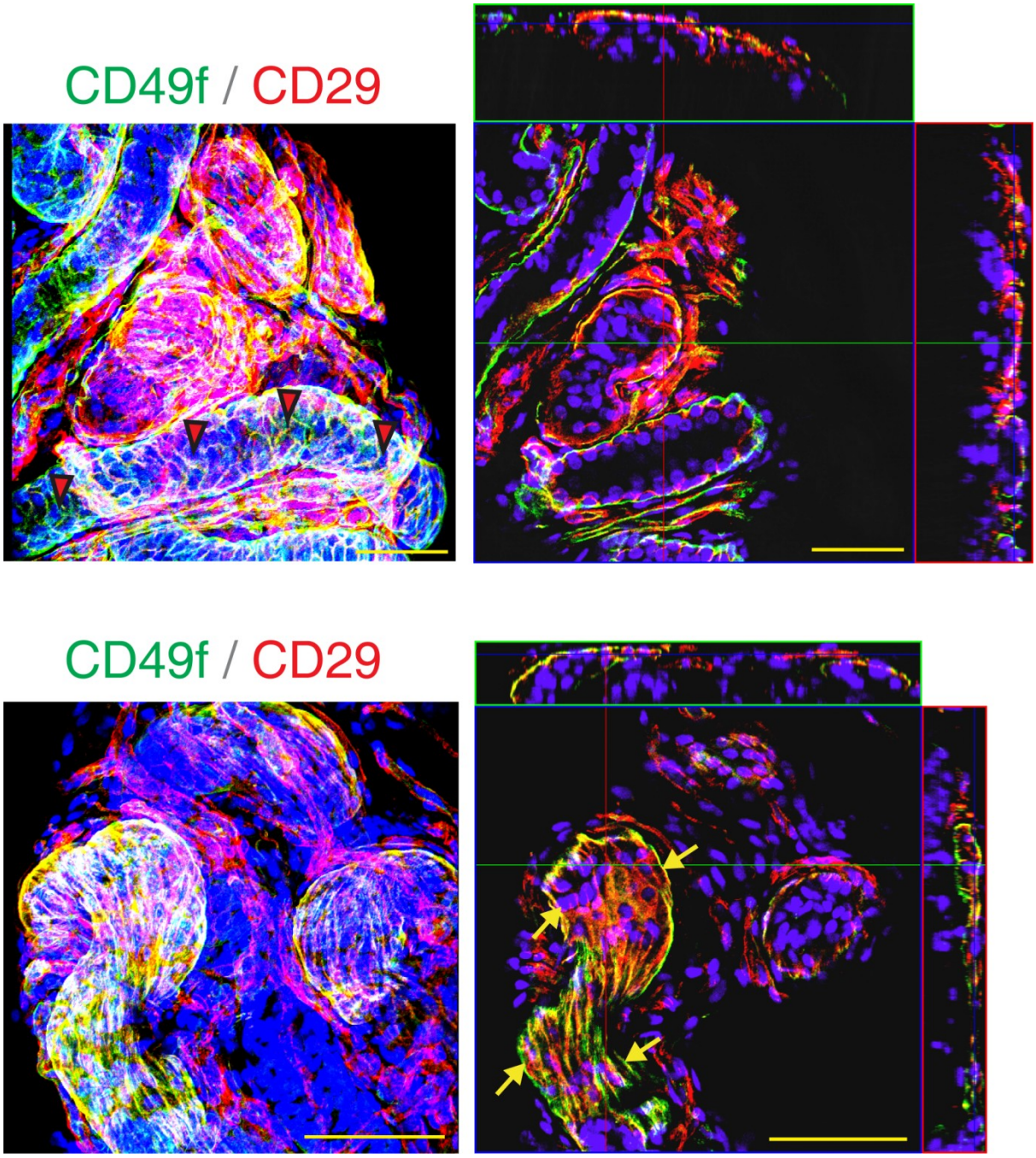

Figure 14. Double-immunofluorescence detection of CD49f and CD29 in eccrine sweat glands.
The upper and lower panels show two characteristic portions expressing CD49f and CD29. Left panels show whole-mount 3D confocal images of CD49f and CD29 expression. Right panels show optical sections of the whole-mounted human eccrine sweat glands in the left panels. Arrowheads in the upper left panel indicate the portion comprised of cuboidal-shaped basal cells. Arrows in the lower right panel indicate the portion comprised of elongated cells. Nuclei (blue) were counterstained with Hoechst 33342. Scale bars: 50 μm.

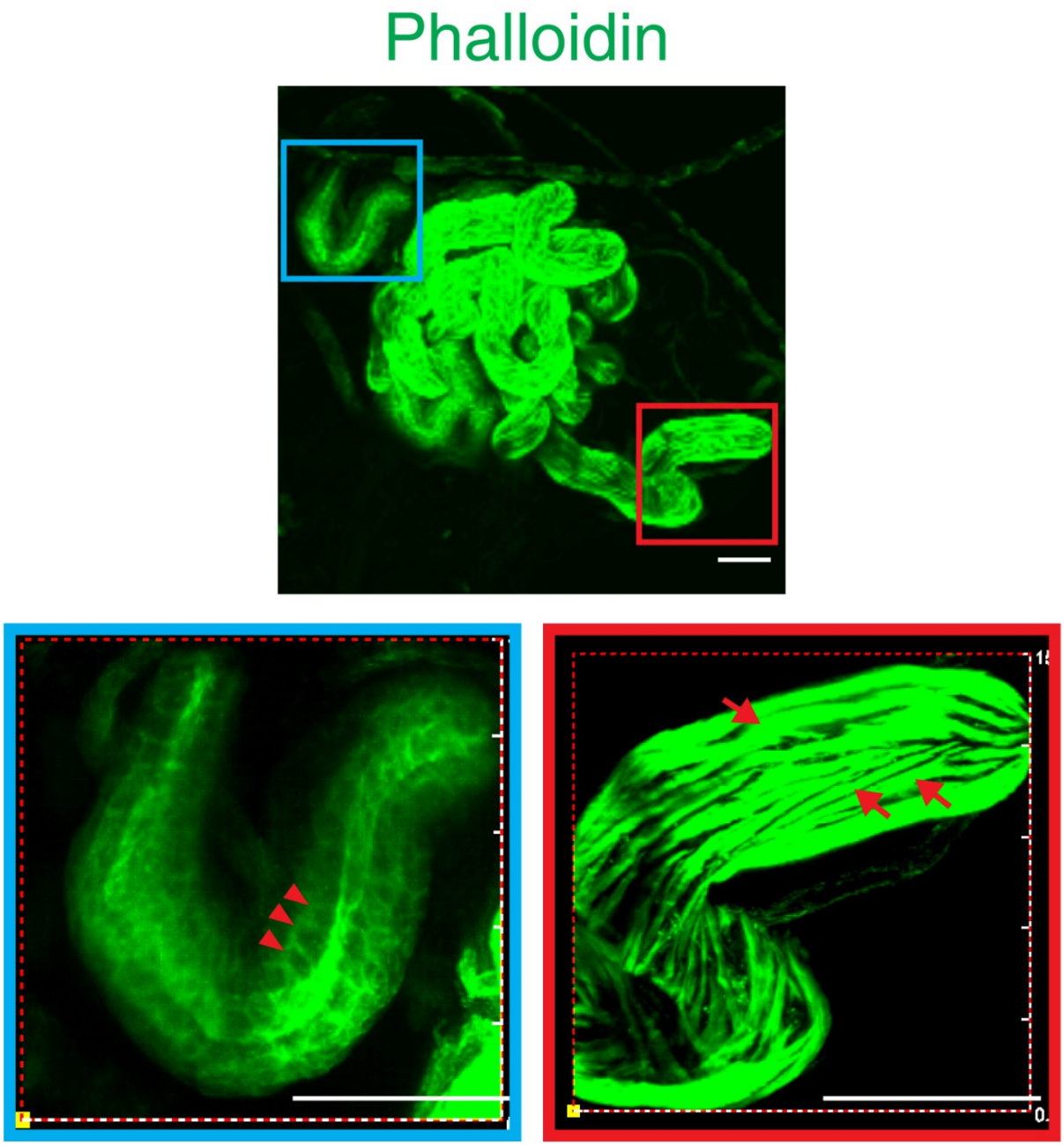

Figure 15. Highly elongated and cuboidal cells form putative ducts and secretory portions, respectively, of eccrine sweat glands.
Patterns of expression of F-actin-phalloidin complex were used to distinguish the ducts and secretory portions of eccrine sweat glands, with the former consisting of cuboidal cells (lower left panel) and the latter of highly elongated cells (lower right panel). Arrowheads and arrows indicate cuboidal and highly elongated cells, respectively. Blue and red boxed areas in the upper panel are shown in the lower panels at higher magnification. Scale bars: 50 μm.

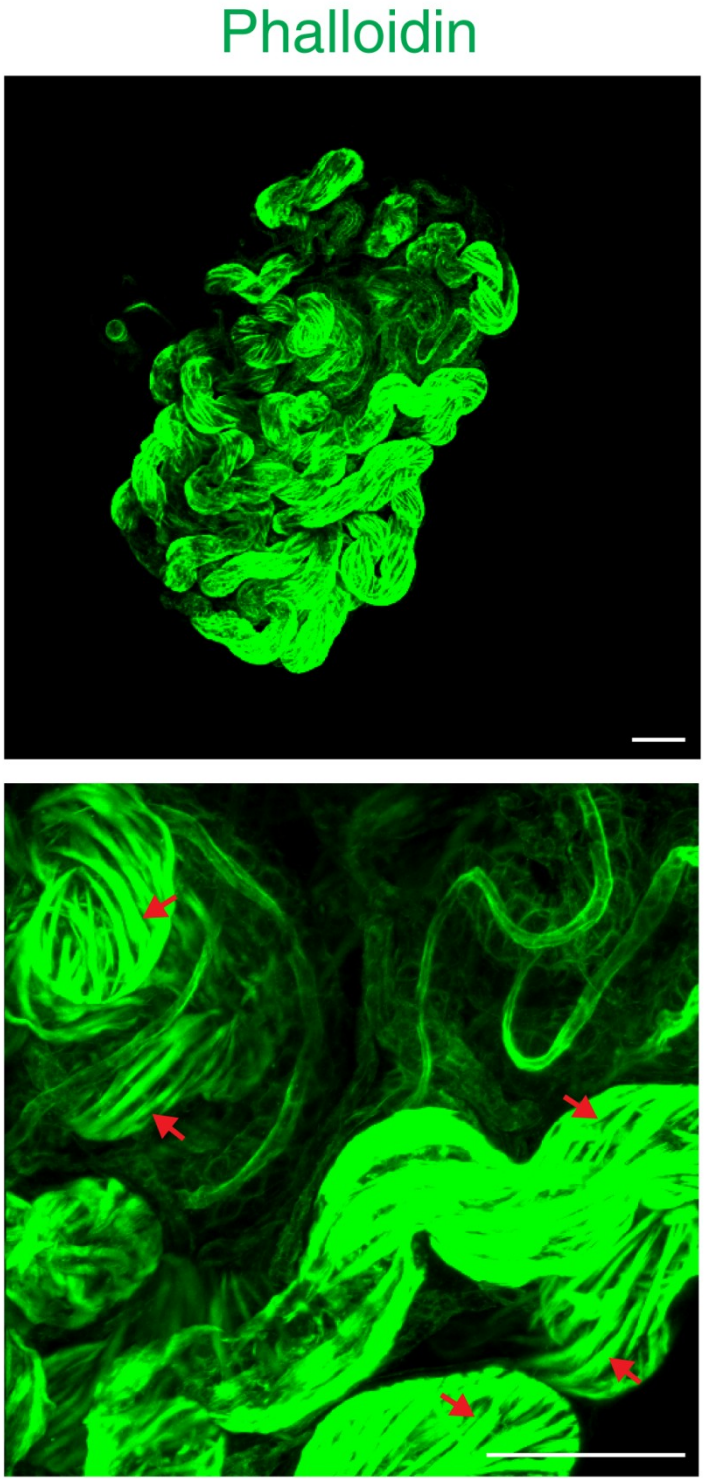

Figure 16. Patterns of F-actin distribution in the two portions of an eccrine sweat gland. Spatial cytoskeletal organization of a human eccrine sweat gland following staining with fluorescent dye-conjugated phalloidin. The lower panel shows a high-magnification view of the micrograph in the upper panel. Arrows indicate the elongated cells that were longitudinally and uniformly arranged on the secretory portion. Scale bars: 50 μm.

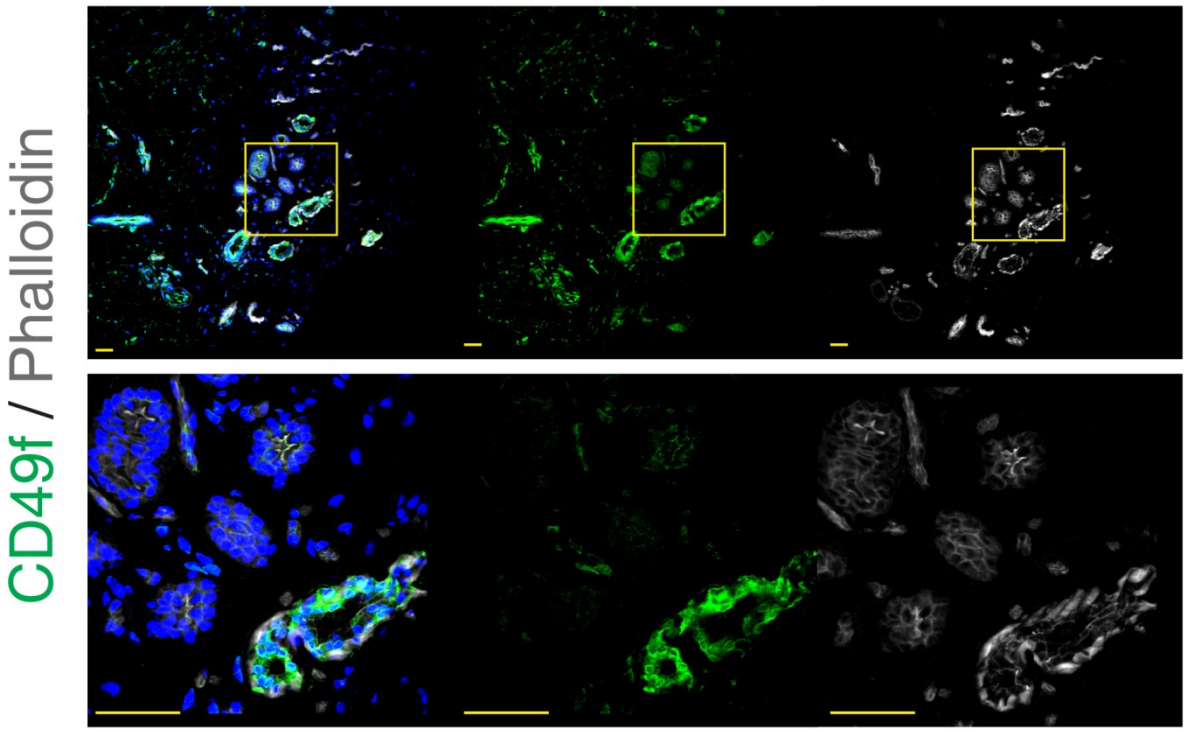

Figure 17. Elongated cells strongly positive for phalloidin are myoepithelial cells expressing CD49f.
Colocalization of F-actin-phalloidin complex with CD49f in cross sections of eccrine sweat glands in human skin. Boxed areas in the upper panels are shown in the lower panels at higher magnification. Nuclei (blue) were counterstained with Hoechst 33342. Scale bars: 50 µm.

the secretory portions, but not the ducts, of the sweat glands. Sweat gland compartments were visualized by both cross-sectional and three-dimensional analyses with phalloidin and the markers K8, αSMA, S100P, and S100A2. Immunohistochemical examination showed that the flattened basal cells strongly positive for phalloidin also expressed αSMA, whereas K8-positive protean-shaped cells were slightly positive for phalloidin (Figure 18). F-actin filaments accumulating at the apical sides were detected in cells expressing S100P, but not S100A2, indicating that the apical sides of ducts, but not secretory portions, are enriched with F-actin filaments (Figure 19). Thus, cross-sectional assays indicated that phalloidin-positive elongated cells are αSMA-positive myoepithelial cells, but not secretory luminal cells, of sweat gland secretory portions. To corroborate this conclusion, three-dimensional anatomical information about myoepithelial cells was obtained at single-cell resolution. αSMA was expressed in the highly elongated cells of entangled secretory portions and co-localized with F-actin-phalloidin complex (Figure 20). In contrast, ducts showing accumulation of F-actin at the apical sides expressed little αSMA, confirming that the elongated cells are myoepithelial cells. Taken together, these whole-mount analyses at single-cell resolution revealed the three-dimensional cell shapes and arrangements of sweat gland coiled structures. These findings indicate that the entangled characteristic structures of secretory portions are due to the three-dimensional arrangements of elongated myoepithelial cells on the secretory portions.

Distributions of sweat gland blood vessels and nerve fibers

Three-dimensional staining successfully visualized not only the detailed coiled structures of eccrine sweat glands but the spatial distributions of blood vessels and nerve fibers that surround these glands and are essential for sweat secretion. Blood vessels support the reabsorption of sweat, whereas nerve

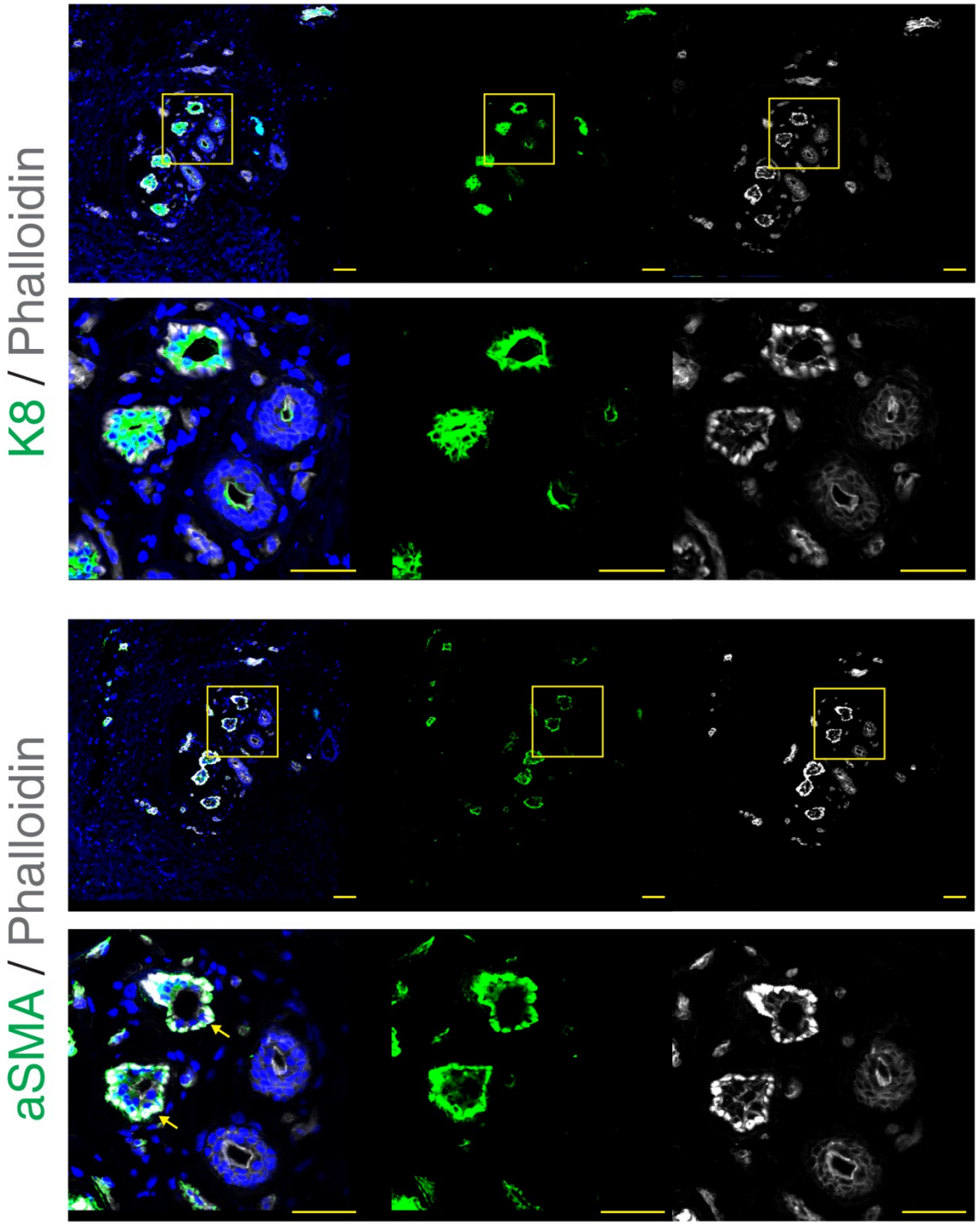

Figure 18. Phalloidin-positive cells express αSMA, but not K8.
Colocalization of phalloidin and sweat gland cell markers (αSMA and K8) in cross sections of eccrine sweat glands in human skin. Arrows indicate colocalization of F-actin and αSMA. Boxed areas in the upper panels are shown at higher magnification in the lower panels. Nuclei (blue) were counterstained with Hoechst 33342. Scale bars: 50 μm.

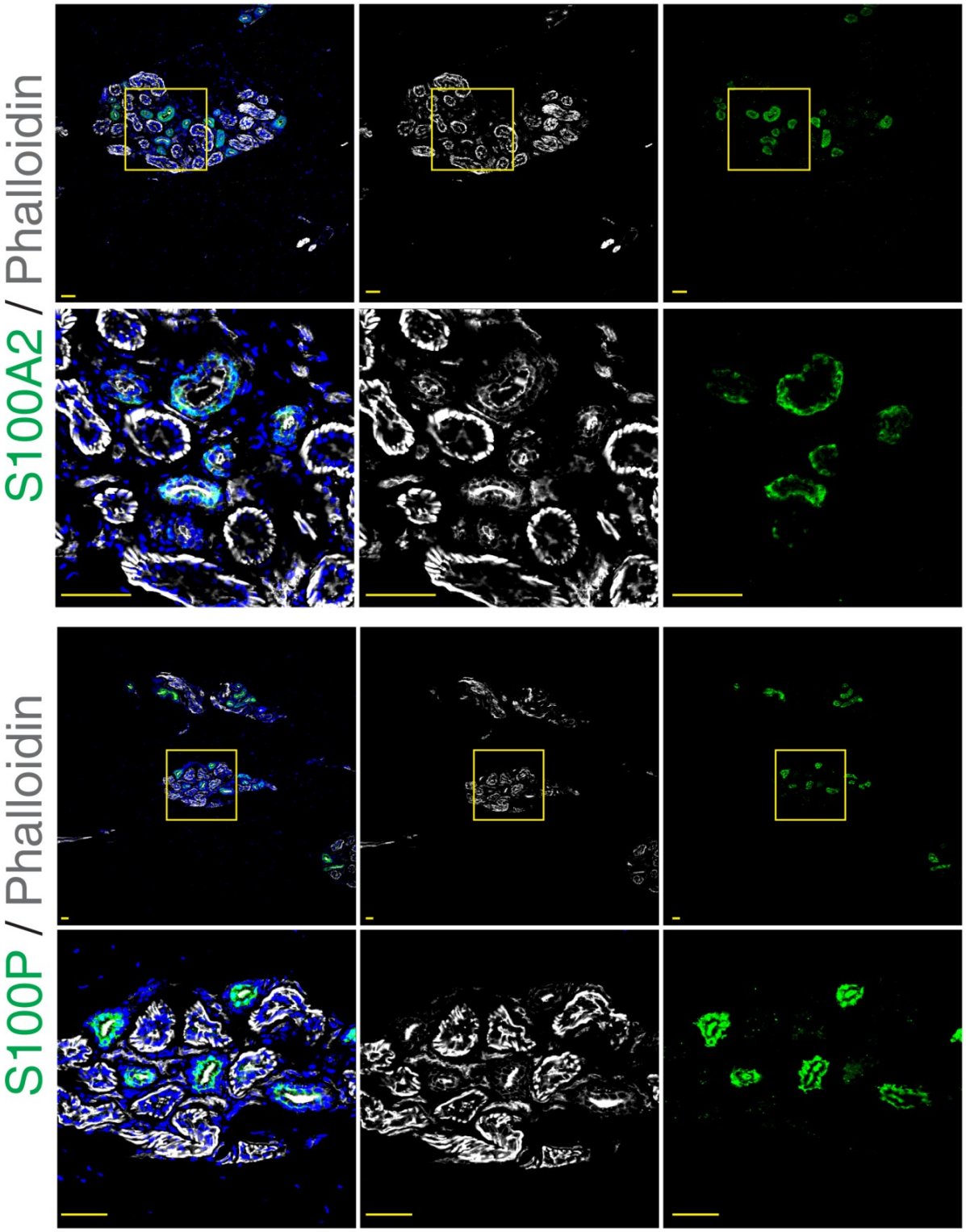

Figure 19. Accumulation of F-actin filaments at the apical sides expressing S100P. Colocalization of phalloidin and sweat gland cell markers (S100A2 and S100P) in cross sections of eccrine sweat glands in human skin. Boxed areas in the upper panels are shown in the lower panels at higher magnification. Nuclei (blue) were counterstained with Hoechst 33342. Scale bars: 50 μm.

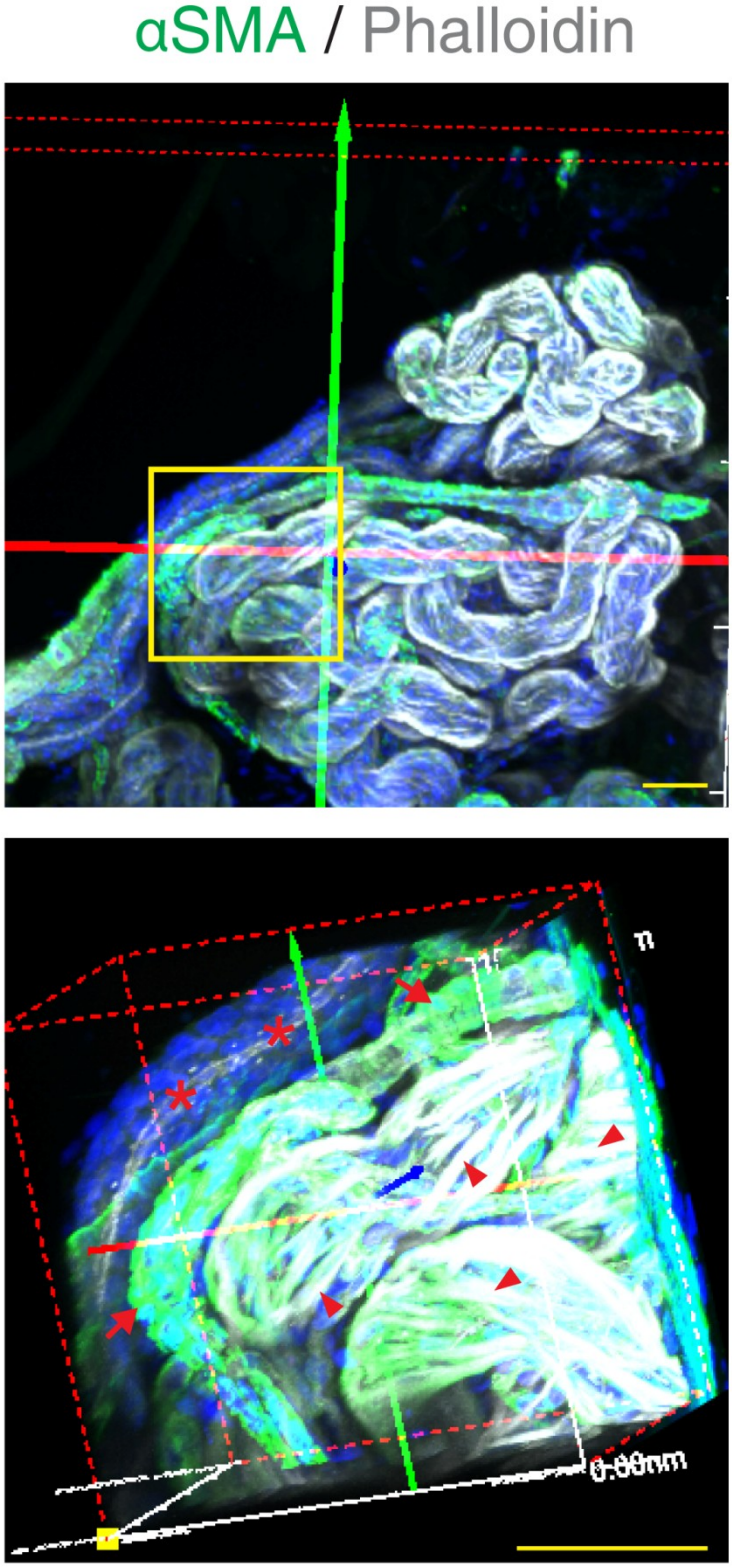

Figure 20. Phalloidin-positive elongated cells express αSMA.
Double-immunofluorescence detection of αSMA and phalloidin in sweat glands. The lower panel shows a high-magnification view of the upper panel. Arrowheads indicate the phalloidin-positive elongated myoepithelial cells expressing αSMA. Arrows indicate the αSMA-positive blood vessels. Asterisks indicate ducts in which the F-actin-phalloidin complex accumulated at the apical side. Nuclei (blue) were counterstained with Hoechst 33342. Scale bars: 50 μm.

fibers are involved in sympathetic innervation. Understanding the detailed structural anatomy of these blood vessels and nerve fibers may clarify the mechanisms that govern sweat gland activity.

The three-dimensional arrangements of blood vessels and nerve fibers surrounding sweat gland coiled structures were analyzed by whole-mount immunostaining with specific markers for blood vessels and nerve fibers. Immunostaining with CD31, a blood vessel marker, revealed that blood vessels ran longitudinally in parallel with sweat gland tubules (Figure 21) and that these blood vessels were three-dimensionally intertwined with sweat gland tubules in the coiled region. Blood vessels in proximity to the ducts are thought to facilitate the reabsorption of sweat components (Kuno, 1956). Whole-mount staining showed that these blood vessels were present not only in the ducts but in the secretory portions of sweat glands, suggesting that blood vessels along sweat gland tubules facilitate the secretion and reabsorption of sweat.

Nerve fibers surrounding eccrine sweat glands were visualized by staining with the neuronal marker PGP9.5. These PGP9.5-positive nerve fibers were found to wrap around the tubules of the sweat glands (Figure 22). Double immunofluorescence staining for PGP9.5 and αSMA showed that these nerve fibers predominantly surrounded the secretory portions of eccrine sweat glands (Figure 23). These nerve fibers covered the flattened myoepithelial cell layers surrounding the secretory portions, suggesting that the latter respond to sympathetic stimuli from nerve fibers.

Thus, blood vessels and nerve fibers are three-dimensionally arranged to facilitate effective sweat secretion. Taken together, whole-mount analyses of eccrine sweat glands provided detailed anatomical information of their coiled structures and the relationships of these structures with blood vessels and nerve fibers.

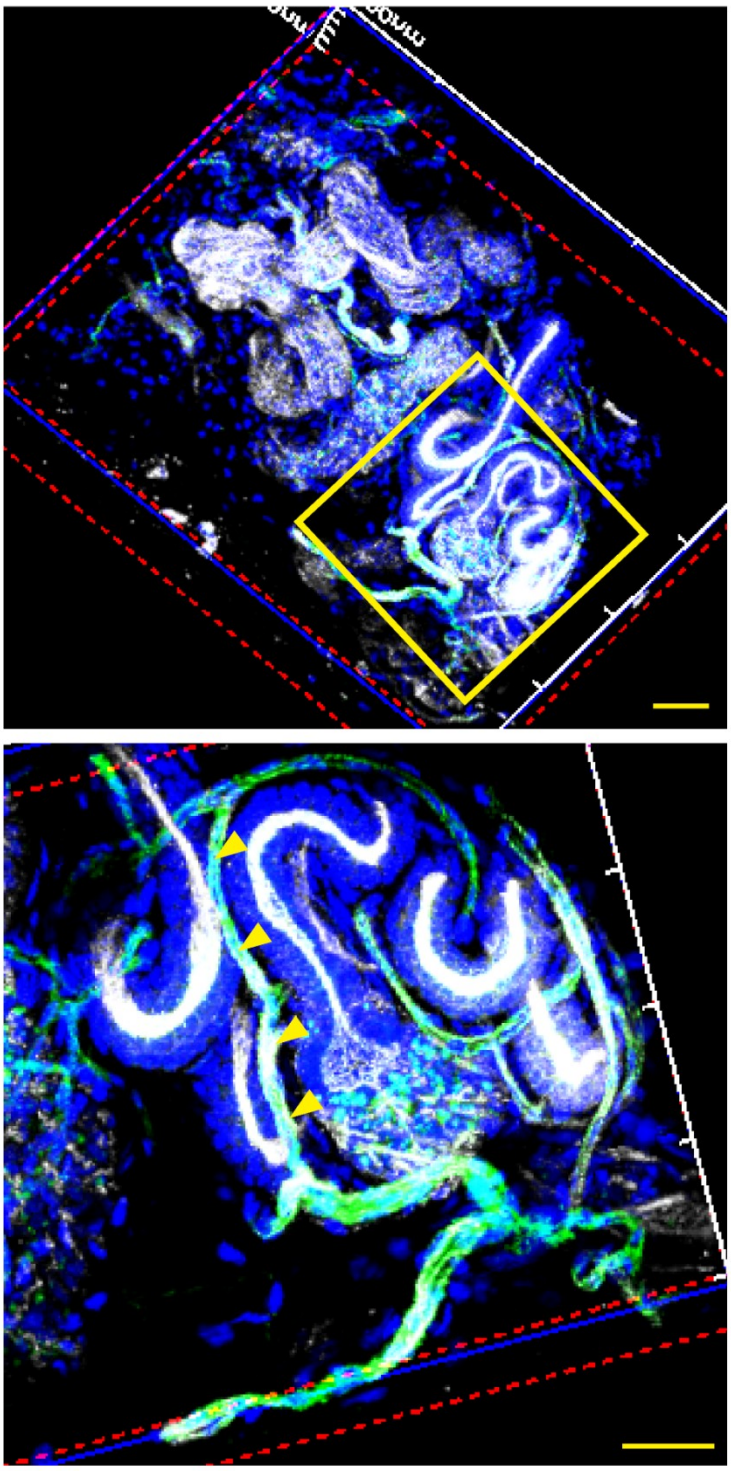

Figure 21. Blood vessels closely run beside the tubular structure of eccrine sweat glands.
Double-immunofluorescence detection of CD31 and phalloidin in sweat glands. The boxed area in the upper panel is shown at higher magnification in the lower panel. Arrowheads indicate blood vessels extending beside the right side tubular structure. Nuclei (blue) were counterstained with Hoechst 33342. Scale bars: 50 μm.

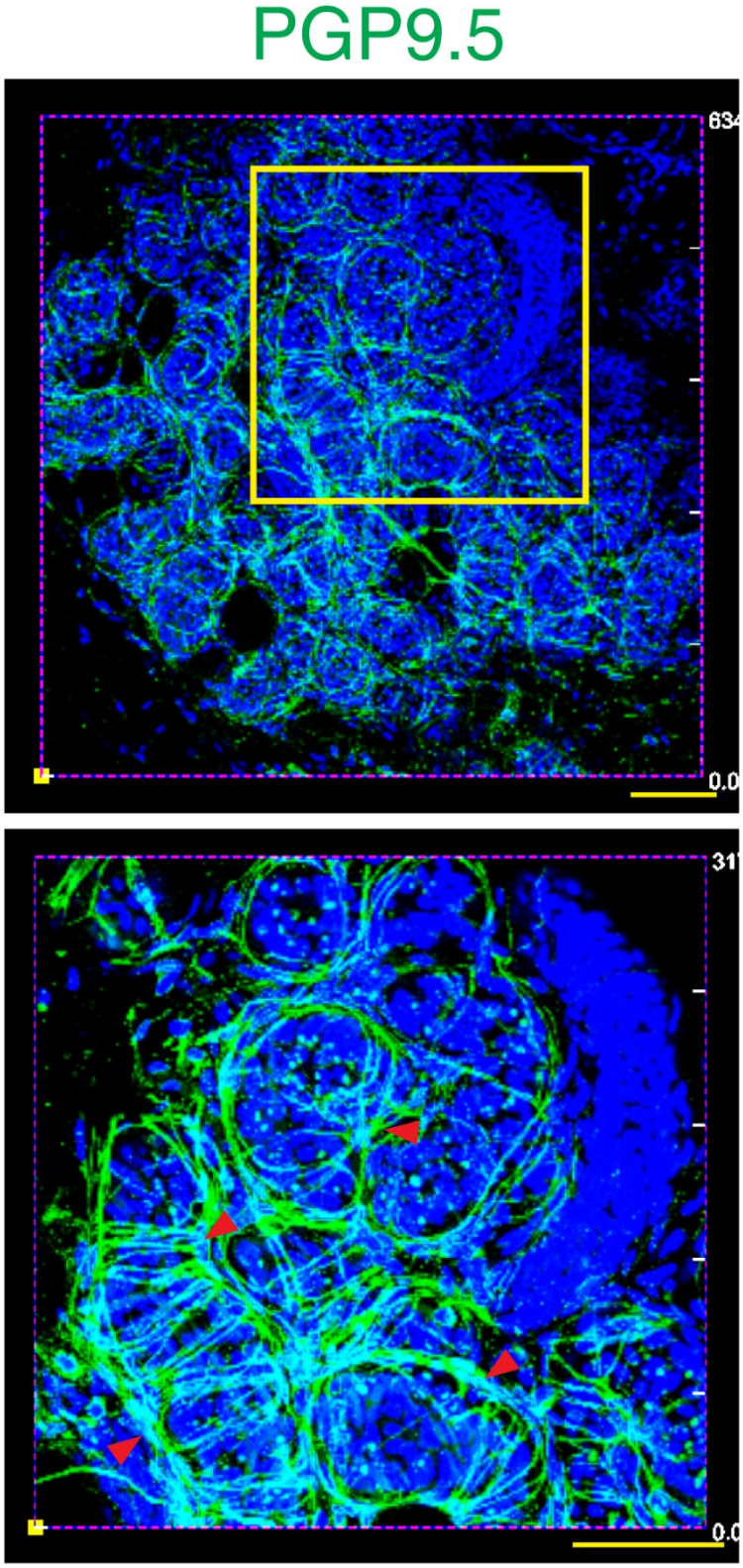

Figure 22. Nerve fibers enwrap the eccrine sweat glands.
Immunofluorescence detection of PGP9.5 in eccrine sweat glands. The boxed area in the upper panel is shown at higher magnification in the lower panel. Arrowheads indicate nerve fibers wrapping the tubules of eccrine sweat glands. Nuclei (blue) were counterstained with Hoechst 33342. Scale bars: 50 μm.

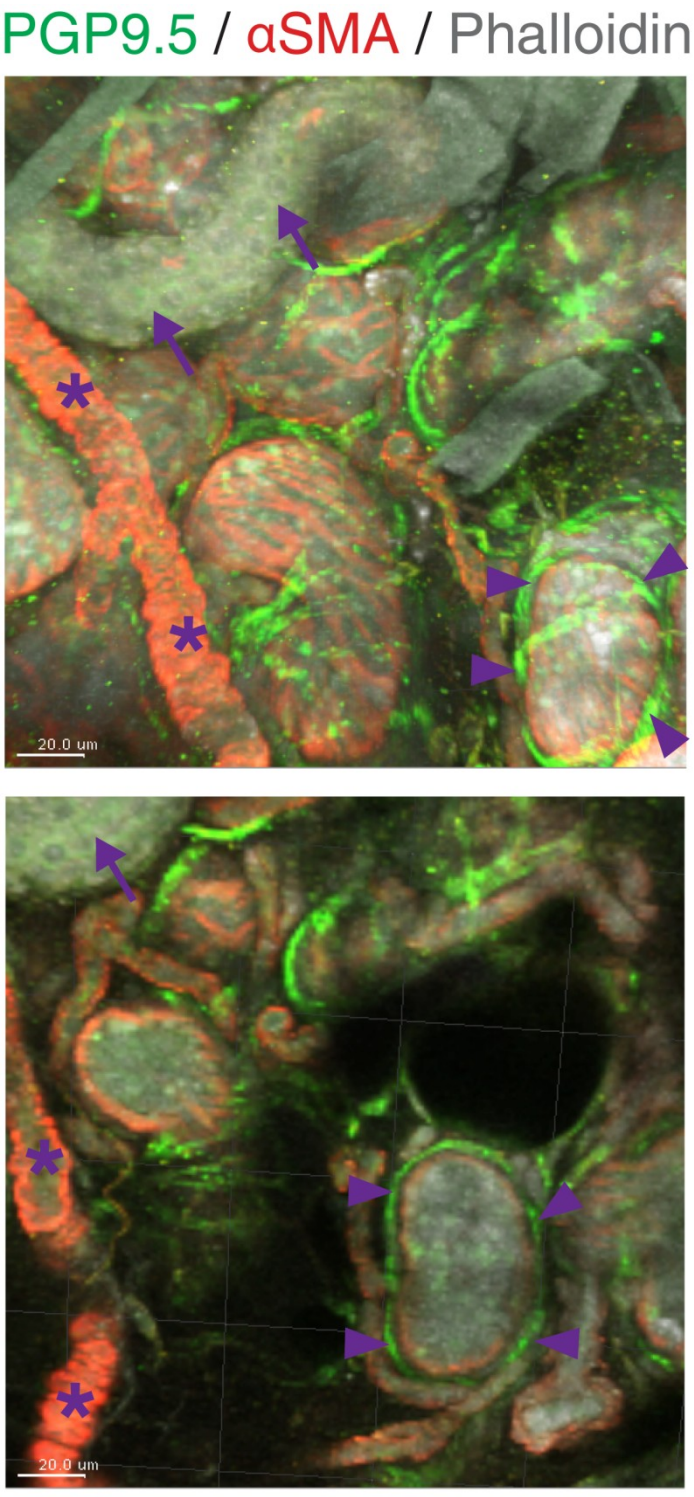

Figure 23. Nerve fibers enwrap the secretory portions, but not the ducts, of eccrine sweat glands.
Immunofluorescence detection of PGP9.5, αSMA, and phalloidin in sweat glands. Upper panels show whole-mount 3D confocal images. Lower panels show optical sections of whole-mounted human eccrine sweat gland in upper panels. The right panels show high-magnification views of the boxed areas in the left panels. Arrowheads indicate nerve fibers that enwrap the αSMA-positive secretory portion. Arrows indicate the αSMA-negative ductal tubules. Asterisks indicate blood vessels. Scale bars: 20 μm.

I-5 Discussion

Although the complex coiled structures of eccrine sweat glands have been investigated by three-dimensional reconstruction of serial histological sections, this anatomical information was limited owing to processing losses between sections. Therefore, determination of the detailed coiled structures requires seamless three-dimensional visualization. This study utilized a whole-mount staining method to determine the detailed three-dimensional anatomy of sweat gland coiled structures, similar to the approach used for seamless visualization of the three-dimensional structures of mammary glands (Rios et al., 2014). Whole-mount staining of eccrine sweat glands allowed visualization of bona fide three-dimensional coiled structures that were compactly formed and frequently folded. Furthermore, the method revealed differences in the three-dimensional structures of the ducts and secretory portions of these glands. The ducts were sometimes hooked and simply folded, while the secretory portions were not only frequently bent but irregularly entangled. Although the secretory portions of mammary and salivary glands were previously found to be round cyst-like structures, no glands have been shown to have secretory portions with such entangled structures (Rios et al., 2014). These structural differences among exocrine gland secretory portions suggest that the tubular secretory portions of sweat glands possess three-dimensionally entangled structural features for effective sweat secretion. In addition, whole-mount staining revealed the three-dimensional locations of junctions between the ducts and secretory portions of eccrine sweat glands. Although these ducts and secretory portions were distributed throughout the surface of the coiled structures, their junctions were located inside the coiled structures, suggesting that eccrine sweat glands possess three-dimensional anatomical rules for the formation of complex coiled

structures. Thus, whole-mount staining not only resulted in visualization of the three-dimensional coiled structures but provided the three-dimensional anatomical features of these coiled structures, which had not been determined by conventional histological methods.

Whole-mount staining for cytoskeletal and cell surface markers succeeded in visualizing the three-dimensional cell shapes and arrangements of each sweat gland compartment. Ductal luminal cells cuboidal in shape were regularly aligned in the luminal layers and F-actin filaments accumulated in the apical regions of ductal luminal cells, indicating that tight junctions were formed between the apical sides of ductal luminal cells. Secretory luminal cells were configured in three-dimensional irregular shapes with little accumulation of F-actin filaments, suggesting that the cell–cell junctions between secretory luminal cells were open, because luminal cells secrete sweat into the lumen through luminal intercellular canaliculi (Munger, 1961). Ductal basal cells cuboidal in shape were regularly arranged in the ductal basal layers, differing from those in mammary glands, which are spindle-shaped myoepithelial cells longitudinally surrounding the mammary gland ducts (Rios et al., 2014). The differences in cell shapes and arrangement of ductal basal cells in sweat and mammary glands suggest that sweat gland ducts may do not possess contractile ability to expel fluid. Secretory basal cells, i.e., myoepithelial cells, highly elongated in shape were arranged longitudinally parallel to the entangled secretory tubules. These results indicate that the entangled tubular structures may be due to the shapes and arrangements of elongated myoepithelial cells on the secretory portions. The shapes and arrangements of sweat gland myoepithelial cells are distinct from those of mammary and salivary myoepithelial cells, which are stellate-shaped and scattered throughout the acinar secretory portions (Rois et al, 2014), suggesting that myoepithelial cells exhibit gland-specific shapes and arrangements to effectively induce the contraction of individual

three-dimensional structures of exocrine gland secretory portions. Thus, whole-mount analyses of eccrine sweat glands can determine the three-dimensional cell shapes and arrangements of their compartments, and provide insights into the three-dimensional mechanical behaviors of the coiled structures in sweat secretion.

Whole-mount analyses not only showed the three-dimensional arrangements of the coiled structures of eccrine sweat glands but also the blood vessels and nerve fibers that facilitate sweat gland activity. Although blood vessels and nerve fibers are abundant in sweat glands, their three-dimensional arrangements have been difficult to determine by conventional histological methods. The whole-mount analyses presented here revealed that the blood vessels ran longitudinally parallel to the tubular structures of the sweat glands. Intriguingly, these blood vessels were consistently close to, but separate from, the sweat gland tubules, comprising a parallel arrangement similar to that of peritubular capillaries and proximal renal tubules in the kidney (Mimura and Nangaku, 2010). In the kidney, the peritubular capillaries are distributed in close proximity to the proximal renal tubules and reabsorb their filtrates. Thus, the adjacent arrangement of blood vessels and eccrine sweat glands may result in the effective provision and reabsorption of sweat components. Whole-mount analyses also revealed the three-dimensional distributions of the nerve fibers that enwrapped the multiple myoepithelial cells surrounding the secretory portions. In salivary exocrine glands, however, the nerve fibers extend to, but do not wrap, the stellate-shaped myoepithelial cells on secretory acini (Knox et al., 2013; Knox et al., 2010). The difference between sweat and salivary glands in the spatial arrangement of nerve fibers relative to myoepithelial cells suggest that the myoepithelial cells of salivary glands individually contract their secretory acini, while the multiple myoepithelial cells of sweat glands synchronously contract their secretory portions.

Collectively, these whole-mount analyses make possible the determination of the complex coiled structures of eccrine sweat glands. The coiled structures possess three-dimensionally entangled secretory portions. The entangled orientation of these secretory portions is consistent with the three-dimensional arrangements of myoepithelial cells. Furthermore, these myoepithelial cells are closely covered by nerve fibers, indicating that myoepithelial cells effectively contract the secretory portions following innervations. Thus, the three-dimensional anatomical information provided by whole-mount staining of eccrine sweat glands provides insights into understanding the mechanisms of sweat secretion.

Chapter II

Identification of human sweat gland stem cells

II-1 Summary

Stem cells routinely maintain epidermal components, including the interfollicular epidermis, hair follicles, and eccrine sweat glands. Human eccrine sweat glands present throughout the body are glandular exocrine organs that mainly play a role in thermoregulation by secreting sweat. Although emerging evidence points to the presence of stem cells, defined as self-renewing multipotent, cells in eccrine sweat glands, it remains unclear whether these stem cells are present in human eccrine sweat glands. To assess whether these cells in are present in human eccrine sweat glands, I first assessed whether the myoepithelial cells in these glands that express the stem cell marker CD29 also express other stem cell markers, finding that the stem cell marker Notch was expressed by α-smooth muscle actin-positive myoepithelial cells in human sweat glands. To determine whether these myoepithelial cells in eccrine sweat gland are stem cells, I established a procedure for isolating myoepithelial cells from human skin tissue as a $CD29^{hi}CD49f^{hi}$ subpopulation. This cell subpopulation possessed the ability to differentiate into sweat gland luminal cells in sphere-forming assays, as well as exhibiting long-term proliferative potential upon multiple passaging, indicating that the $CD29^{hi}CD49f^{hi}$ myoepithelial subpopulation includes stem cells with self-renewal ability. These findings provide evidence that the myoepithelial cells in human eccrine sweat glands contain stem cells that possess both self-renewal ability and multipotency to differentiate into sweat glands.

II-2 Introduction

The human epidermis mainly consists of three components: the interfollicular epidermis, hair follicles, and eccrine sweat glands. These components are maintained by stem cells characterized by self-renewal ability and multipotency. The basal layer of keratinocytes in human interfollicular epidermis contains clusters of stem cells, characterized by long-term self-renewal ability in culture. These cells express a range of markers, including high levels of CD29, the transmembrane proteoglycan MCSP, and the EGFR antagonist LRIG1 (Jensen and Watt, 2006; Jones and Watt, 1993; Legg et al., 2003). In human hair follicles, the best-characterized stem cell population resides in a region known as the bulge. These cells, which express keratin 15 and CD200, regenerate hair follicles, as shown by engraftment experiments (Lyle et al., 1998; Ohyama et al., 2006; Toyoshima et al., 2012). In contrast, much less is known about the stem cells in human eccrine sweat glands. Mouse eccrine sweat gland myoepithelial cells were recently shown to generate sweat glands *in vivo* (Lu *et al.*, 2012), suggesting that human eccrine sweat glands also contain a source of stem cells, analogous to those observed in mice.

Mammalian sweat glands are single tubules consisting of functionally distinct ducts and secretory portions. Sweat ducts are composed of a helical epidermal duct, a straight dermal duct, and a short coiled extension of the dermal duct that continues into the coiled secretory portion. This secretory portion, which is primed to respond to stimuli from sympathetic nerves, includes secretory luminal cells and myoepithelial cells (Saga, 2002). Mammalian sweat gland germs emerge from the basal layer of the epidermis and elongate downward into the dermis where they form glandular globules. The morphogenesis of sweat glands in human skin begins at 12 weeks of gestation, and is essentially

completed by 22 weeks (Hashimoto et al., 1965). Because human sweat glands mainly function to maintain body temperature by sweating, they are distributed throughout the body (Sato et al., 1989b).

I sought to isolate sweat gland cells from human skin using a protocol described for the isolation of mammary gland cells (Shackleton et al., 2006). Mammary glands are exocrine glands that evolved from sweat glands (Oftedal, 2002). While sweat glands include "clear" (serous) and "dark" (mucous) secretory cells and surrounding myoepithelial cells, mammary glands consist of three different cell types: myoepithelial cells and two types of luminal lineage cells, ductal and alveolar epithelial cells (Dontu et al., 2003; Sato et al., 1989b). Ductal cells generate mammary gland ducts and alveolar cells constitute the alveolar units that expand during pregnancy. The myoepithelial and luminal cell subpopulations in mammary glands can be isolated based on their expression of CD29, a stem cell marker in skin (Jones and Watt, 1993); CD49f, an epidermal basal keratinocyte marker (Hertle et al., 1991); and CD24, a heat-stable antigen used to enrich neural stem cells (Rietze et al., 2001). The $CD24^{+}CD29^{hi}$ and $CD24^{+}CD49f^{hi}$ subpopulations, both of which are comprised of mammary gland myoepithelial cells, show properties of mammary stem cells, being both multipotent and self-renewing (Shackleton et al., 2006; Stingl et al., 2006).

In this study, I show that myoepithelial cell layers in human eccrine sweat glands express stem cell markers. These myoepithelial cells, isolated as $CD29^{hi}CD49f^{hi}$ cells, include cells with self-renewal ability and multipotency and can generate three-dimensional spheres, similar to mammary stem cells, thereby corroborating that they act as sweat gland stem cells.

II-3 Materials and Methods

Human skin tissues

Frozen human skin tissue samples were obtained with informed consent from ILSbio (Chestertown, MD). Fresh human skin tissues were obtained with informed consent from Osaka University Hospital (Osaka, Japan) and Biopredic International (Rennes, France). Experiments using human skin were approved by the Ethics Committee of Osaka University.

Antibodies

Antibodies for immunohistochemistry and immunofluorescence included anti-Ki67 (Santa Cruz Biotechnology, Santa Cruz, CA), anti-Notch1 (Cell Signaling, Beverly, MA), anti-p63 (Santa Cruz Biotechnology), anti-keratin 8 (Progen), anti-αSMA (Abcam), anti-aquaporin 5 (AQP5; in house), anti-CD29 (Abcam), anti-CD49f (Millipore), anti-S100P (Novus Biologicals), anti-S100A2 (Novus Biologicals), HRP-conjugated sheep anti-mouse (Amersham), Envision+System/HRP rabbit (Dako), HRP-conjugated donkey anti-goat (Santa Cruz Biotechnology), HRP-conjugated goat anti-chicken (Abcam), HRP-conjugated goat anti-rat (American Qualex), and species-specific fluorescent secondary antibodies (Invitrogen). Antibodies for flow cytometry and cell sorting included allophycocyanin-conjugated anti-CD29 (BD Pharmingen, San Diego, CA), Brilliant Violet 421-conjugated anti-CD49f (Biolegend, San Diego, CA), anti-AQP5 (in house) and Alexa Fluor 488-conjugated donkey anti-chicken (Jackson ImmunoResearch Laboratories, West Grove, PA).

Immunohistochemical analysis

Human skin tissues were embedded in OCT compound (Sakura Finetechnical Co.) and frozen in 2-methylbutane chilled in liquid nitrogen. Cryosections were prepared, fixed in 4% formaldehyde in PBS, cold methanol, or cold acetone, and blocked with 1% goat serum (Dako) in PBS, followed by incubation with primary antibodies at 4°C overnight. After three washes with PBS, the sections were treated with HRP-conjugated secondary antibodies, followed by color development using 3,3-diaminobenzidine. After counterstaining with hematoxylin, the sections were examined with an Eclipse E800 microscope (Nikon). For double immunofluorescence staining, sections were prepared, fixed in 4% formaldehyde in PBS, cold methanol, or cold acetone, and incubated with primary antibodies at 4°C overnight. After washing in PBS, the sections were treated with secondary antibodies for 1 h, washed with PBS, and stained with Hoechst 33342 to visualize the nuclei. All procedures were performed at room temperature. Immunofluorescence images were recorded using an LSM5 confocal microscope. Table III details the sources, clones, and concentrations of primary and secondary antibodies used for immunohistochemical staining.

Tissue dissociation and cell preparation

Isolated sweat glands from human skin tissue were enzymatically disaggregated for 6 h at 37°C in Complete MammoCult Human Medium (Stem Cell Technologies, Vancouver, BC) with 300 U/ml collagenase type II (Worthington Biochemicals, Freehold, NJ) and 100 U/ml hyaluronidase (Sigma) on a tube rotator. After centrifugation at 200 × *g* for 10 min, red blood cells were removed by treatment with 0.16% NH_4Cl/0.02 mM EDTA. Single-cell suspensions were prepared by repeated pipetting for 3 min in prewarmed 0.5% trypsin/1 mM EDTA, followed by repeated pipetting for 1 min in prewarmed 5 mg/ml dispase (Gibco, Paisley, UK)/0.1 mg/ml DNase I (Sigma). The resulting

Table III. Primary and secondary antibodies used for immunohistochemistry, immunofluorescence and flow cytometry.

Primary Antibody	Secondary Antibody	Usage
Anti-Ki-67 (1:400 dilution) Santa Cruz, California, USA	Horseradish peroxidase (HRP)-conjugated donkey anti-goat (1:400 dilution) Santa Cruz, California, USA	Immunohistochemistry
Anti-keratin 8 (K8) (1:100 dilution) Progen, Heidelberg, Germany	Alexa Fluor 488 conjugated goat anti-mouse (1:1000 dilution) Alexa Fluor 546 conjugated goat anti-mouse (1:1000 dilution) Invitrogen, Carlsbad, CA	Immunofluorescence
Anti-α smooth muscle actin (αSMA) (1:100 dilution) Abcam, Cambridge, MA	Alexa Fluor 488 conjugated goat anti-rabbit (1:1000 dilution) Alexa Fluor 546 conjugated goat anti-rabbit (1:1000 dilution) Invitrogen, Carlsbad, CA	Immunofluorescence
Anti-S100 calcium binding protein P (S100P) (1:100 dilution) Novus Biologicals, Littleton, CO	Alexa Fluor 488 conjugated goat anti-rabbit (1:1000 dilution) Alexa Fluor 546 conjugated goat anti-rabbit (1:1000 dilution) Invitrogen, Carlsbad, CA	Immunofluorescence
Anti-S100 calcium binding protein A2 (S100A2) (1:100 dilution) Novus Biologicals, Littleton, CO	Alexa Fluor 488 conjugated goat anti-rabbit (1:1000 dilution) Alexa Fluor 546 conjugated goat anti-rabbit (1:1000 dilution) Invitrogen, Carlsbad, CA	Immunofluorescence
Anti-Notch1 (1:100 dilution) Cell Signaling, Beverly, MA	Envision system (HRP for rabbit) Dako Cytomation, Glostrup, Denmark	Immunohistochemistry
	Alexa Fluor 488 conjugated goat anti-rabbit (1:1000 dilution) Alexa Fluor 546 conjugated goat anti-rabbit (1:1000 dilution) Invitrogen, Carlsbad, CA	Immunofluorescence
Anti-p63 (1:100 dilution) Santa Cruz, California, USA	Horseradish peroxidase (HRP)-conjugated donkey anti-goat (1:400 dilution) Santa Cruz, California, USA	Immunohistochemistry
	Alexa Fluor 488 conjugated donkey anti-goat (1:1000 dilution) Alexa Fluor 546 conjugated donkey anti-goat (1:1000 dilution) Invitrogen, Carlsbad, CA	Immunofluorescence
Anti-aquaporine 5 (AQP5) (1:100 dilution) In house	HRP-conjugated goat anti-chicken (1:1000 dilution) Abcam, Cambridge, MA	Immunohistochemistry
	Alexa Fluor 488 conjugated goat anti-chicken (1:1000 dilution) Alexa Fluor 546 conjugated goat anti-chicken (1:1000 dilution) Invitrogen, Carlsbad, CA	Immunofluorescence
	Alexa Fluor 488 conjugated donkey anti-chicken (1:100 dilution) Jackson ImmunoResearch Laboratories, West Grove, PA	Flow cytometry
Anti-integrin β1 (CD29) (1:100 dilution) Abcam, Cambridge, MA	HRP-conjugated sheep anti-mouse (1:500) Amersham, San Francisco, CA	Immunohistochemistry
	Alexa Fluor 488 conjugated goat anti-mouse (1:1000 dilution) Alexa Fluor 546 conjugated goat anti-mouse (1:1000 dilution) Invitrogen, Carlsbad, CA	Immunofluorescence
Anti-integrin β1 (CD29) Allophycocyanin conjugated (1:6 dilution) BD Pharmingen, San Diego, CA		Flow cytometry
Anti-integrin α6 (CD49f) (1:100 dilution) Millipore, Milford, MA	HRP-conjugated goat anti-rat (1:400) American Qualex, San Clemente, CA	Immunohistochemistry
	Alexa Fluor 488 conjugated goat anti-rat (1:1000 dilution) Alexa Fluor 546 conjugated goat anti-rat (1:1000 dilution) Invitrogen, Carlsbad, CA	Immunofluorescence
Anti-integrin α6 (CD49f) Brilliant Violet 421 conjugated (1:20 dilution) Biolegend, San Diego, CA		Flow cytometry

suspensions were filtered through 40-μm mesh (BD Biosciences, San Jose, CA). Surgically separated epidermis samples were minced and enzymatically disaggregated for 16 h at 4°C in 0.25% trypsin. The resulting suspensions were filtered through 40-μm mesh.

Cell labeling, flow cytometry, and cell sorting

Cells were labeled with antibodies at 4°C for 20 min in PBS containing 2% BSA (Sigma). After two washes in PBS, the cells were resuspended in PBS containing 2% BSA, filtered through 40-μm mesh, and kept on ice until sorting. Flow cytometric analysis and cell sorting were performed with a FACSAria (BD Biosciences).

Quantitative reverse-transcription polymerase chain reaction (qRT-PCR)

Total RNA was isolated using ISOGEN-LS (Nippon Gene, Tokyo, Japan) and Ethachinmate (Wako Pure Chemical Industries, Osaka, Japan), and cDNA synthesized using SuperScript III with random hexamers (Invitrogen). Real-time monitored quantitative PCR was performed using SYBR Green Super Mix and an ABI PRISM 7000 (Applied Biosystems, Foster City, CA). The levels of expression of the target genes were normalized relative to the levels of expression of GAPDH in the same samples using a standard curve method. The primer sets for qRT-PCR included those for αSMA (forward, 5′-ATAGAACATGGCATCATCACCAAC-3′; reverse, 5′-GGGCAACACGAAGCTCATTGTA-3′), keratin 18 (K18) (forward, 5′-CCCTGCTGAACATCAAGGTCAA-3′; reverse, 5′- GCTGTCCAAGGCATCACCAA-3′), S100A2 (forward, 5′-GCCAAGAGGGCGACAAGTT-3′; reverse, 5′-AGGAAAACAGCATACTCCTGGA-3′), S100P (forward, 5′-AAGGATGCCGTGGATAAATTGC-3; reverse, 5′-

ACACGATGAACTCACTGAAGTC-3′), and GAPDH (forward, 5′-GCACCGTCAAGGCTGAGAAC-3′; reverse, 5′- TGGTGAAGACGCCAGTGGA-3′), all produced by Custom Primer Greiner Bio-One Co., Japan.

Immunocytochemistry

Cell suspensions were fixed in 4% formaldehyde in PBS and placed on Matsunami adhesive silane-coated slides (Matsunami Glass, Osaka, Japan). After incubation for 8 h at 37°C, the cells were incubated with primary antibodies, followed by incubation with secondary antibodies. Nuclei were visualized with Hoechst 33342. Fluorescence images were recorded under an LSM 5 PASCAL confocal microscope (Carl Zeiss).

In vitro *sphere cultures*

Procedures for suspension sphere cultures have been described (Spike et al., 2012). Briefly, freshly sorted cells were plated on ultralow-adherence plates (Corning, Corning, NY) at 1000 cells/cm^2 in sphere culture medium (Complete MammoCult Human Medium containing 0.5 μg/ml hydrocortisone 21-hemisuccinate (Sigma), 10 ng/ml recombinant human epidermal growth factor (PeproTech, Rocky Hill, NJ), 10 ng/ml recombinant human basic fibroblast growth factor (Stem Cell Technologies), 4 μg/ml heparin (Stem Cell Technologies), and 100 μg/ml penicillin/streptomycin (Gibco)), with or without 2% Matrigel (growth factor-reduced; BD Biosciences). For long-term serial passages, spheres grown on plates as described above were recovered from Matrigel using Cell Recovery Solution (BD Biosciences), and then treated with trypsin followed by dispase, as described (Spike et al., 2012). Dissociated cells were collected by passing through a 40-μm mesh prior to

plating on ultra-low adherence plates at 1000 cells/cm^2 in sphere culture medium containing 2% Matrigel. For clonal sphere cultures, freshly sorted single cells were seeded into separate wells of 96-well ultralow-adherence plates at one cell/well in sphere culture medium with 2% Matrigel.

II-4 Results

Localization of stem cell markers in human eccrine sweat glands

Stem cells in adult mammalian tissues possess slow-cycling properties during normal homeostasis, whereas their descendants display fast cycling. I therefore assessed the proliferative activity of human sweat glands and epidermis. Ki-67-labeled cells, which are actively cycling cells, were concentrated in the epidermis, with few detected in the sweat glands (Figure 24), suggesting that eccrine sweat glands are comprised of infrequently dividing cells. To explore whether eccrine sweat glands contain slow-cycling stem cells, the levels of expression of stem cell markers were assessed in adult human sweat glands. CD29 and Notch are cell surface receptors expressed on stem cells and have been shown to be involved in niche recognition through cell–extracellular matrix and cell–cell interactions, respectively (Campos et al., 2006). In Chapter I, I provided evidence that CD29 is expressed on myoepithelial cells, but not on secretory luminal cells (Figure 7). The expression of CD29 was more pronounced in sweat glands than in the epidermis (Figure 5, 25), and Notch was more strongly expressed on the basal side of sweat glands than in the epidermis (Figure 26). Double immunofluorescence staining showed that Notch was expressed in the secretory portion and coexpressed with αSMA, but not K8 (Figure 27). p63 is an epidermal stem cell marker induced by Notch signaling. Moreover, the cross-talk between p63 and Notch is involved in the balance between keratinocyte self-renewal and differentiation (Nguyen et al., 2006). p63 was strongly expressed in the epidermis and moderately expressed in sweat glands (Figure 26). Double immunofluorescence staining showed that the p63 expression levels were lower in the αSMA- and K8-positive secretory portions than in the αSMA- and K8-negative ducts (Figure 28). These findings indicate that cells

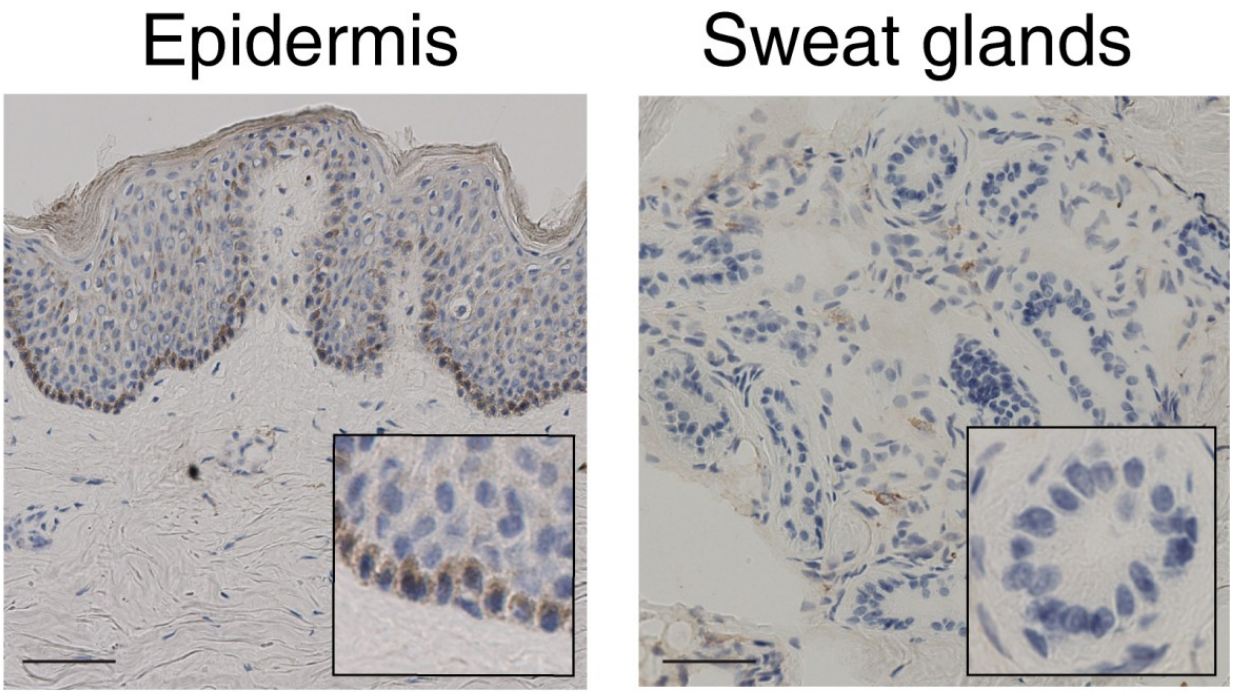

Figure 24. Detection of Ki-67 in the basal layers of epidermis, but not in eccrine sweat glands.
Immunohistochemical localization of Ki-67 in human skin. Ki-67^{+} cells were located in the epidermis (left panel). Sweat gland cells did not express Ki-67 (right panel). Insets show magnified views of the epidermis (left panel) and eccrine sweat glands (right panel). Scale bars: 50 μm.

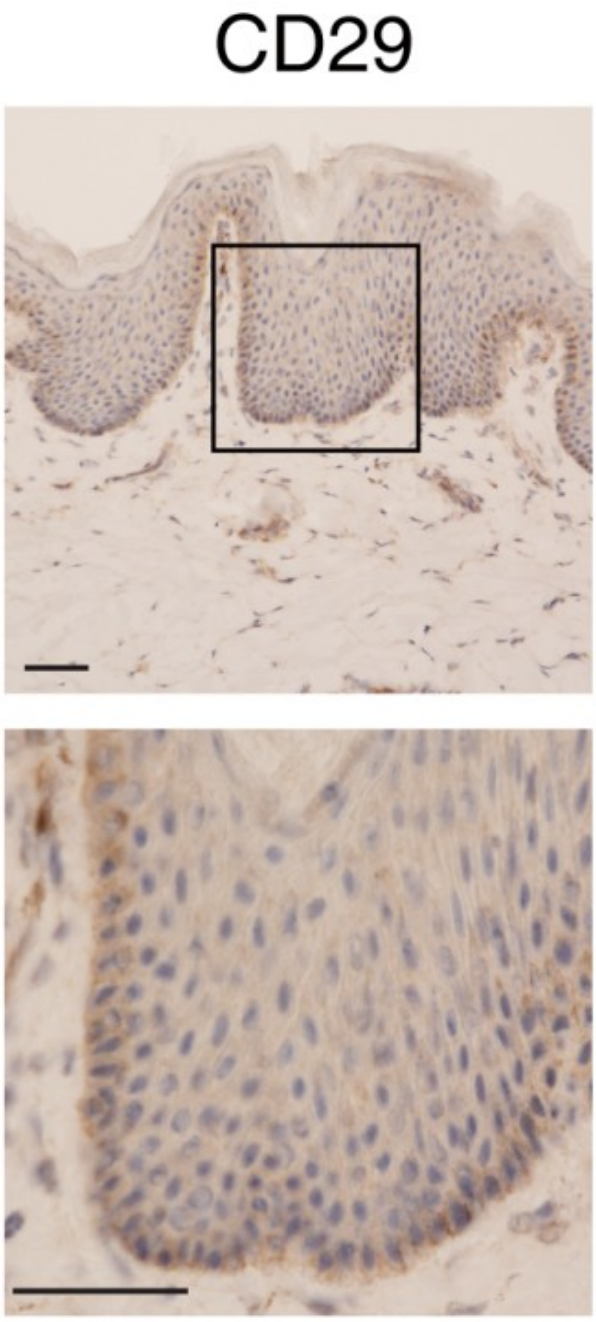

Figure 25. Detection of CD29 in the basal layers of interfollicular epidermis.
Pattern of expression of CD29 in human skin. The boxed area in the upper panel is shown in the lower panel at higher magnification. Scale bars: 50 μm.

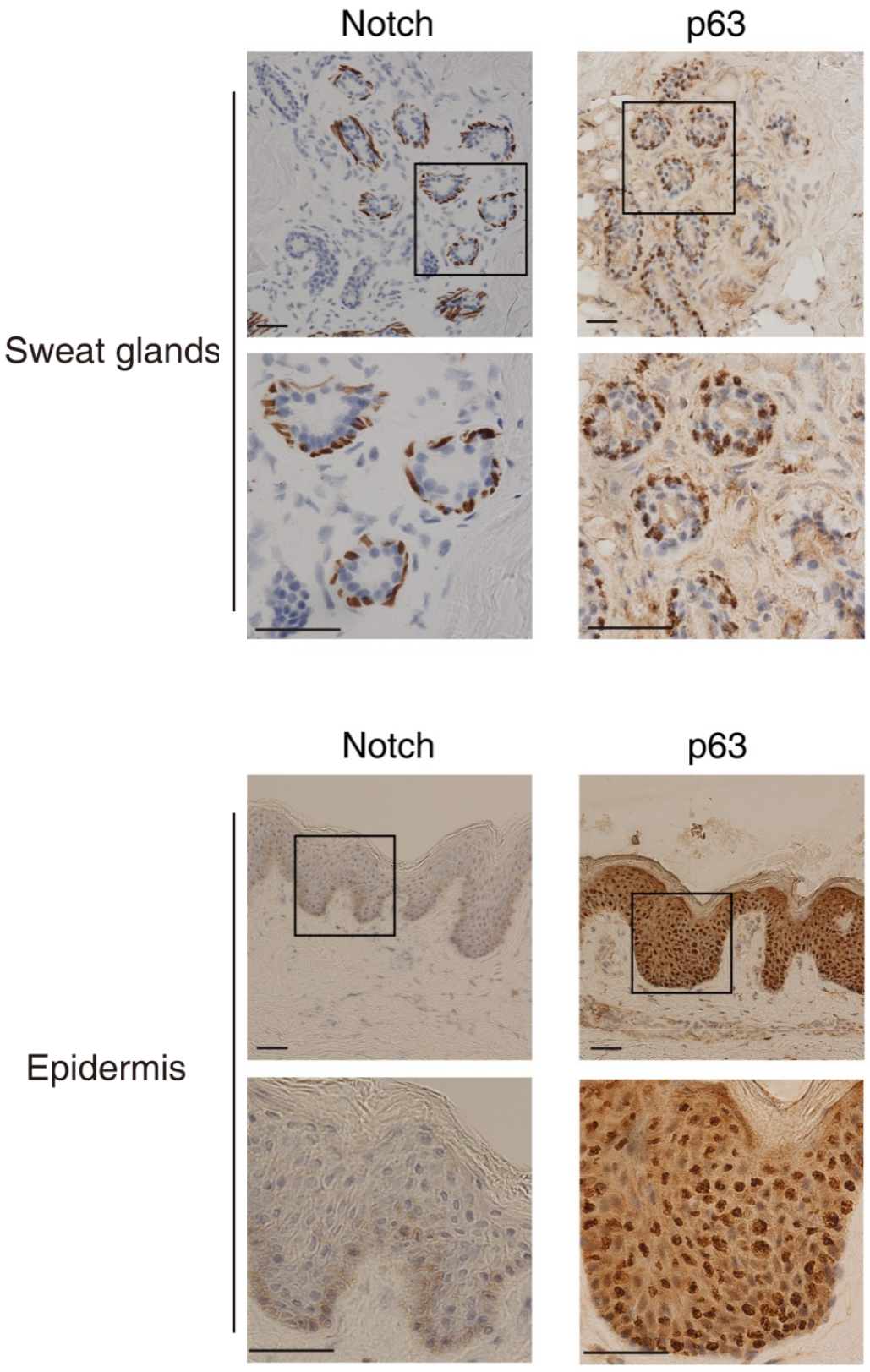

Figure 26. Detection of the stem cell markers Notch and p63 in the basal layers of human eccrine sweat glands.
Expression patterns of Notch and p63 in human skin. Boxed areas in the upper panels are shown in the lower panels at higher magnification. Scale bars: 50 μm.

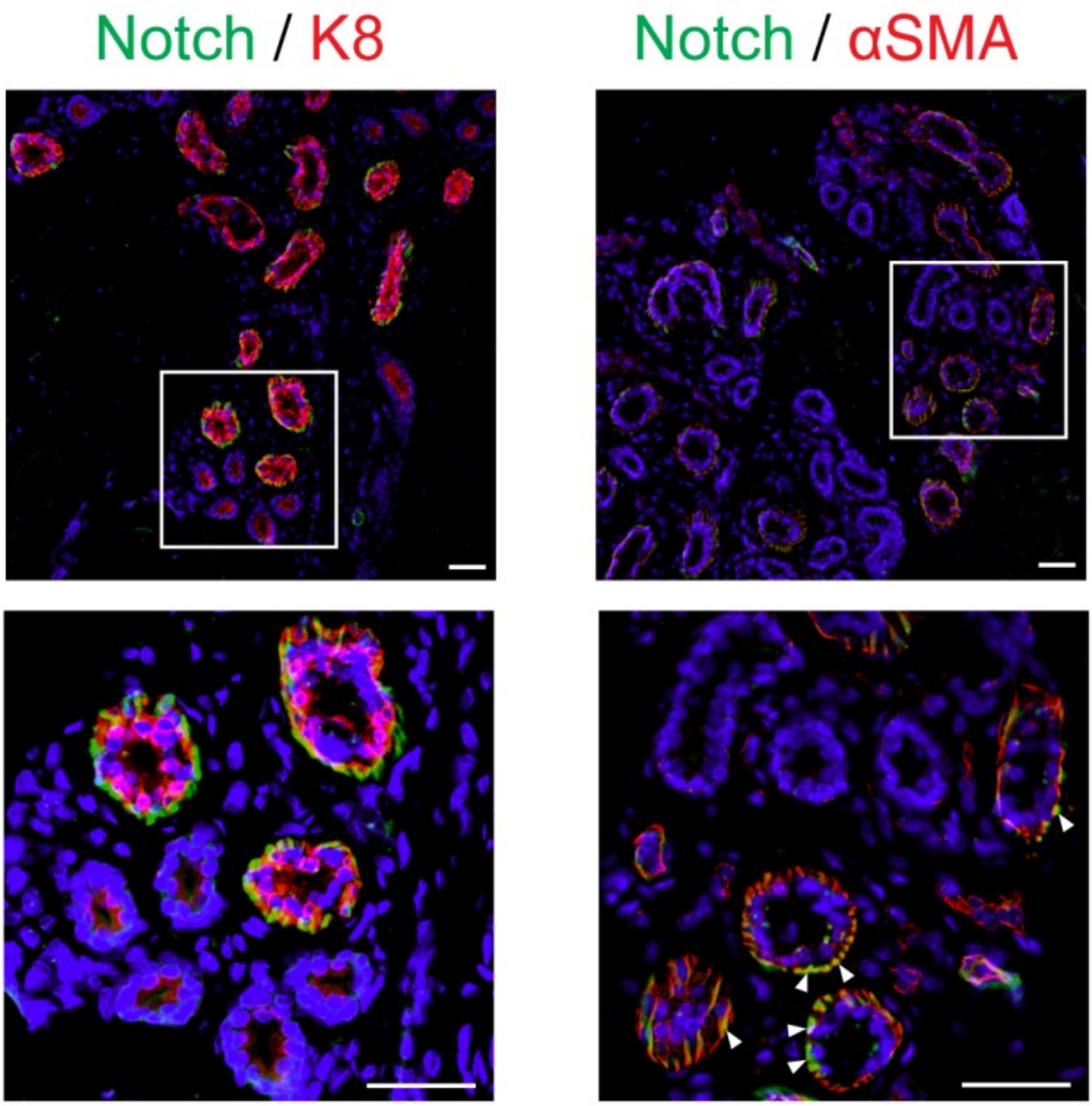

Figure 27. Expression of Notch in myoepithelial, but not secretory luminal, cells. Colocalization of the epidermal stem cell marker Notch and the sweat gland cell markers (αSMA and K8) in human sweat glands. Boxed areas in the upper panels are magnified in the lower panels. Arrowheads indicate colocalization of αSMA and Notch. Nuclei (blue) were counterstained with Hoechst 33342. Scale bars: 50 μm.

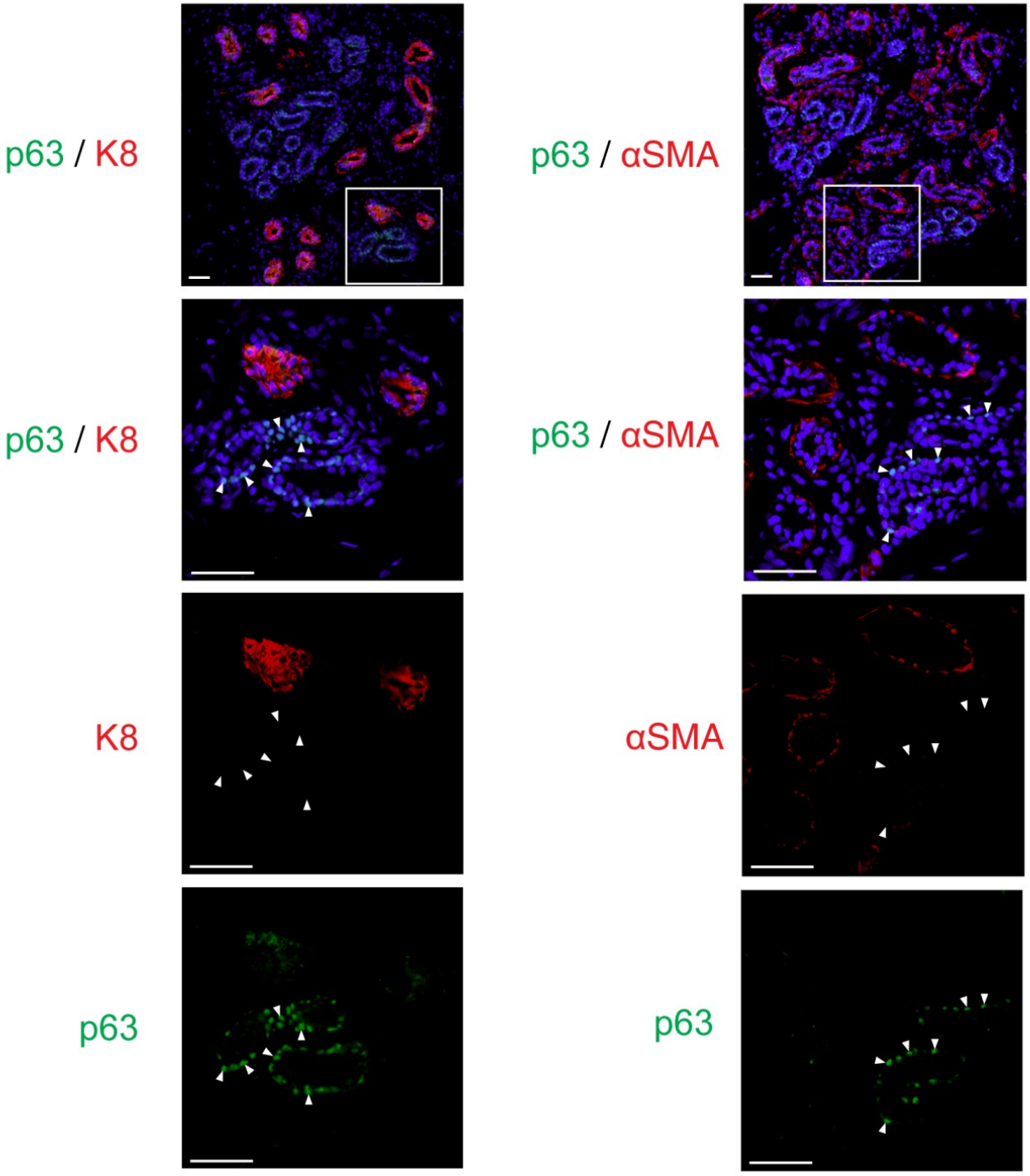

Figure 28. p63 expression levels were lower in the secretory portions than in the ducts of human sweat glands.
Colocalization of p63 and the sweat gland cell markers αSMA and K8 in human sweat glands. Boxed areas in the upper panels are magnified in the lower panels. p63 was expressed in K8- and αSMA-negative cells (arrowheads). Nuclei (blue) were counterstained with Hoechst 33342. Scale bars: 50 μm.

positive for stem cell markers reside among the αSMA-positive myoepithelial cells of human sweat glands, except for cells positive for p63.

Procedure for isolating human eccrine sweat gland populations

To further explore the stem cell nature of myoepithelial cells in human eccrine sweat glands, I established protocols for the isolation of these cells from human skin tissue. Because of the anatomical similarities between eccrine sweat glands and mammary glands, I employed the cell surface markers CD29, CD49f, and CD24 used for the isolation of mammary cells (Dontu et al., 2003; Sato et al., 1989b; Shackleton et al., 2006; Stingl et al., 2006), and investigated their expression patterns in eccrine sweat glands. In Chapter I, I showed that CD29 and CD49f were strongly expressed in human eccrine sweat glands, similar to mammary glands (Figure 5). These expression patterns were subsequently compared with the expression patterns of AQP5, a cell surface marker almost exclusively expressed by sweat glands (Figure 29). Although CD29 and CD49f were strongly expressed in the basal regions of sweat glands (Figure 6), AQP5 was expressed in the luminal regions (Figure 30). Furthermore, CD29 was strongly expressed in the secretory portions expressing K8 and αSMA (Figure 7) but was less strongly expressed in the ducts expressing S100P and S100A2 (Figure 31). CD49f was also intensely expressed in the secretory portions (Figure 7) but to a lesser extent in the ducts (Figure 32), whereas AQP5 was specifically expressed in the secretory portions but not in the ducts (Figure 33).

Based on these observations, I sought to isolate sweat gland myoepithelial cells from human skin by flow cytometry. CD29, CD49f, and AQP5 were expressed in the basal epidermal cells (Figure 25, 34), and CD29 and CD49f, but not AQP5, were expressed in basal layers of human hair follicles

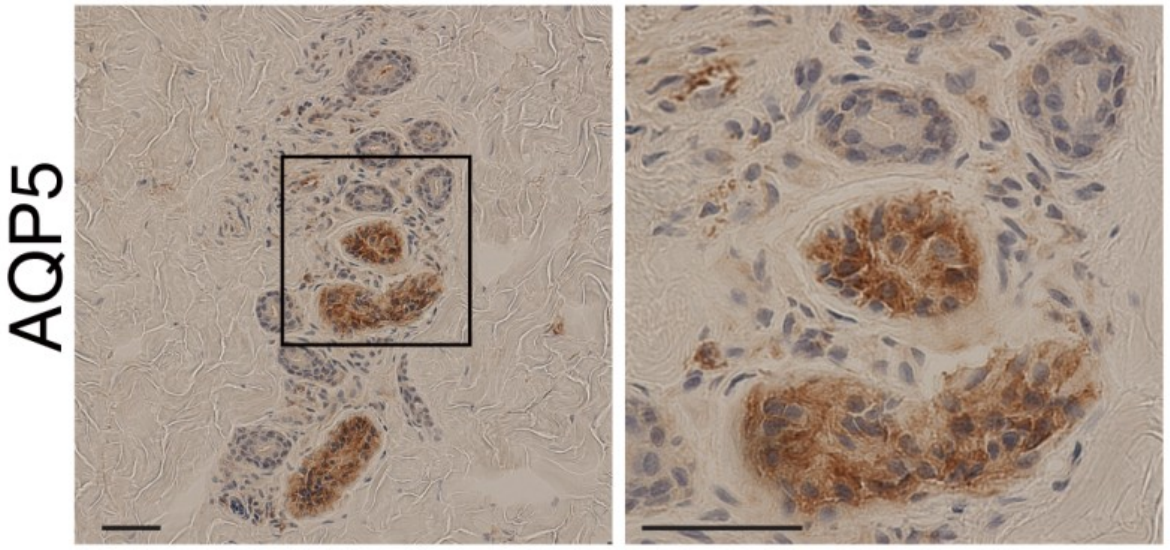

Figure 29. AQP5 was strongly expressed in parts of human eccrine sweat glands. Expression pattern of AQP5 in human sweat glands. The boxed area in the left panel is shown in the right panel at higher magnification. Scale bars: 50 μm.

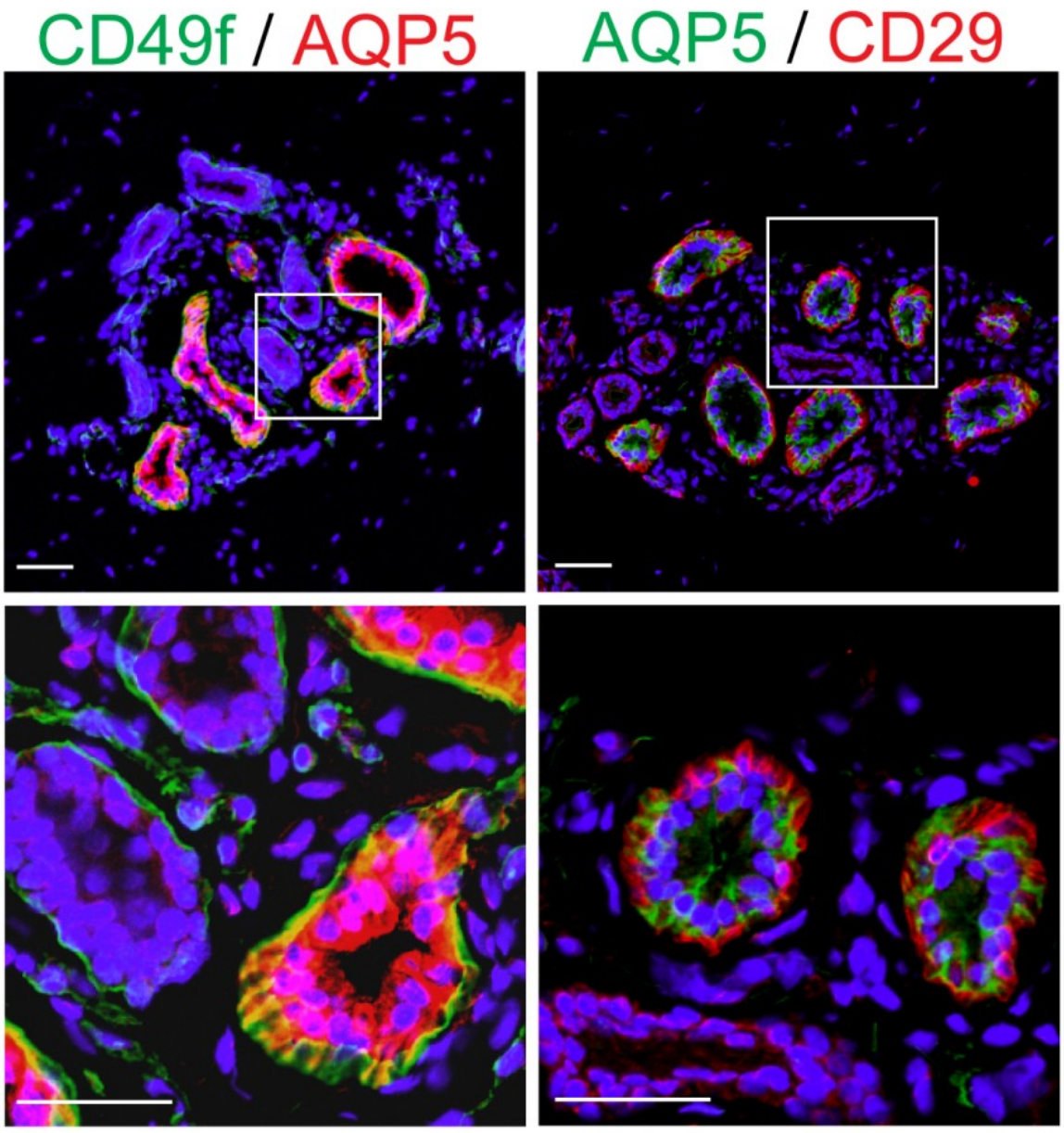

Figure 30. AQP5 was expressed by luminal cells, but not by basal cells expressing CD49f and CD29, of eccrine sweat glands.
Double-immunofluorescence detection of CD29, CD49f, and AQP5 in sweat glands. Nuclei (blue) were counterstained with Hoechst 33342. Boxed areas in the upper panels are shown in the lower panels at higher magnification. Scale bars: 50 μm.

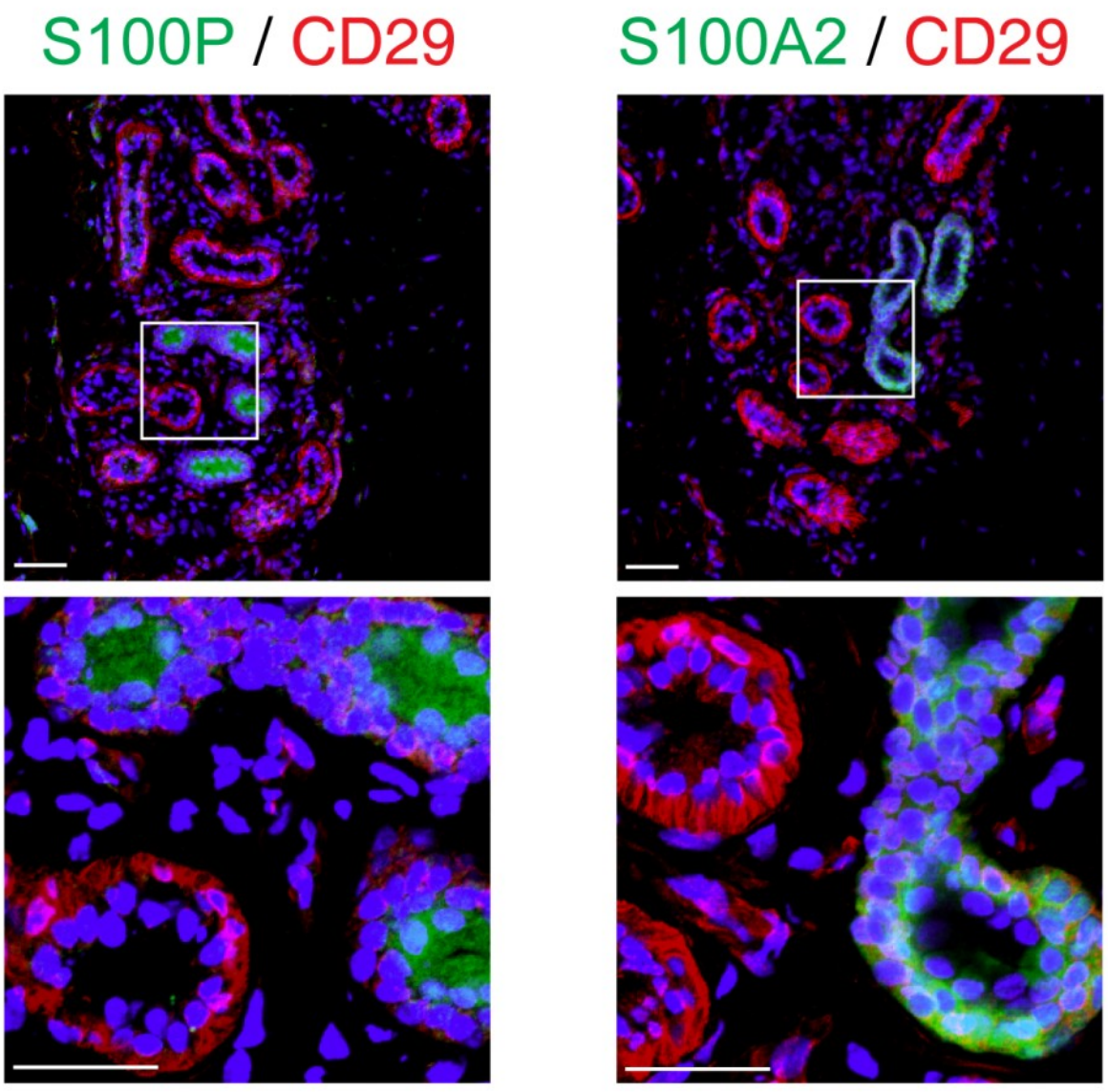

Figure 31. Reduced levels of expression of CD29 in ducts of human sweat glands expressing S100P and S100A2.
Colocalization of CD29 and the ductal markers S100A2 and S100P in human sweat glands. Boxed areas in the upper panels are shown in the lower panels at higher magnification. Nuclei (blue) were counterstained with Hoechst 33342. Scale bars: 50 μm.

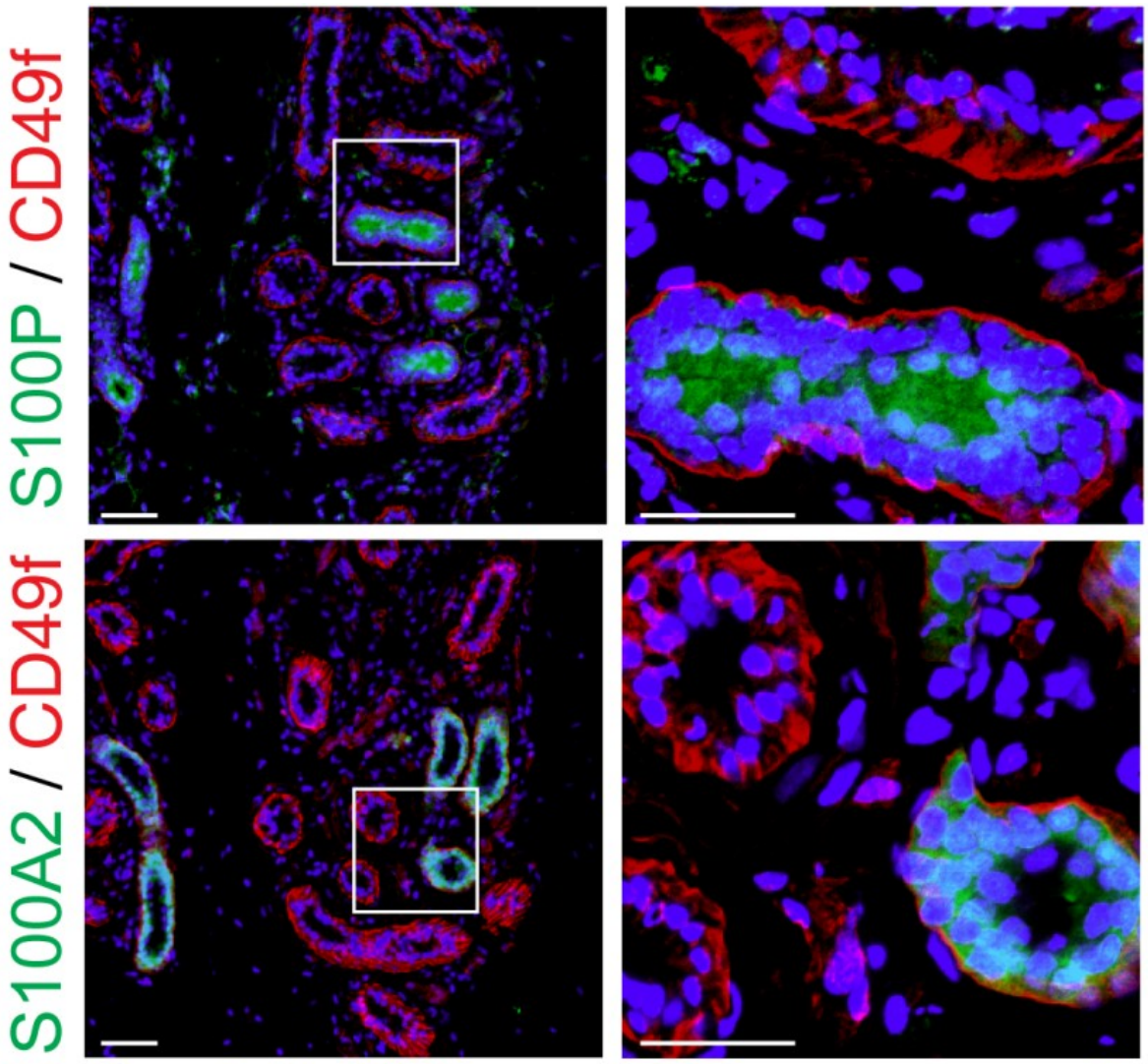

Figure 32. Reduced levels of expression of CD49f in ducts expressing S100P and S100A2 than in secretory portions of human sweat glands.
Colocalization of CD49f and the sweat gland cell markers S100A2 and S100P in human sweat glands. Boxed areas in the left panels are shown in the right panels at higher magnification. Nuclei (blue) were counterstained with Hoechst 33342. Scale bars: 50 μm.

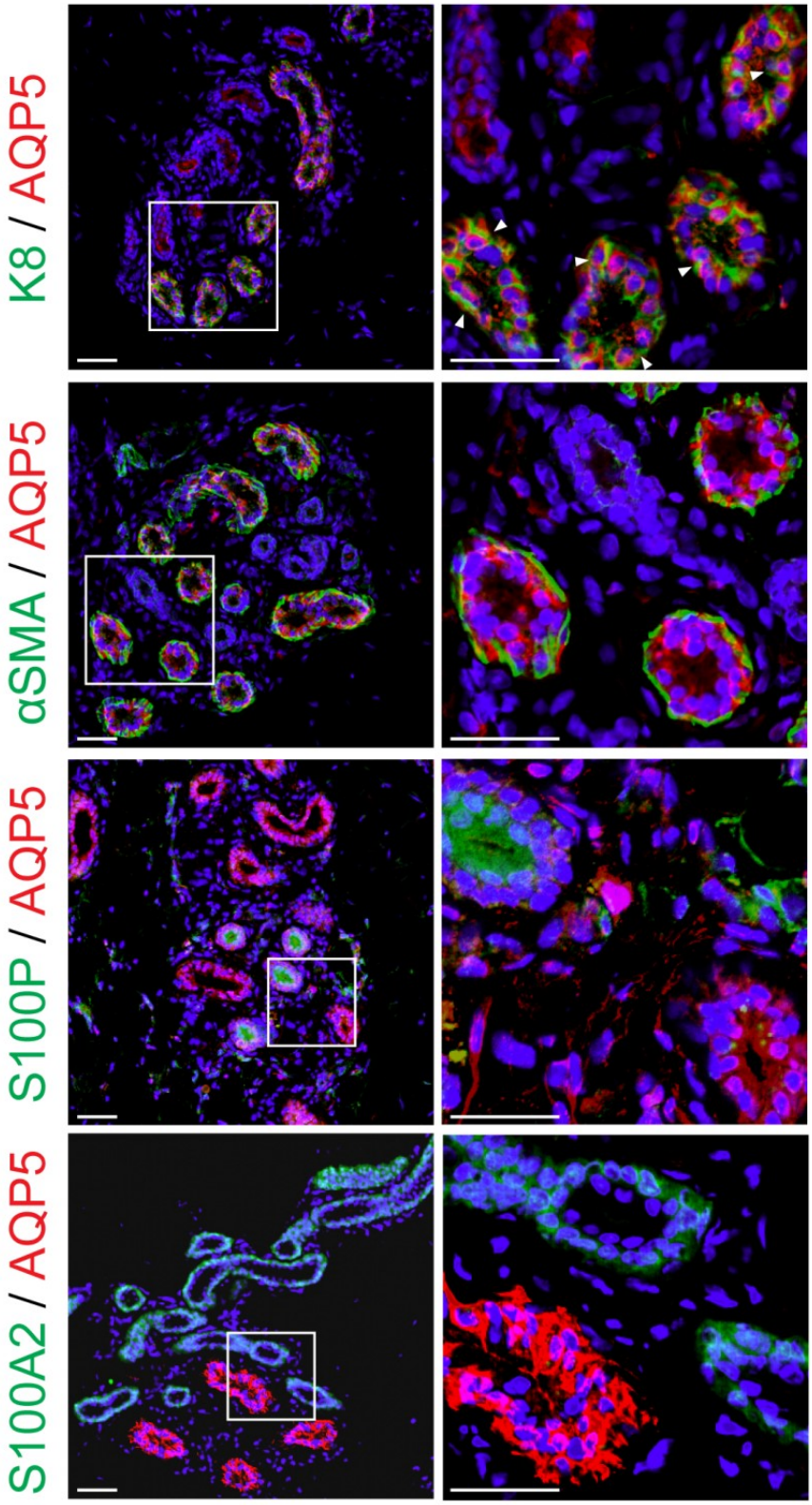

Figure 33. Expression of AQP5 in secretory portions expressing αSMA and K8, but not in ducts expressing S100P and S100A2.
Colocalization of AQP5 and the sweat gland cell markers αSMA, K8, S100A2, and S100P in human sweat glands. Arrowheads indicate colocalization of AQP5 with K8. Boxed areas in the left panels are shown in the right panels at higher magnification. Nuclei (blue) were counterstained with Hoechst 33342. Scale bars: 50 μm.

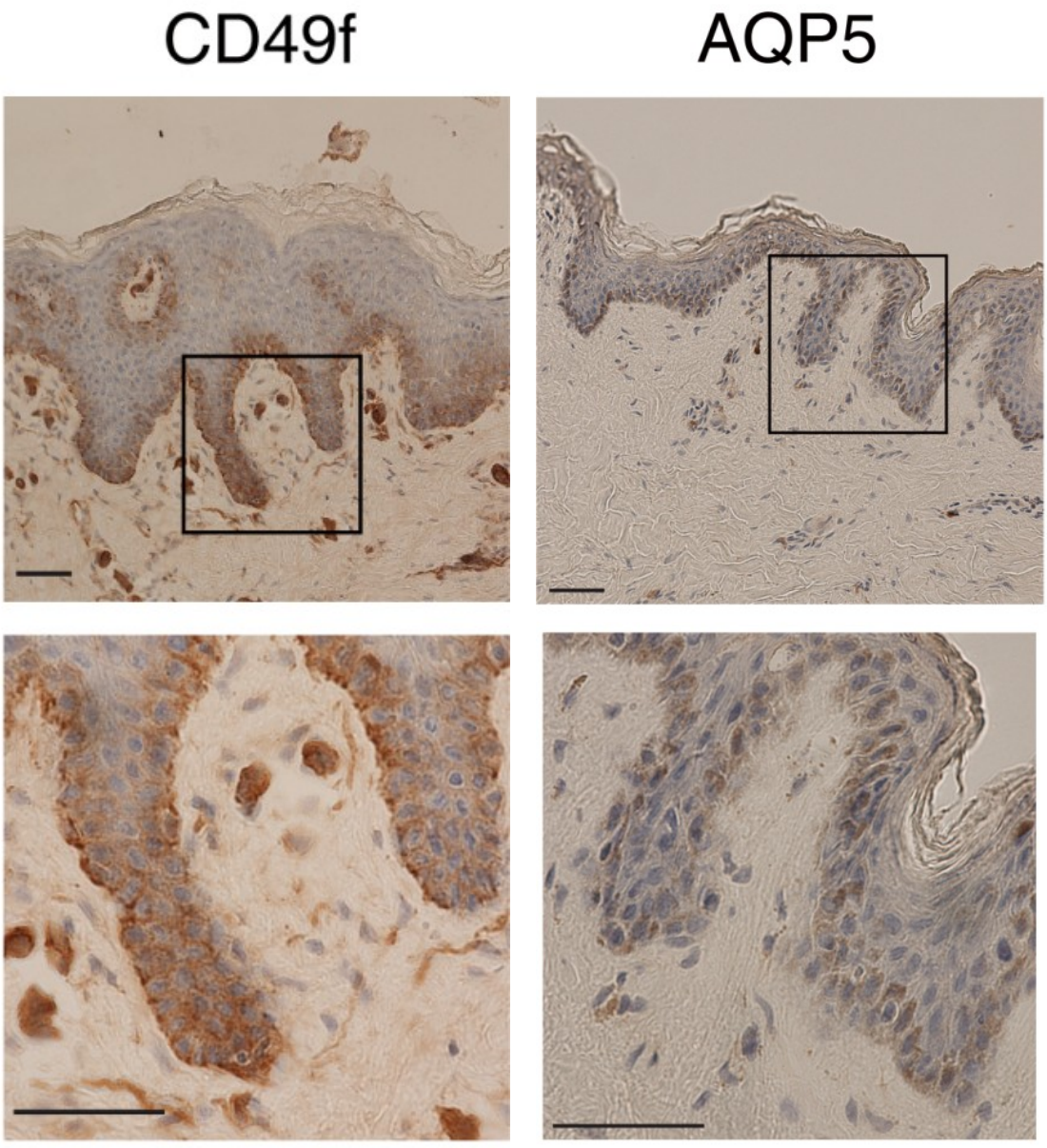

Figure 34. Slight expression of CD49f and AQP5 in the basal layers of human epidermis. Expression patterns of CD49f and AQP5 in human epidermis. Boxed areas in the upper panels are shown in the lower panels at higher magnification. Scale bars: 50 μm.

(Figure 35). Therefore, the cells isolated from the skin using these cell surface markers contain not only sweat gland cells but also epidermal keratinocytes and hair follicle cells. To avoid the contamination of cells derived from the epidermis and hair follicles, the eccrine sweat glands were collected from human skin as shown in chapter I. Individual sweat gland organs were isolated microsurgically from human skin tissue stained with neutral red (Figure 9). The collagenous connective tissue surrounding these isolated eccrine sweat glands was enzymatically disaggregated in medium containing collagenase/hyaluronidase for 6 h at 37°C (Figure 36). The organs were then dissociated into single-cell suspensions by a two-step treatment with trypsin/EDTA and dispase, and subjected to flow cytometry (Figure 37).

Using a combination of CD29, CD49f, and AQP5, four distinct subpopulations were isolated: P1, $CD29^{hi}CD49f^{hi}$; P2, $CD29^{mid}CD49f^{mid}AQP5^{-}$; P3, $CD29^{mid}CD49f^{mid}AQP5^{+}$; and P4, $CD29^{lo}CD49f^{lo}$ (Figure 38). The levels of expression of these sweat gland marker genes in these cell subpopulations were assayed by qRT-PCR (Figure 39). The epidermal $CD29^{mid}CD49f^{hi}$ subpopulation was also collected as a control for epidermal basal keratinocytes. The expression of αSMA, a myoepithelial cell marker, was restricted to P1 ($CD29^{hi}CD49f^{hi}$), while the expression of K18, a secretory luminal cell marker, was preferentially detected in P3 ($CD29^{mid}CD49f^{mid}AQP5^{+}$). S100A2, a basal duct cell marker, was highly expressed in P2 ($CD29^{mid}CD49f^{mid}AQP5^{-}$), while the expression of S100P, a luminal duct cell marker, was preferentially detected in P4 ($CD29^{lo}CD49f^{lo}$). These results indicated that myoepithelial cells and secretory luminal cells were enriched in the $CD29^{hi}CD49f^{hi}$ and $CD29^{mid}CD49f^{mid}AQP5^{+}$ subpopulations, respectively. Similarly, immunohistochemical assays showed that the P1 ($CD29^{hi}CD49f^{hi}$) and P3 ($CD29^{mid}CD49f^{mid}AQP5^{+}$) subpopulations were enriched with αSMA- and K8-positive cells, respectively (Figure 40). Quantification of these

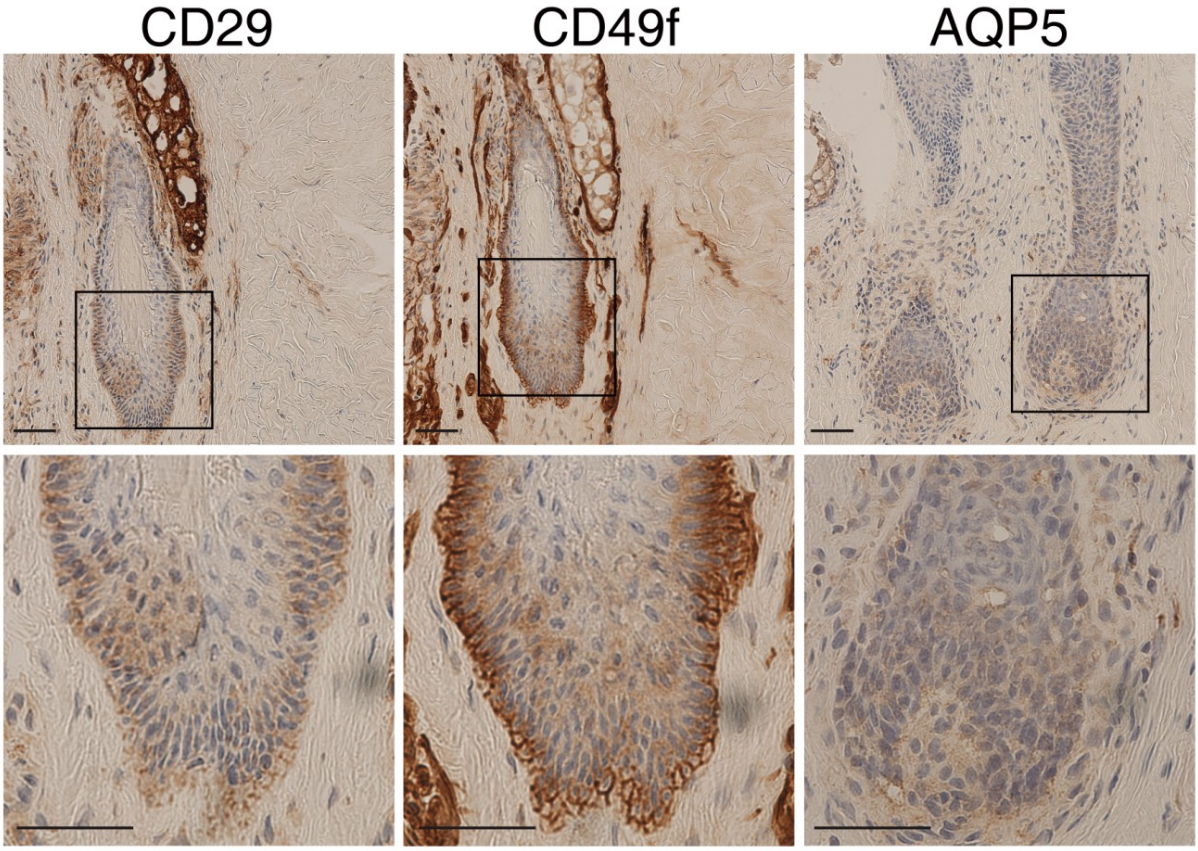

Figure 35. Expression of CD29 and CD49, but not AQP5, in basal cells of human hair follicles.
Expression patterns of CD29, CD49f, and AQP5 in human hair follicles. Boxed areas in the upper panels are shown in the lower panels at higher magnification. Scale bars: 50 μm.

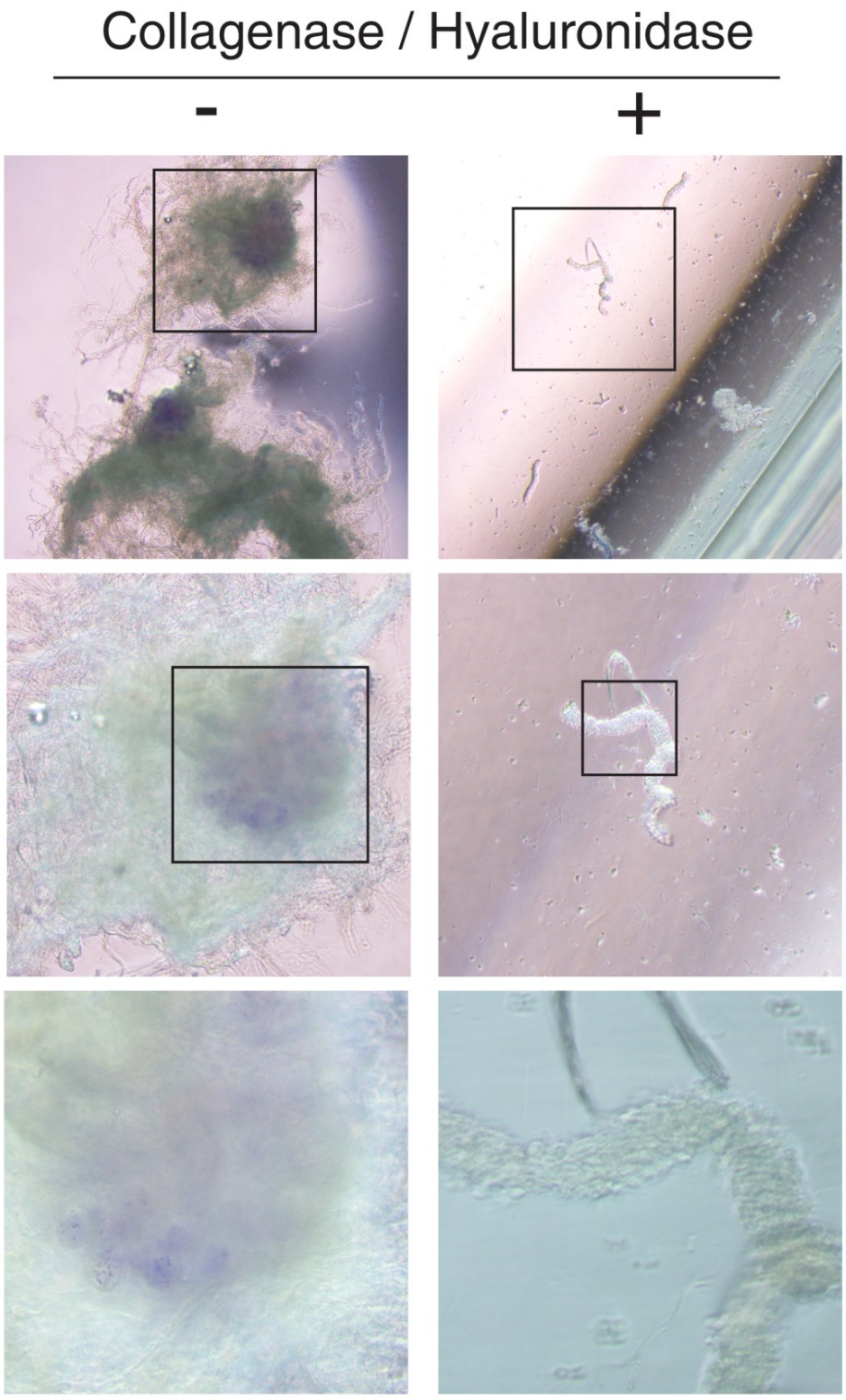

Figure 36. Disaggregation of collagenous connective tissue attached to sweat gland organs by collagenase/hyaluronidase.
The left panels show neutral red staining of sweat glands on a collagen background. The right panels show sweat gland organs following enzymatic disaggregation. Boxed areas in the upper panels are shown in the lower panels at higher magnification.

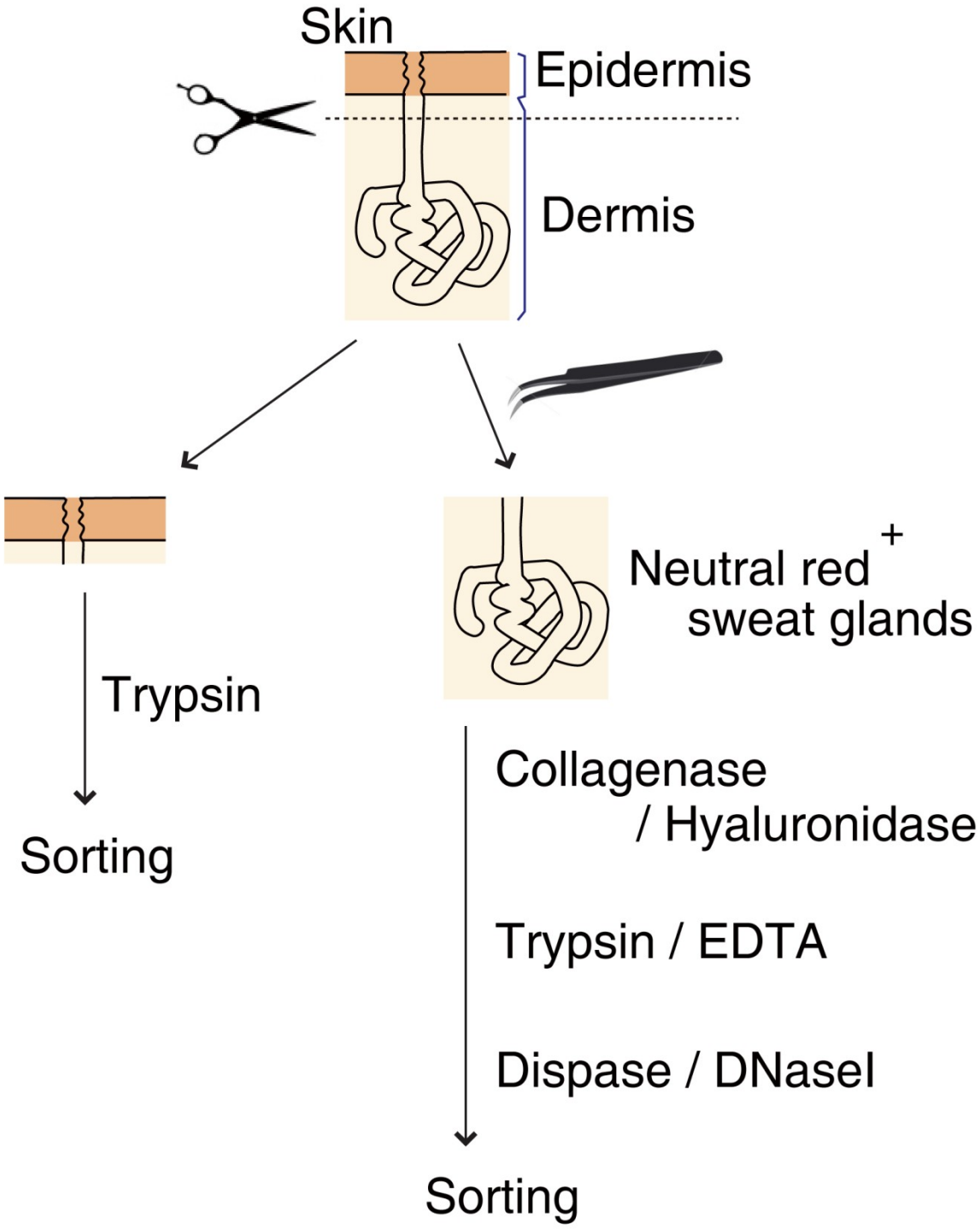

Figure 37. Schematic representation of the experimental design for isolation of sweat gland cells and epidermal basal keratinocytes.
The dermis was separated from the epidermis using surgical scissors. The sweat glands in the dermis were visualized by staining with neutral red and collected with fine forceps. Single-cell suspensions were prepared from sweat glands and epidermis by enzymatic disaggregation. Sweat gland cells and basal keratinocytes were isolated from single-cell suspensions by cell sorting.

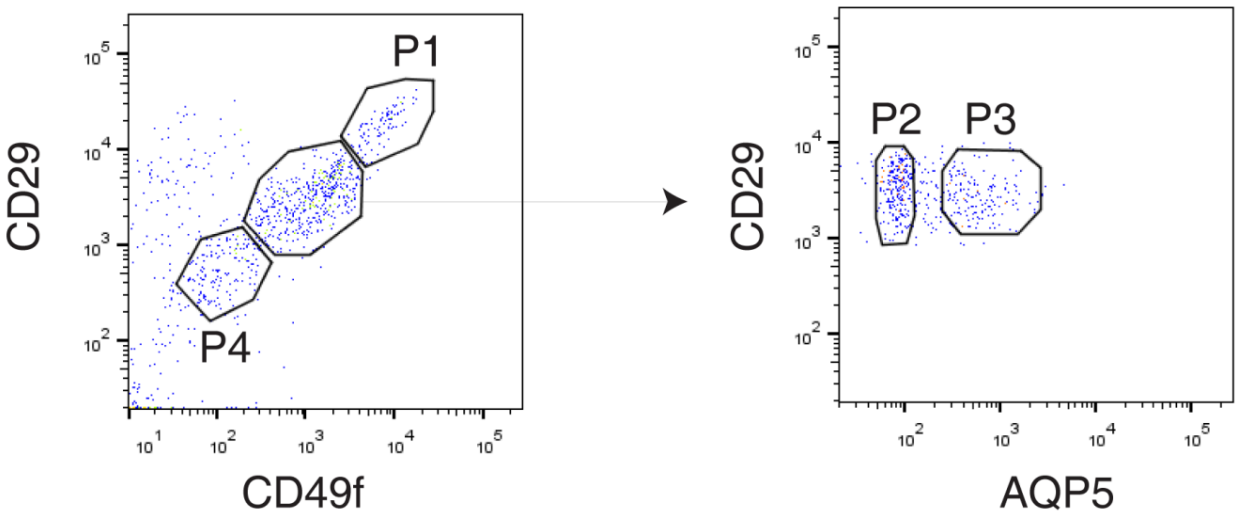

Figure 38. Expression of CD29, CD49f, and AQP5 in four distinct subpopulations of sweat gland cells.
Flow cytometric analysis, gating, and sorting of dissociated sweat gland cells from human skin. Cells were sorted by expression of CD29, CD49f, and AQP5. The following gates were used to define the four subpopulations: P1, $CD29^{hi}CD49f^{hi}$; P2, $CD29^{mid}CD49f^{mid}AQP5^{-}$; P3, $CD29^{mid}CD49f^{mid}AQP5^{+}$; and P4, $CD29^{lo}CD49f^{lo}$ cells.

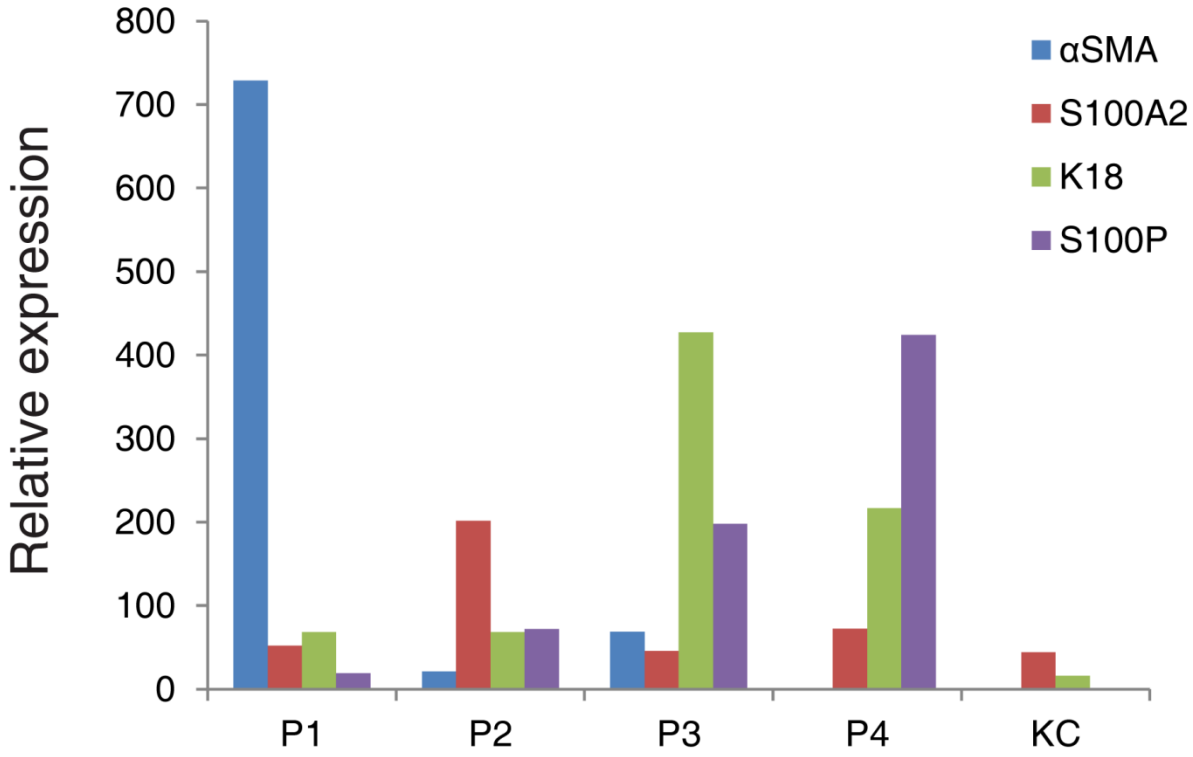

Figure 39. Enrichment of myoepithelial cells in the CD29^{hi}CD49f^{hi} (P1) subpopulation of human sweat glands.
qRT-PCR analysis of the expression of mRNAs encoded sweat gland marker genes in the four subpopulations. The levels of expression of each gene were normalized relative to the levels of expression of glyceraldehyde-3-phosphate dehydrogenase (GAPDH) in the same samples.

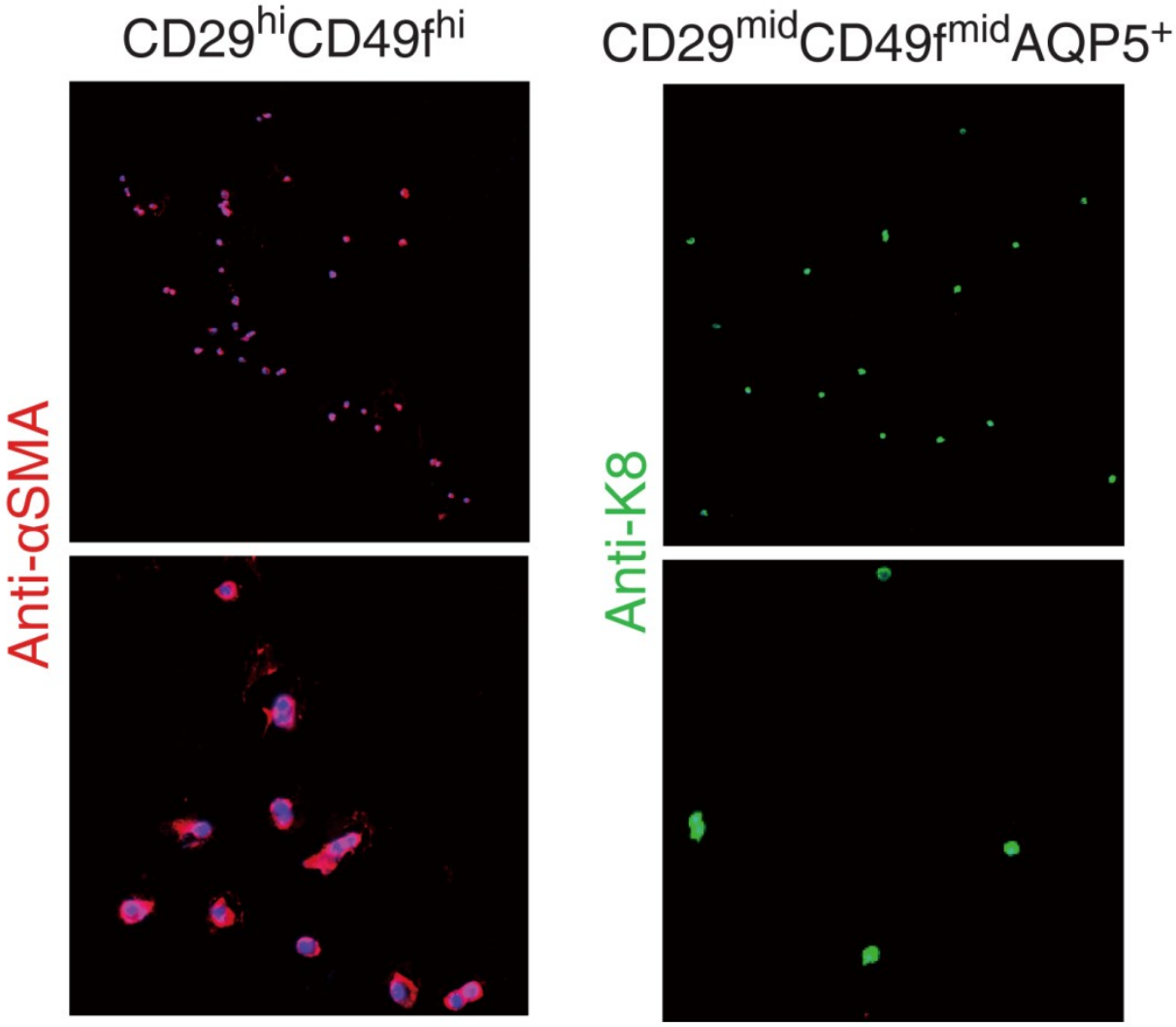

Figure 40. Concentration of αSMA- and K8-positive cells in the CD29^{hi}CD49f^{hi} and CD29^{mid}CD49f^{mid}AQP5^{+} subpopulations, respectively.
CD29^{hi}CD49f^{hi} and CD29^{mid}CD49f^{mid}AQP5^{+} cells were plated onto MAS-coated slides immediately after sorting and stained for αSMA and K8. The lower panels show high-magnification photomicrographs of the upper panels. Nuclei (blue) were counterstained with Hoechst 33342.

αSMA- and K8-positive cells revealed that 95% of the P1 ($CD29^{hi}CD49f^{hi}$) subpopulation was αSMA-positive, while 90% of the P3 ($CD29^{mid}CD49f^{mid}AQP5^{+}$) subpopulation was K8-positive (Figure 41), confirming that the P1 ($CD29^{hi}CD49f^{hi}$) and P3 ($CD29^{mid}CD49f^{mid}AQP5^{+}$) subpopulations represented myoepithelial and luminal cells, respectively, in sweat glands. These findings indicate that myoepithelial cells in human sweat glands can be isolated as a $CD29^{hi}CD49f^{hi}$ subpopulation.

Multipotency of the myoepithelial subpopulation of human eccrine sweat glands

Next, I investigated whether these myoepithelial cells possessed the ability to regenerate the secretory portion of sweat glands. The P1 ($CD29^{hi}CD49f^{hi}$) subpopulation was cultured on ultralow-adherence plates at 1000 cells/cm^2 in sphere culture medium with or without 2% Matrigel. The P2 ($CD29^{mid}CD49f^{mid}AQP5^{-}$), P3 ($CD29^{mid}CD49f^{mid}AQP5^{+}$), and P4 ($CD29^{lo}CD49f^{lo}$) subpopulations and the epidermal $CD29^{mid}CD49f^{hi}$ subpopulation were similarly seeded as controls. Similar to mammary gland cells, the myoepithelial cell-enriched P1 ($CD29^{hi}CD49f^{hi}$) subpopulation generated spheres in the presence, but not the absence, of Matrigel (Figure 42 A, B). Spheres were also generated from the P2 ($CD29^{mid}CD49f^{mid}AQP5^{-}$) subpopulation in the presence of Matrigel, but few spheres were generated from the P3 ($CD29^{mid}CD49f^{mid}AQP5^{+}$), P4 ($CD29^{lo}CD49f^{lo}$), and epidermal $CD29^{mid}CD49f^{hi}$ subpopulations irrespective of the presence or absence of Matrigel (Figure 42 A). The P1 ($CD29^{hi}CD49f^{hi}$) subpopulation-derived spheres exhibited exocrine gland-like hollow structures, with the markers for luminal (K8) and myoepithelial (αSMA) cells expressed in apical and basal cell layers, respectively (Figure 43). These results suggest that human sweat gland myoepithelial cells possess the ability to differentiate into luminal cells and regenerate secretory

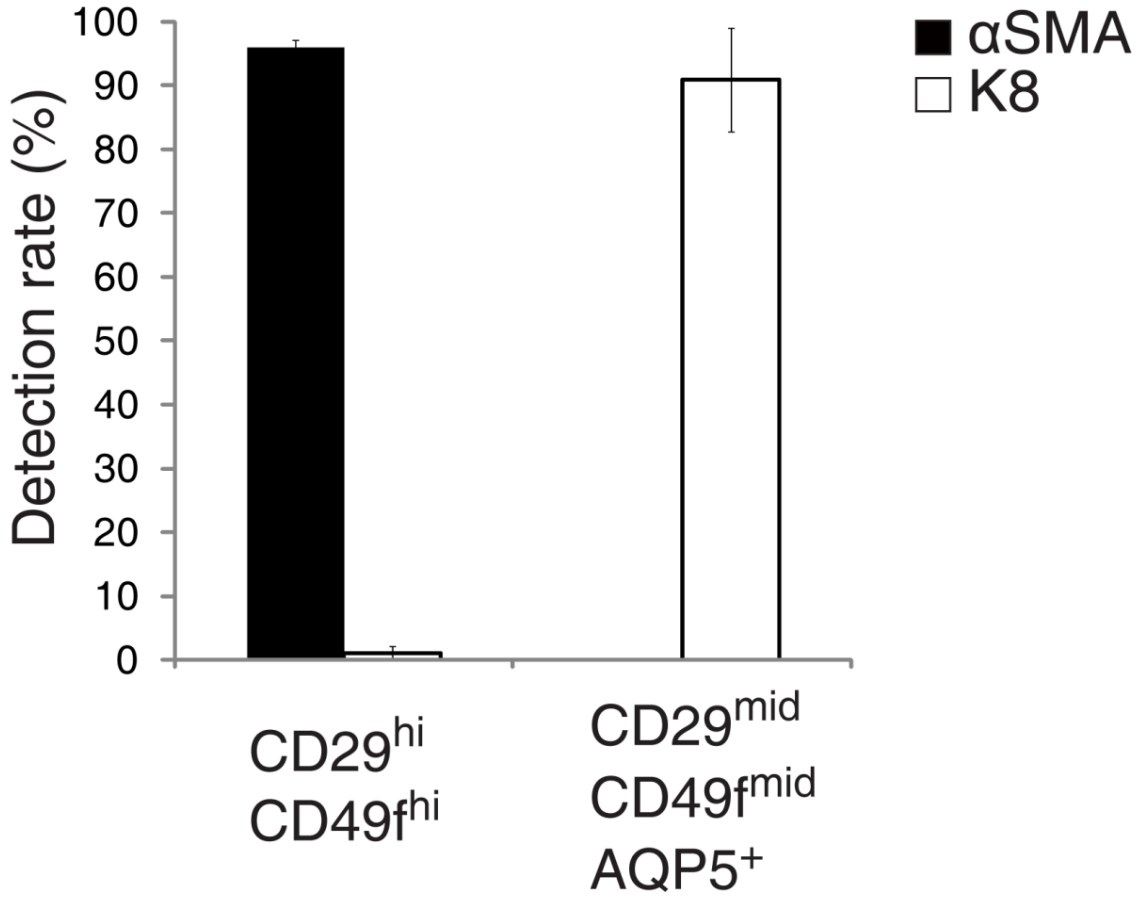

Figure 41. Enrichment of the CD29^{hi}CD49f^{hi} and CD29^{mid}CD49f^{mid}AQP5^{+} subpopulations for αSMA- and K8-positive cells, respectively.
αSMA- and K8-positive cells in the CD29^{hi}CD49f^{hi} and CD29^{mid}CD49f^{mid}AQP5^{+} subpopulations were quantified in five representative fields each.

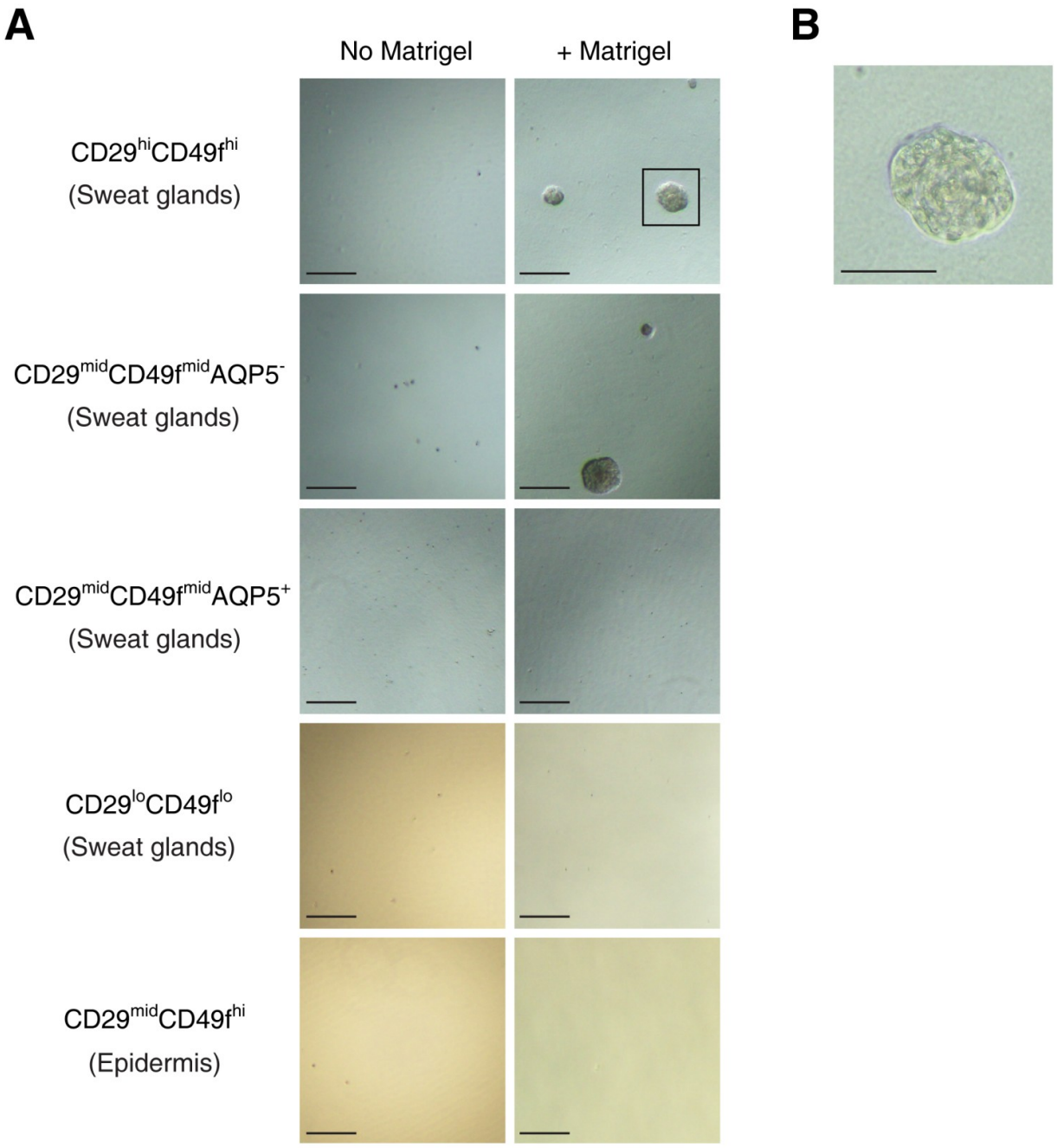

Figure 42. Generation of spheres by the CD29^{hi}CD49f^{hi} and CD29^{mid}CD49f^{mid}AQP5^{-} subpopulations of human sweat glands.
(A) Morphologies of the CD29^{hi}CD49f^{hi}, CD29^{mid}CD49f^{mid}AQP5^{-}, CD29^{mid}CD49f^{mid}AQP5^{+}, and CD29^{lo}CD49f^{lo} subpopulations and the epidermal CD29^{mid}CD49f^{hi} subpopulation grown under nonadherent conditions in the presence or absence of Matrigel. (B) Enlarged view of the boxed area in (A). Scale bars: 100 μm (A); 50 μm (B).

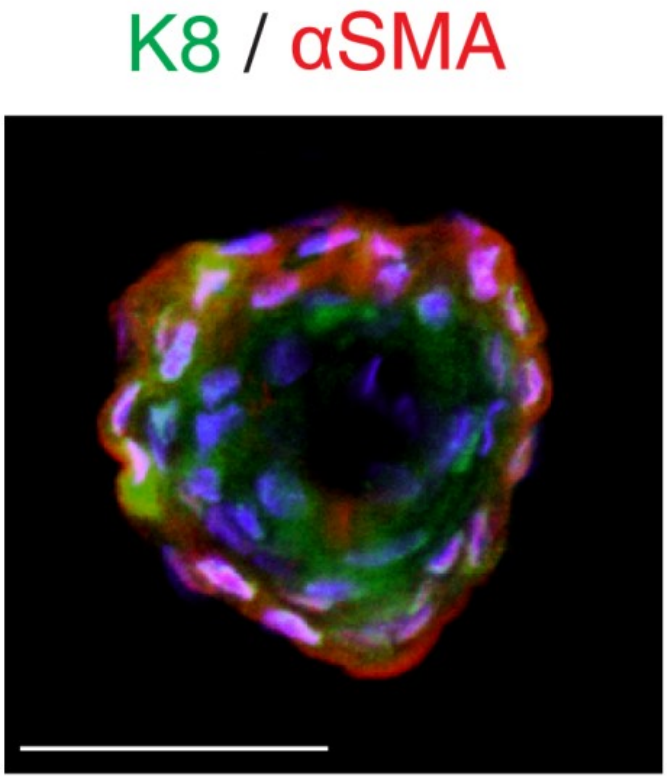

Figure 43. Expression of luminal cell markers by myoepithelial cell subpopulation-derived spheres.
Confocal immunofluorescence staining of spheres derived from the $CD29^{hi}CD49f^{hi}$ subpopulation, showing the expression of K8 (green) and αSMA (red) with nuclear counterstaining (Hoechst 33342; blue). The outer cells of the spheres were positive for αSMA, while the inner cells were positive for K8. Scale bars: 50 μm.

portions.

Self-renewal ability of the sweat gland myoepithelial subpopulation

The self-renewal ability of stem cells is usually assessed by measuring their sphere-forming ability. I therefore assessed the self-renewal ability of the $CD29^{hi}CD49f^{hi}$ myoepithelial subpopulation in human eccrine sweat glands. First, to test the long-term proliferative potential of these myoepithelial cells, I evaluated the secondary and tertiary sphere-forming abilities of the P1 ($CD29^{hi}CD49f^{hi}$) subpopulation (Spike et al., 2012). P1 ($CD29^{hi}CD49f^{hi}$)-derived spheres were dissociated and seeded onto ultralow-adherence plates at 1000 cells/cm^2 in sphere culture medium containing 2% Matrigel. The sphere-derived cells were capable of generating secondary and tertiary spheres (Figure 44). To verify the clonal growth of the myoepithelial cells, I examined whether single myoepithelial cells are capable of generating spheres. P1 ($CD29^{hi}CD49f^{hi}$) cells were cultured at clonal density on 96-well ultralow-adherence plates for 14 days in sphere culture medium containing 2% Matrigel. Single cells from the P1 ($CD29^{hi}CD49f^{hi}$) subpopulation formed spheres (sphere-forming efficiency = 2.3%), whereas single cells from the P3 ($CD29^{mid}CD49f^{mid}AQP5^{+}$) subpopulation did not (Figure 45, 46). The spheres generated by the P1 ($CD29^{hi}CD49f^{hi}$) cells showed little evidence of the enlarged lumen and branch-like morphogenesis shown by mammary glands *in vitro* (Figure 47). These findings indicated that the myoepithelial $CD29^{hi}CD49f^{hi}$ subpopulation contains stem cells with high proliferative potential.

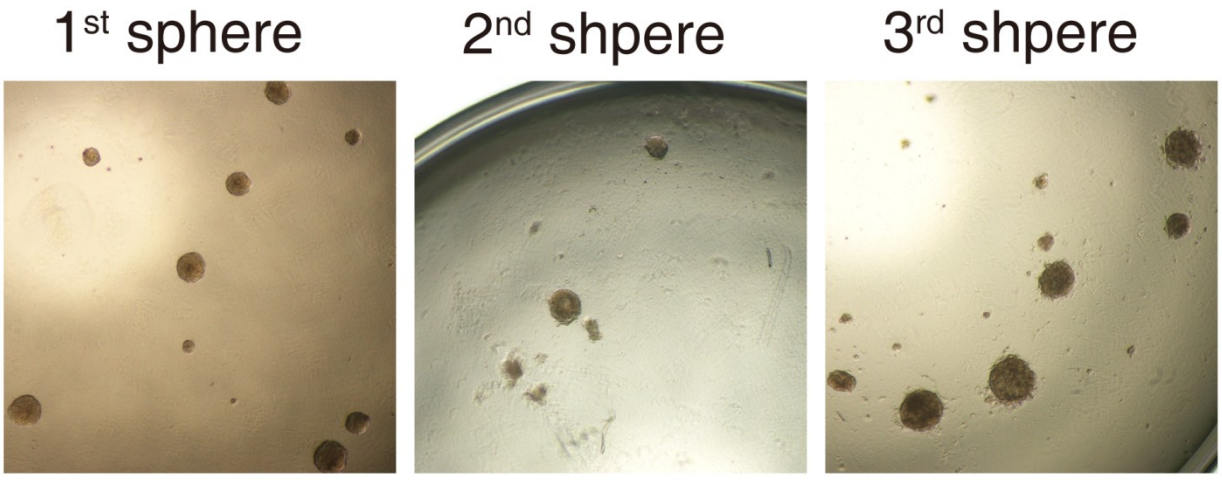

Figure 44. Generation of secondary and tertiary spheres from the CD29^{hi}CD49f^{hi} subpopulation.
Morphologies of cell spheres generated from CD29^{hi}CD49f^{hi} cells. Secondary and tertiary spheres were generated from enzymatically disaggregated cell suspensions derived from primary and secondary spheres, respectively.

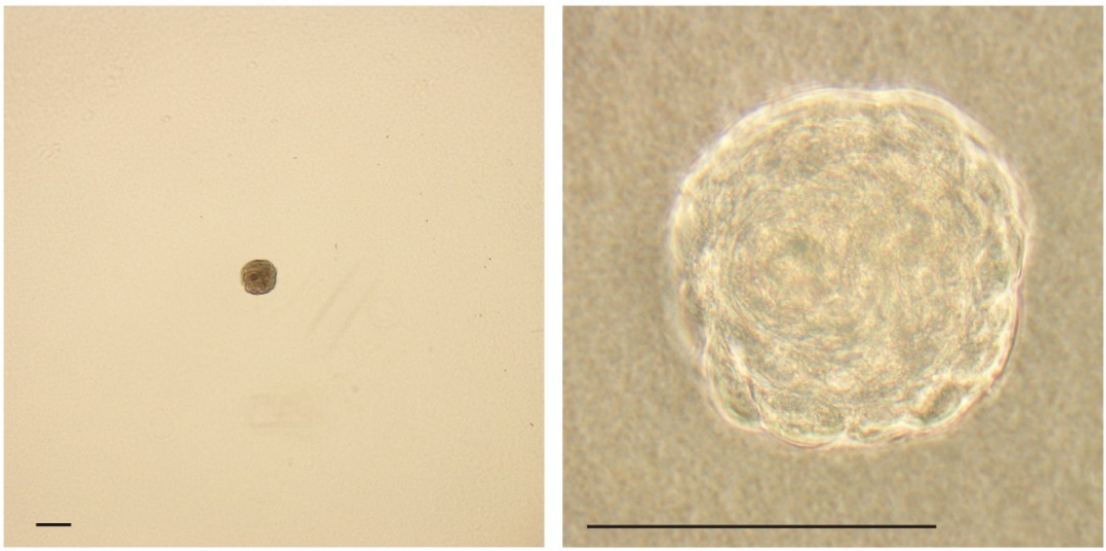

Figure 45. Generation of spheres from single myoepithelial cells.
Spheres generated by clonal expansion of single cells within the $CD29^{hi}CD49f^{hi}$ myoepithelial subpopulation. The right panel shows a high-magnification view of the micrograph in the left panel. Scale bars: 100 μm.

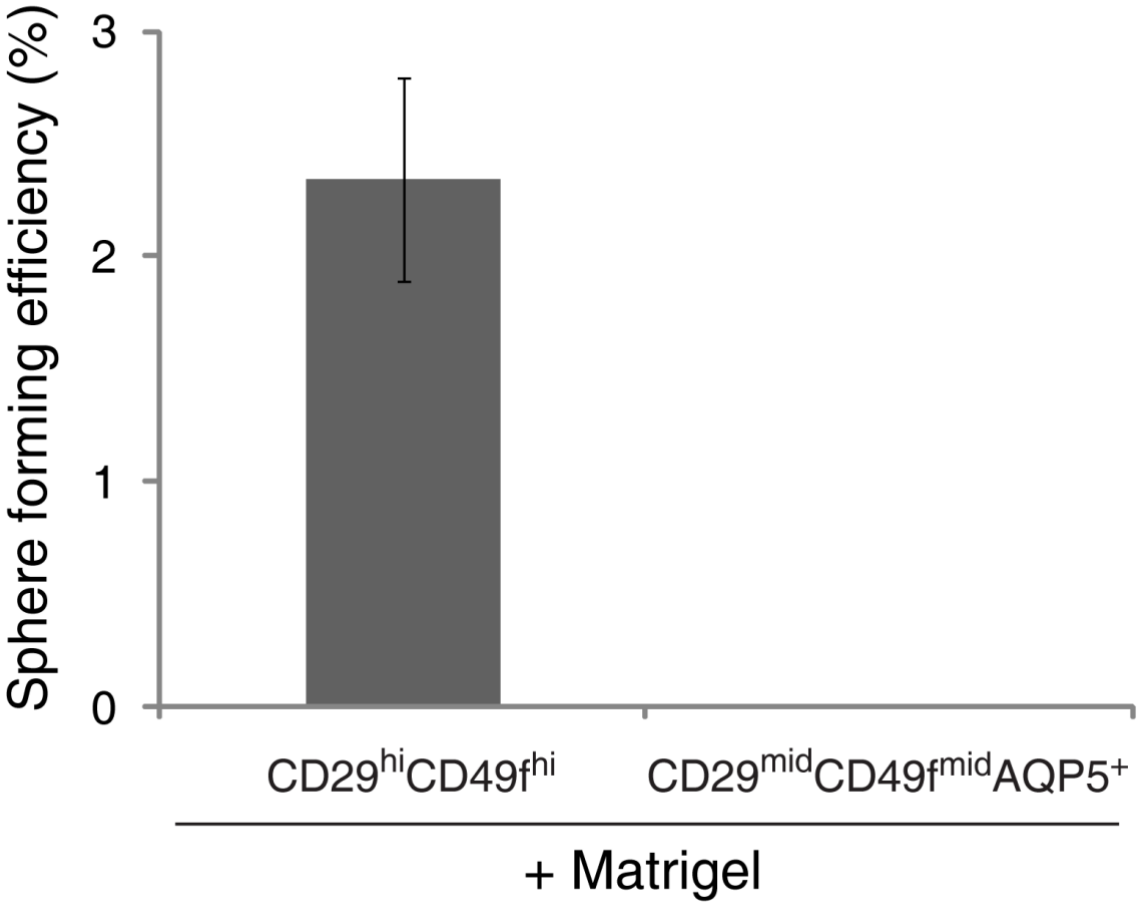

Figure 46. Formation of spheres by single cells from the CD29^{hi}CD49f^{hi}, but not the CD29^{mid}CD49f^{mid}AQP5^{+}, subpopulation.
Single cells from the CD29^{hi}CD49f^{hi} and CD29^{mid}CD49f^{mid}AQP5^{+} subpopulations were seeded in 96-well plates at clonal density. The sphere-forming efficiency was assessed as the percentage of cells that formed spheres.

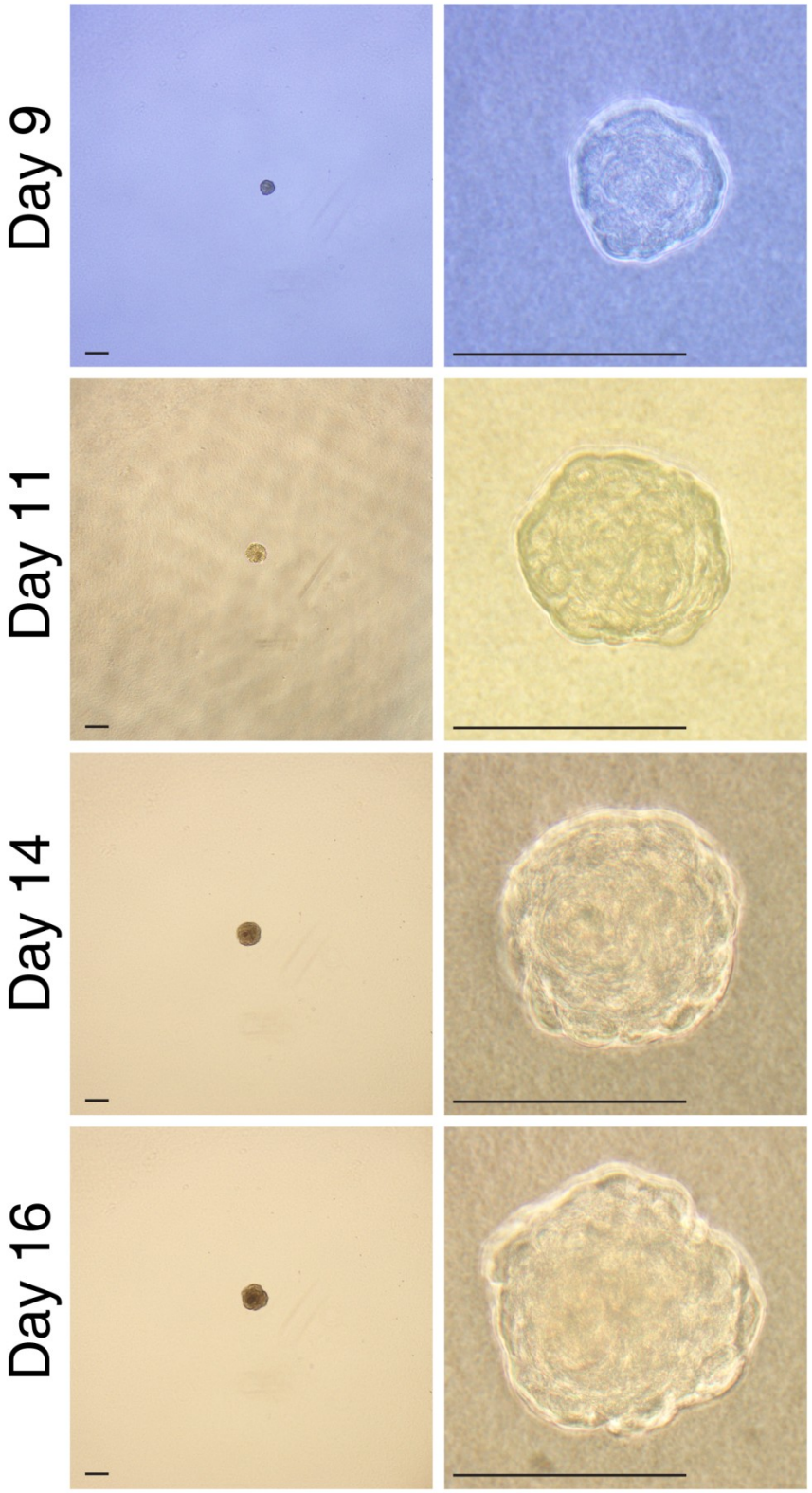

Figure 47. Lack of mammary gland-like branching morphogenesis by myoepithelial cell-derived spheres.
Shapes of spheres formed by single $CD29^{hi}CD49f^{hi}$ cells over 16 days. The right panel shows a high magnification view of the micrograph in the left panel. Scale bars: 100 μm.

II-5 Discussion

The existence of human sweat gland stem cells was originally suggested by histological studies on skin wound repair. “Partial” sweat glands, from which the epidermal sweat duct unit was removed after superficial epidermal injury, were found to regenerate epidermal ducts (Lobitz et al., 1954). This ability of sweat glands to regenerate straight ducts was supported by findings showing that the residues of human sweat glands present after dermal trauma regenerated the dermal ducts of sweat glands (Lobitz et al., 1956). Furthermore, cells derived from microsurgically isolated sweat gland organs were found capable of reconstituting a multilayered epidermis-like structure *in vitro*, suggesting that human sweat glands contain multipotent cells. (Biedermann et al., 2010). Nevertheless, the compartments of sweat glands that contribute to duct regeneration and possess self-renewal ability remained unclear. In this study, I identified human sweat gland stem cells residing among the myoepithelial cells of the secretory portion. Myoepithelial cells showed high levels of expression of the stem cell markers CD29 and Notch and were isolated as a $CD29^{hi}CD49f^{hi}$ subpopulation. These freshly isolated cells exhibited multipotency, as evidenced by the generation of sweat gland-like spheres composed of both cell types expressing secretory luminal and myoepithelial cell markers, respectively. Furthermore, the $CD29^{hi}CD49f^{hi}$ myoepithelial subpopulation exhibited self-renewal ability and high proliferative potential in sphere-forming assays. Taken together, these findings indicate that the myoepithelial cell-enriched $CD29^{hi}CD49f^{hi}$ subpopulation contains stem cells with multipotency and self-renewal ability. However, it remains to be determined whether other cell types contribute to the stem cell characteristics of the $CD29^{hi}CD49f^{hi}$ subpopulation.

Mouse sweat glands contain two multipotent stem cell populations, myoepithelial and basal duct

cells (Lu et al., 2012). The basal duct cells form straight and coiled duct-like structures, while the myoepithelial cells generate a sweat gland-like structure that expresses ATP1a1 when transplanted into mammary fat pads. Consistent with these observations, the results presented here suggest that the basal duct cells of human sweat glands also contain stem cells distinct from those present among myoepithelial cells. These basal duct cells, isolated as the $CD29^{mid}CD49f^{mid}AQP5^{-}$ subpopulation, were capable of generating spheres, making it likely that these cells, in addition to the $CD29^{hi}CD49f^{hi}$ myoepithelial cells in the secretory portion, contain stem cells that are both self-renewing and multipotent. These human sweat gland stem cells may therefore contribute to the construction and maintenance of the glandular organization of sweat glands.

Similar to sweat glands, mammary glands are glandular organs consisting of myoepithelial and luminal cells. Several lines of evidence indicate that mammary glands have evolved from sweat glands (Jenness, 1974; Long, 1969; Oftedal, 2002). I found that sweat gland stem cells share many features with mammary gland stem cells (Shackleton et al., 2006; Spike et al., 2012; Stingl et al., 2006). Similar to mammary gland stem cells, sweat gland stem cells predominantly reside among myoepithelial cells and are capable of generating exocrine gland-like hollow spheres *in vitro*. Furthermore, both mammary and sweat gland stem cells require Matrigel, a reconstituted gel composed of basement membrane molecules, to form spheres *in vitro*. These similarities suggest that mammary and sweat gland stem cells share common mechanisms of exocrine tissue organogenesis. However, there are also differences between mammary and sweat gland stem cells. Mammary gland stem cells contribute to mammary gland development during multiple cycles of pregnancy, whereas sweat glands undergo little periodic cycling (Shackleton et al., 2006). Human sweat gland cells are generally in a dormant state and are detected as label-retaining cells in 5-bromo-2′-deoxyuridine

pulse-chase experiments *in vivo* (Morimoto and Saga, 1995), suggesting that human sweat gland myoepithelial cells are generally quiescent.

Another feature distinguishing mammary and sweat gland stem cells is their patterns of expression of Notch, a cell surface protein that controls the choice between self-renewal and differentiation. Notch is expressed predominantly by myoepithelial cells in sweat glands, but by luminal cells in mammary glands (Bouras et al., 2008). Constitutive Notch activation in mammary gland stem cells promotes commitment to luminal cell differentiation and eventually causes the development of tumors, whereas constitutive inhibition of Notch signaling leads to expansion of mammary stem cells (Bouras et al., 2008). Therefore, the opposing expression pattern of Notch in sweat glands may account, at least in part, for the infrequency of sweat gland tumors. Further comparative studies of sweat gland stem cells and other epithelial stem cells, including hair follicle and mammary stem cells, may lead to a better understanding of the mechanisms regulating epithelial morphogenesis and homeostasis of these stem cells.

In conclusion, I have provided evidence that human sweat gland stem cells reside among myoepithelial cells, similar to findings for mammary stem cells. Human sweat gland myoepithelial cells can be isolated as a $CD29^{hi}CD49f^{hi}$ subpopulation. Sweat gland stem cells are normally in a quiescent state in secretory portions, but exhibit high proliferative potential and the ability to regenerate sweat gland-like spheres comprising both luminal and myoepithelial cells *in vitro*. The identification of human sweat gland stem cells may provide new insights for the development of bioengineered glandular organs.

General Discussion

Eccrine sweat glands are important in maintaining human body homeostasis, making them a topic of intensive histological and physiological investigations for many decades. However, studies of eccrine sweat glands utilizing the techniques of modern structural and molecular biology, such as four-dimensional visualization, lineage-tracing, and nucleotide-labeling techniques, have lagged behind studies of other glands, because *Homo sapiens* is the only species in which eccrine sweat glands are distributed throughout the body. Therefore, the properties of human eccrine sweat glands, including their glandular structure, functions such as sweating, morphogenesis, and glandular homeostasis and regeneration, have remained largely unknown. Recent studies of other exocrine glands have enabled the features of human eccrine sweat glands to be clarified. The experiments described here have revealed the complex coiled structures and glandular stem cells of these glands. A human eccrine sweat gland is a three-dimensional coiled structure more intricate than the structural scheme delineated from histological analyses. Especially, the secretory portions of sweat glands are frequently entangled and the myoepithelial cells are oriented along the direction of these entangled secretory tubules. Furthermore, the myoepithelial cells are stem cells possessing self-renewal ability and multipotency. These myoepithelial cells are housed in a unique environment in which they are encircled by closely neighboring blood vessels and nerve fibers. These findings provided not only knowledge of the structural and cell biological natures of eccrine sweat glands but also delineate methods of studying these glands, including three-dimensional structural analysis and methods of isolating each sweat gland compartment. These results will likely contribute greatly to further understanding of the structure and functions of human eccrine sweat glands.

Regeneration of functional eccrine sweat glands

There are major challenges in regenerating functional eccrine sweat glands for patients with impaired thermoregulation. In humans, transplanted epidermal cells were thought to form eccrine sweat gland-like structures in the dermis (Shikiji et al., 2003), but these regenerated constructs hardly expressed sweat gland cell markers and formed few rounded tubules (Figure 2). Sweat gland stem cells transplanted into mammary fat pads of mice formed sweat gland-like structures, which were histologically observed as unbranched hollow tubules (Lu et al., 2012). However, the ability of these regenerated glands to form coiled structures has remained unclear. Furthermore, regenerated sweat glands must function as a thermoregulatory apparatus capable of sweating. Some eccrine sweat glands have sweating ability (active sweat glands), whereas others do not (inactive sweat glands), with their ratio remaining constant after age 2.5 years and being affected by the thermal environment during this period (Kuno, 1956), suggesting that neurogenic stimuli are essential for the generation of active sweat glands. Thus, regeneration of functional eccrine sweat glands requires reconstruction of not only unbranched coiled tubular structures but also their dermal components, i.e., nerve fibers, to facilitate effective sweat secretion.

In this study, I showed that myoepithelial cells are enriched in sweat gland stem cells, with the latter possessing the ability to regenerate sweat gland-like spheres with apical and basal cell layers that express luminal (K8) and myoepithelial (αSMA) markers, respectively. Additionally, I was able to determine the three-dimensional coiled structure of eccrine sweat glands. The coiled secretory portion is not only frequently bent but also irregularly entangled, suggesting that regenerated sweat glands require three-dimensional entangled structures for sweat secretion. I also determined the

three-dimensional arrangements of glandular nerve fibers in the sweat glands. Intriguingly, the glandular nerve fibers surrounded the myoepithelial cell layers, containing abundant stem cells, of the secretory portions. These results suggest that the myoepithelial cells not only possess the ability to regenerate eccrine sweat gland structures but also modulate sweating ability in response to neurogenic stimuli from glandular nerve fibers. Thus, these findings provide insights into the regeneration of functional eccrine sweat glands, which may be useful for patients with impaired thermoregulation, including burn victims.

Epidermal regeneration derived from eccrine sweat gland cells

Eccrine sweat glands that function as a thermoregulatory apparatus have the ability to regenerate the epidermis after injury. The epidermis is maintained and regenerated by epidermal stem cells present in the interfollicular epidermis and hair follicles. Keratinocyte stem cells in the interfollicular epidermis routinely generate stratified epidermis in vivo (Ghazizadeh and Taichman, 2001; Jones et al., 1995). Hair follicle stem cells are in a quiescent state in the bulge region of the hair shaft, but they proliferate and give rise to epidermis during wound healing (Ito et al., 2005). The existence of sweat gland epidermal stem cells was originally suggested in histological studies of dermal wound repair. Sweat glands were reported to regenerate the epidermis in response to superficial injury to human skin, although traumatized skin includes hair follicles, a recognized source of epidermal stem cells (Lobitz et al., 1954). The ability of sweat glands to regenerate the epidermis was supported by results showing that porcine sweat glands can regenerate the epidermis in wounds completely stripped of hair follicles (Miller et al., 1998). Regeneration of the epidermis by sweat glands was further demonstrated by the ability of enzymatically isolated human sweat glands to form stratified

epidermis *in vitro* (Biedermann et al., 2010). Recently, the combination of immunohistochemistry and computer-assisted three-dimensional reconstruction showed that sweat glands could reconstitute the epidermis after partial-thickness wounds in human forearms (Rittie et al., 2013). These results indicate that sweat glands contain cells that regenerate the epidermis, but the epidermal stem cells that contribute to re-epithelialization have not been identified. Label retaining cells, stem-like cells possessing slow-cycling properties, have been localized in human sweat glands and found to express the epidermal stem cell marker, K15 (Nakamura and Tokura, 2009). This finding suggests that epidermal stem cells are present in sweat glands, although their potential for self-renewal and multipotency has not yet been demonstrated. The results shown in this study suggest that human sweat gland myoepithelial cells are a third type of epidermal stem cell. Similar to hair follicle stem cells, human sweat gland myoepithelial cells showed a low level of expression of the proliferative marker Ki-67, indicating that they have low proliferative activity. Isolated human sweat gland myoepithelial cells showed high proliferative potential during *in vitro* sphere culture. These results suggest that sweat gland epidermal stem cells are normally quiescent and transiently acquire a high proliferative potential during the wound healing process, similar to hair follicle bulge stem cells. Similarly, mouse sweat gland myoepithelial cells were shown to regenerate the epidermis when transplanted into back skin *in vivo* (Lu et al., 2012). Collectively, human eccrine sweat glands distributed throughout the entire skin surface have been widely implicated in skin homeostasis, including thermoregulation and epidermal regeneration. Further understanding of the structure and functions of eccrine sweat glands may strongly contribute to skin regeneration.

Sweat gland stem cell niche

The structural and cell biological analyses of eccrine sweat glands showed that myoepithelial cells possessing self-renewal ability and multipotency are housed in a unique environment, closely surrounded by neighboring blood vessels and nerve fibers. Stem cells of various tissues exist within unique microenvironments, called niches (Fuchs et al., 2004; Moore and Lemischka, 2006). These niches are composed of microenvironmental cells that nurture stem cells and enable them to maintain tissue homeostasis (Hall and Watt, 1989; Watt and Hogan, 2000). Key components of these niches include direct interactions between stem cells and neighboring cells, secreted factors, extracellular matrix, environmental signals, and physical factors, including elasticity and stiffness. Blood vessels are categorized as cellular components that constitute niches (Levenberg, 2005). In the skin, for example, growing hair follicles are surrounded by blood vessels. Follicle vascularization promotes hair growth and increases hair follicles and hair size, indicating that the vascular niche maintains epidermal stem cells in hair follicles (Yano et al., 2001). I found that sweat gland blood vessels are spatially distributed along with the tubular structure of eccrine sweat glands. The distributions of blood vessels in eccrine sweat glands are similar to those in seminiferous tubules. The testicular blood vessels form networks along with seminiferous tubules (Oatley and Brinster, 2012). The spermatogonial stem cells in seminiferous tubules are preferentially located adjacent to blood vessels and are maintained by factors supplied by these blood vessels (Oatley and Brinster, 2012). However, it remains unclear whether the sweat gland blood vessels are part of the microenvironments that maintain sweat gland stem cells. Nerve cells are also known to comprise the cellular component of the niche. The nerve fibers that wrap the upper bulge regions of hair follicles secrete sonic hedgehog, a signaling molecule vital for neural development, and create a molecularly and phenotypically distinct hair follicle stem cell population (Brownell et al., 2011). In salivary

glands, parasympathetic innervation occurs in parallel with salivary gland development (Coughlin, 1975) and is essential for regeneration after injury (Proctor and Carpenter, 2007). Furthermore, parasympathetic innervation has been shown to maintain the salivary gland progenitor population in an undifferentiated state, which was required for organogenesis (Knox et al., 2010). Although the eccrine sweat glands are innervated by parasympathetic nerves, it remains unknown whether these nerves are part of the niches that maintain sweat gland stem cells. I found that nerve fibers surround the sweat gland secretory portions, but hardly surround the ducts. Myoepithelial cells respond to neurotransmitters secreted by parasympathetic nerves and induce the contraction of glandular tubules for sweat secretion, suggesting that the sweat gland stem cells within myoepithelial cells adjacent to the parasympathetic nerves may be largely influenced by their neural microenvironment. In addition, eccrine sweat glands are also encased by adipocytes. Adipocyte lineage cells have been shown to contribute to the skin stem cell niche by expressing platelet-derived growth factor, regulating follicular stem cell activity and promoting hair cycling (Festa et al., 2011). Mammary glands are also embedded in fat pads, which contain adipocytes that provide nutrients and energy during lactation and are regulated by pregnancy-associated hormones (Gimble et al., 2007). Eccrine sweat glands rarely undergo the expansion and regression of hair follicles and mammary glands, but homeostasis of sweat glands may be maintained by soluble factors secreted by sweat gland adipocytes. Thus, sweat gland stem cells may be governed by the specialized niches comprised of a variety of cell types, each with a distinct function (Figure D-1). Clarifying the properties of sweat gland stem cells and the distributions of glandular dermal components may provide further insight into the nature of stem cells and their niches in spatially intricate eccrine sweat glands.

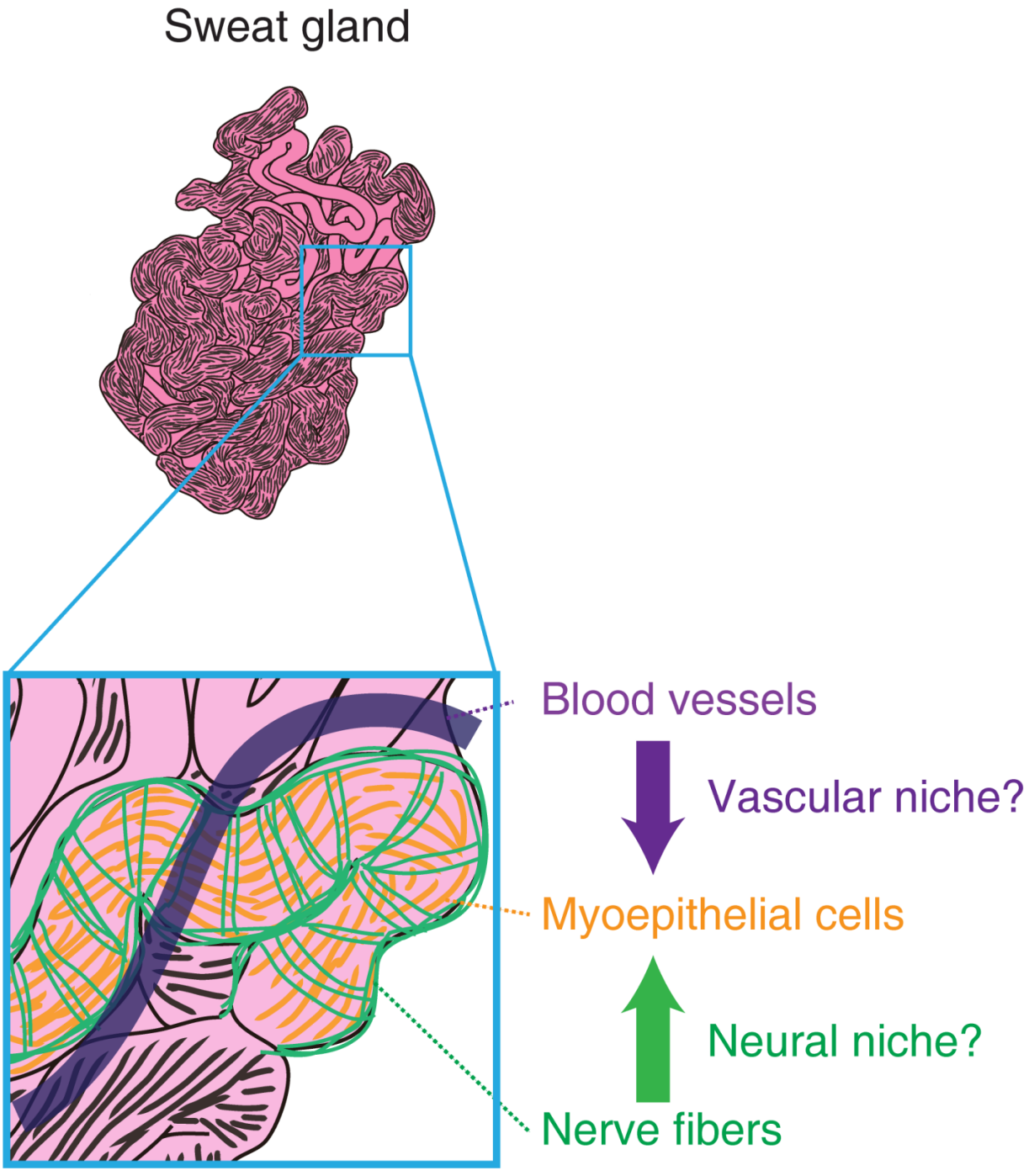

Figure D-1. Possible schematic presentation of sweat gland stem cell niche.
Sweat gland blood vessels are spatially distributed along the tubular structure of eccrine sweat glands, with these structures wrapped by sweat gland nerve fibers.

References

Alonso L and Fuchs E 2006. The hair cycle. *J Cell Sci*, **119**: 391-393.

Biedermann T, Pontiggia L, Bottcher-Haberzeth S, Tharakan S, Braziulis E, Schiestl C, Meuli M and Reichmann E 2010. Human eccrine sweat gland cells can reconstitute a stratified epidermis. *The Journal of investigative dermatology*, **130**: 1996-2009.

Blanpain C and Fuchs E 2009. Epidermal homeostasis: a balancing act of stem cells in the skin. *Nature reviews Molecular cell biology*, **10**: 207-217.

Blanpain C, Lowry WE, Geoghegan A, Polak L and Fuchs E 2004. Self-renewal, multipotency, and the existence of two cell populations within an epithelial stem cell niche. *Cell*, **118**: 635-648.

Bouras T, Pal B, Vaillant F, Harburg G, Asselin-Labat ML, Oakes SR, Lindeman GJ and Visvader JE 2008. Notch signaling regulates mammary stem cell function and luminal cell-fate commitment. *Cell stem cell*, **3**: 429-441.

Brayden DJ and Fitzpatrick J 1995. Cultured human sweat gland epithelia: isolation of glands using neutral red. *Pharm Res*, **12**: 171-175.

Brownell I, Guevara E, Bai CB, Loomis CA and Joyner AL 2011. Nerve-derived sonic hedgehog defines a niche for hair follicle stem cells capable of becoming epidermal stem cells. *Cell*

stem cell, **8**: 552-565.

Campos LS, Decker L, Taylor V and Skarnes W 2006. Notch, epidermal growth factor receptor, and beta1-integrin pathways are coordinated in neural stem cells. *J Biol Chem*, **281**: 5300-5309.

Coughlin MD 1975. Early development of parasympathetic nerves in the mouse submandibular gland. *Dev Biol*, **43**: 123-139.

Debnath J and Brugge JS 2005. Modelling glandular epithelial cancers in three-dimensional cultures. *Nature reviews Cancer*, **5**: 675-688.

Dodt HU, Leischner U, Schierloh A, Jahrling N, Mauch CP, Deininger K, Deussing JM, Eder M, Zieglgansberger W and Becker K 2007. Ultramicroscopy: three-dimensional visualization of neuronal networks in the whole mouse brain. *Nature methods*, **4**: 331-336.

Dontu G, Abdallah WM, Foley JM, Jackson KW, Clarke MF, Kawamura MJ and Wicha MS 2003. In vitro propagation and transcriptional profiling of human mammary stem/progenitor cells. *Genes Dev*, **17**: 1253-1270.

Driskell RR, Clavel C, Rendl M and Watt FM 2011. Hair follicle dermal papilla cells at a glance. *J Cell Sci*, **124**: 1179-1182.

Eiraku M, Takata N, Ishibashi H, Kawada M, Sakakura E, Okuda S, Sekiguchi K, Adachi T and Sasai Y 2011. Self-organizing optic-cup morphogenesis in three-dimensional culture.

Nature, **472**: 51-56.

Erturk A, Becker K, Jahrling N, Mauch CP, Hojer CD, Egen JG, Hellal F, Bradke F, Sheng M and Dodt HU 2012. Three-dimensional imaging of solvent-cleared organs using 3DISCO. *Nature protocols*, **7**: 1983-1995.

Ferraris C, Chevalier G, Favier B, Jahoda CA and Dhouailly D 2000. Adult corneal epithelium basal cells possess the capacity to activate epidermal, pilosebaceous and sweat gland genetic programs in response to embryonic dermal stimuli. *Development*, **127**: 5487-5495.

Festa E, Fretz J, Berry R, Schmidt B, Rodeheffer M, Horowitz M and Horsley V 2011. Adipocyte lineage cells contribute to the skin stem cell niche to drive hair cycling. *Cell*, **146**: 761-771.

Fuchs E 2009. Finding one's niche in the skin. *Cell stem cell*, **4**: 499-502.

Fuchs E, Tumbar T and Guasch G 2004. Socializing with the neighbors: stem cells and their niche. *Cell*, **116**: 769-778.

Fujiwara H, Ferreira M, Donati G, Marciano DK, Linton JM, Sato Y, Hartner A, Sekiguchi K, Reichardt LF and Watt FM 2011. The basement membrane of hair follicle stem cells is a muscle cell niche. *Cell*, **144**: 577-589.

Ghazizadeh S and Taichman LB 2001. Multiple classes of stem cells in cutaneous epithelium: a lineage analysis of adult mouse skin. *EMBO J*, **20**: 1215-1222.

Gimble JM, Katz AJ and Bunnell BA 2007. Adipose-derived stem cells for regenerative medicine.

Circ Res, **100**: 1249-1260.

Hall PA and Watt FM 1989. Stem cells: the generation and maintenance of cellular diversity. *Development*, **106**: 619-633.

Hama H, Kurokawa H, Kawano H, Ando R, Shimogori T, Noda H, Fukami K, Sakaue-Sawano A and Miyawaki A 2011. Scale: a chemical approach for fluorescence imaging and reconstruction of transparent mouse brain. *Nat Neurosci*, **14**: 1481-1488.

Hashimoto K, Gross BG and Lever WF 1965. The ultrastructure of the skin of human embryos. I. The intraepidermal eccrine sweat duct. *The Journal of investigative dermatology*, **45**: 139-151.

Hertle MD, Adams JC and Watt FM 1991. Integrin expression during human epidermal development in vivo and in vitro. *Development*, **112**: 193-206.

Holyoke JB and Lobitz WC, Jr. 1952. Histologic variations in the structure of human eccrine sweat glands. *The Journal of investigative dermatology*, **18**: 147-167.

Ito M, Liu Y, Yang Z, Nguyen J, Liang F, Morris RJ and Cotsarelis G 2005. Stem cells in the hair follicle bulge contribute to wound repair but not to homeostasis of the epidermis. *Nat Med*, **11**: 1351-1354.

Jenkinson DM, Elder HY and Bovell DL 2007. Equine sweating and anhidrosis Part 2: anhidrosis. *Veterinary dermatology*, **18**: 2-11.

Jenness R 1974. Proceedings: Biosynthesis and composition of milk. *The Journal of investigative dermatology*, **63**: 109-118.

Jensen KB and Watt FM 2006. Single-cell expression profiling of human epidermal stem and transit-amplifying cells: Lrig1 is a regulator of stem cell quiescence. *Proc Natl Acad Sci U S A*, **103**: 11958-11963.

Jones PH, Harper S and Watt FM 1995. Stem cell patterning and fate in human epidermis. *Cell*, **80**: 83-93.

Jones PH and Watt FM 1993. Separation of human epidermal stem cells from transit amplifying cells on the basis of differences in integrin function and expression. *Cell*, **73**: 713-724.

Ke MT, Fujimoto S and Imai T 2013. SeeDB: a simple and morphology-preserving optical clearing agent for neuronal circuit reconstruction. *Nat Neurosci*, **16**: 1154-1161.

Knox SM, Lombaert IM, Haddox CL, Abrams SR, Cotrim A, Wilson AJ and Hoffman MP 2013. Parasympathetic stimulation improves epithelial organ regeneration. *Nature communications*, **4**: 1494.

Knox SM, Lombaert IM, Reed X, Vitale-Cross L, Gutkind JS and Hoffman MP 2010. Parasympathetic innervation maintains epithelial progenitor cells during salivary organogenesis. *Science*, **329**: 1645-1647.

Kunisada M, Cui CY, Piao Y, Ko MS and Schlessinger D 2009. Requirement for Shh and Fox

family genes at different stages in sweat gland development. *Hum Mol Genet*, **18**: 1769-1778.

Kuno Y 1956. Human Perspiration. *Amer Lect Ser*, **285**.

Leblond CP 1964. Classification of Cell Populations on the Basis of Their Proliferative Behavior. *Natl Cancer Inst Monogr*, **14**: 119-150.

Legg J, Jensen UB, Broad S, Leigh I and Watt FM 2003. Role of melanoma chondroitin sulphate proteoglycan in patterning stem cells in human interfollicular epidermis. *Development*, **130**: 6049-6063.

Levenberg S 2005. Engineering blood vessels from stem cells: recent advances and applications. *Curr Opin Biotechnol*, **16**: 516-523.

Lobitz WC, Jr., Holyoke JB and Brophy D 1956. Response of the human eccrine sweat duct to dermal injury. *The Journal of investigative dermatology*, **26**: 247-259; discussion, 259-262.

Lobitz WC, Jr., Holyoke JB and Montagna W 1954. Responses of the human eccrine sweat duct to controlled injury: growth center of the epidermal sweat duct unit. *The Journal of investigative dermatology*, **23**: 329-344.

Lombaert IM, Brunsting JF, Wierenga PK, Faber H, Stokman MA, Kok T, Visser WH, Kampinga HH, de Haan G and Coppes RP 2008. Rescue of salivary gland function after stem cell transplantation in irradiated glands. *PloS one*, **3**: e2063.

Long CA 1969. The Origin and Evolution of Mammary Glands. *Bioscience*, **19**: 519-523.

Lu CP, Polak L, Rocha AS, Pasolli HA, Chen SC, Sharma N, Blanpain C and Fuchs E 2012. Identification of stem cell populations in sweat glands and ducts reveals roles in homeostasis and wound repair. *Cell*, **150**: 136-150.

Luebberding S, Krueger N and Kerscher M 2013. Skin physiology in men and women: in vivo evaluation of 300 people including TEWL, SC hydration, sebum content and skin surface pH. *International journal of cosmetic science*, **35**: 477-483.

Lyle S, Christofidou-Solomidou M, Liu Y, Elder DE, Albelda S and Cotsarelis G 1998. The C8/144B monoclonal antibody recognizes cytokeratin 15 and defines the location of human hair follicle stem cells. *J Cell Sci*, **111 (Pt 21)**: 3179-3188.

Miller SJ, Burke EM, Rader MD, Coulombe PA and Lavker RM 1998. Re-epithelialization of porcine skin by the sweat apparatus. *The Journal of investigative dermatology*, **110**: 13-19.

Mimura I and Nangaku M 2010. The suffocating kidney: tubulointerstitial hypoxia in end-stage renal disease. *Nature reviews Nephrology*, **6**: 667-678.

Moll I and Moll R 1992. Changes of expression of intermediate filament proteins during ontogenesis of eccrine sweat glands. *The Journal of investigative dermatology*, **98**: 777-785.

Montagna W, Chase HB and Lobitz WC, Jr. 1953. Histology and cytochemistry of human skin. IV. The eccrine sweat glands. *The Journal of investigative dermatology*, **20**: 415-423.

Moore KA and Lemischka IR 2006. Stem cells and their niches. *Science*, **311**: 1880-1885.

Morimoto Y and Saga K 1995. Proliferating cells in human eccrine and apocrine sweat glands. *J Histochem Cytochem*, **43**: 1217-1221.

Munger BL 1961. The ultrastructure and histophysiology of human eccrine sweat glands. *The Journal of biophysical and biochemical cytology*, **11**: 385-402.

Murakami M, Ohtake T, Dorschner RA, Schittek B, Garbe C and Gallo RL 2002. Cathelicidin anti-microbial peptide expression in sweat, an innate defense system for the skin. *The Journal of investigative dermatology*, **119**: 1090-1095.

Nakamura M and Tokura Y 2009. The localization of label-retaining cells in eccrine glands. *The Journal of investigative dermatology*, **129**: 2077-2078.

Nguyen BC, Lefort K, Mandinova A, Antonini D, Devgan V, Della Gatta G, Koster MI, Zhang Z, Wang J, Tommasi di Vignano A, Kitajewski J, Chiorino G, Roop DR, Missero C and Dotto GP 2006. Cross-regulation between Notch and p63 in keratinocyte commitment to differentiation. *Genes Dev*, **20**: 1028-1042.

Oatley JM and Brinster RL 2012. The germline stem cell niche unit in mammalian testes. *Physiol Rev*, **92**: 577-595.

Oftedal OT 2002. The mammary gland and its origin during synapsid evolution. *J Mammary Gland Biol Neoplasia*, **7**: 225-252.

Ohyama M, Terunuma A, Tock CL, Radonovich MF, Pise-Masison CA, Hopping SB, Brady JN, Udey MC and Vogel JC 2006. Characterization and isolation of stem cell-enriched human hair follicle bulge cells. *J Clin Invest*, **116**: 249-260.

Proctor GB and Carpenter GH 2007. Regulation of salivary gland function by autonomic nerves. *Autonomic neuroscience : basic & clinical*, **133**: 3-18.

Proksch E, Brandner JM and Jensen JM 2008. The skin: an indispensable barrier. *Exp Dermatol*, **17**: 1063-1072.

Quinton PM 1983. Sweating and its disorders. *Annu Rev Med*, **34**: 429-452.

Rietze RL, Valcanis H, Brooker GF, Thomas T, Voss AK and Bartlett PF 2001. Purification of a pluripotent neural stem cell from the adult mouse brain. *Nature*, **412**: 736-739.

Rios AC, Fu NY, Lindeman GJ and Visvader JE 2014. In situ identification of bipotent stem cells in the mammary gland. *Nature*, **506**: 322-327.

Rittie L, Sachs DL, Orringer JS, Voorhees JJ and Fisher GJ 2013. Eccrine sweat glands are major contributors to reepithelialization of human wounds. *The American journal of pathology*, **182**: 163-171.

Saga K 2002. Structure and function of human sweat glands studied with histochemistry and cytochemistry. *Prog Histochem Cytochem*, **37**: 323-386.

Sato K 1977. Pharmacology and function of the myoepithelial cell in the eccrine sweat gland.

Experientia, **33**: 631-633.

Sato K, Kang WH, Saga K and Sato KT 1989a. Biology of sweat glands and their disorders. I. Normal sweat gland function. *J Am Acad Dermatol*, **20**: 537-563.

Sato K, Kang WH, Saga K and Sato KT 1989b. Biology of sweat glands and their disorders. I. Normal sweat gland function. *J Am Acad Dermatol*, **20**: 537-563.

Schittek B, Hipfel R, Sauer B, Bauer J, Kalbacher H, Stevanovic S, Schirle M, Schroeder K, Blin N, Meier F, Rassner G and Garbe C 2001. Dermcidin: a novel human antibiotic peptide secreted by sweat glands. *Nature immunology*, **2**: 1133-1137.

Schmidt-Nielsen K, Schmidt-Nielsen B, Jarnum SA and Houpt TR 1957. Body temperature of the camel and its relation to water economy. *Am J Physiol*, **188**: 103-112.

Schon M, Benwood J, O'Connell-Willstaedt T and Rheinwald JG 1999. Human sweat gland myoepithelial cells express a unique set of cytokeratins and reveal the potential for alternative epithelial and mesenchymal differentiation states in culture. *J Cell Sci*, **112 (Pt 12)**: 1925-1936.

Shackleton M, Vaillant F, Simpson KJ, Stingl J, Smyth GK, Asselin-Labat ML, Wu L, Lindeman GJ and Visvader JE 2006. Generation of a functional mammary gland from a single stem cell. *Nature*, **439**: 84-88.

Shelmire JB, Jr. 1959. Some interrelations between sebum, sweat and the skin surface. *The Journal*

of investigative dermatology, **32**: 471-472.

Shikiji T, Minami M, Inoue T, Hirose K, Oura H and Arase S 2003. Keratinocytes can differentiate into eccrine sweat ducts in vitro: involvement of epidermal growth factor and fetal bovine serum. *J Dermatol Sci*, **33**: 141-150.

Shiohara T, Doi T and Hayakawa J 2011. Defective sweating responses in atopic dermatitis. *Curr Probl Dermatol*, **41**: 68-79.

Spike BT, Engle DD, Lin JC, Cheung SK, La J and Wahl GM 2012. A mammary stem cell population identified and characterized in late embryogenesis reveals similarities to human breast cancer. *Cell stem cell*, **10**: 183-197.

Stingl J, Eirew P, Ricketson I, Shackleton M, Vaillant F, Choi D, Li HI and Eaves CJ 2006. Purification and unique properties of mammary epithelial stem cells. *Nature*, **439**: 993-997.

Sun TT, Shih C and Green H 1979. Keratin cytoskeletons in epithelial cells of internal organs. *Proc Natl Acad Sci U S A*, **76**: 2813-2817.

Tomer R, Ye L, Hsueh B and Deisseroth K 2014. Advanced CLARITY for rapid and high-resolution imaging of intact tissues. *Nature protocols*, **9**: 1682-1697.

Toyoshima KE, Asakawa K, Ishibashi N, Toki H, Ogawa M, Hasegawa T, Irie T, Tachikawa T, Sato A, Takeda A and Tsuji T 2012. Fully functional hair follicle regeneration through the rearrangement of stem cells and their niches. *Nature communications*, **3**: 784.

Watt FM and Fujiwara H 2011. Cell-extracellular matrix interactions in normal and diseased skin. *Cold Spring Harbor perspectives in biology*, **3**.

Watt FM and Hogan BL 2000. Out of Eden: stem cells and their niches. *Science*, **287**: 1427-1430.

Yano K, Brown LF and Detmar M 2001. Control of hair growth and follicle size by VEGF-mediated angiogenesis. *J Clin Invest*, **107**: 409-417.

Zhu L, Okano S, Takahara M, Chiba T, Tu Y, Oda Y and Furue M 2013. Expression of S100 protein family members in normal skin and sweat gland tumors. *J Dermatol Sci*, **70**: 211-219.

Publication

Kurata R, Futaki S, Nakano I, Tanemura A, Murota H, Katayama I, Sekiguchi K.

Isolation and characterization of sweat gland myoepithelial cells from human skin.

Cell Struct Funct. 2014 Oct 8;39(2):101-12.

Acknowledgments

The studies described in this dissertation were performed under the direction of Prof. Kiyotoshi Sekiguchi, the Principal Investigator in the Laboratory for Extracellular Matrix Biochemistry, Institute for Protein Research, Osaka University. I would like to express my deepest gratitude to Prof. Sekiguchi for his firm guidance, essential criticisms, and kind consideration. His pointed comments have always been extremely helpful for my research, and I have learned a way of logical thinking from him. I would like to express my sincere gratitude to Dr. Sugiko Futaki for her great suggestions and comments on my work and dissertation.

I would like to express my gratitude to Dr. Kenji Kusumoto, Ms. Itsuko Nakano, and all the members of the Laboratory for Extracellular Matrix Biochemistry for their helpful suggestions and comments. I would like to thank Dr. Fumitaka Fujita of the Technical Development Center, Mandom Corporation, who supported and encouraged me throughout this study.

I also thank Dr. Ichiro Katayama, Dr. Hiroyuki Murota, and Dr. Atsushi Tanemura, who provided me the opportunity to perform experiments using human skin.

I am also grateful to Dr. Kazuaki Yoshikawa and Dr. Masato Okada for their review of my dissertation.

Finally, I am especially grateful to my wife and my children, who have always been supportive of my academic pursuits. To all of my friends and family who have provided support and encouragement, thank you very much.

Ryuichiro Kurata

Osaka, May 2015